6-1985

A Study of Fine Structure Development of Poly(ethylene terephthalate) in High Speed Spinning by Using a Pneumatic Drawdown Device

Chi-Chung Bai
University of Tennessee - Knoxville

To the Graduate Council:

I am submitting herewith a dissertation written by Chi-Chung Bai entitled "A Study of Fine Structure Development of Poly(ethylene terephthalate) in High Speed Spinning by Using a Pneumatic Drawdown Device." I have examined the final electronic copy of this dissertation for form and content and recommend that it be accepted in partial fulfillment of the requirements for the degree of Doctor of Philosophy, with a major in Human Ecology.

J. E. Spruiell, Major Professor

We have read this dissertation and recommend its acceptance:

Larry C. Wadsworth, K. E. Duelud, Jay Stauss

Accepted for the Council:

Carolyn R. Hodges

Vice Provost and Dean of the Graduate School

(Original signatures are on file with official student records.)

To the Graduate Council:

I am submitting herewith a dissertation written by Chi-Chung Bai entitled " A Study of Fine Structure Development of Poly(ethylene terephthalate) in High Speed Spinning by Using a Pneumatic Drawdown Device." I have examined the final copy of this dissertation for form and content and recommend that it be accepted in partial fulfillment of the requirements for the degree of Doctor of Philosophy, with a major in Home Economics.

J. E. Spruiell, Major Professor

We have read this dissertation and recommend its acceptance:

Accepted for the Council:

The Graduate School

A STUDY OF FINE STRUCTURE DEVELOPMENT OF POLY(ETHYLENE TEREPHTHALATE) IN HIGH SPEED SPINNING BY USING A PNEUMATIC DRAWDOWN DEVICE

A Dissertation

Presented for the

Doctor of Philosophy

Degree

The University of Tennessee, Knoxville

Chi-Chung Bai

June 1985

DEDICATION

To my parents Mr. and Mrs. Hsi-Chih Bai (白曦之), my wife Hsin-Shen Bai, (李新生) and my sons Jong-Woen Bai (白仲文) and Young-Weon Bai (白仰文).

ACKNOWLEDGEMENT

The author wishes to express his sincere appreciation to author's advisors, Professors J. E. Spruiell and L. C. Wadsworth, for their guidance, support, and patience throughout this work.

Financial support was provided by the National Science Council and Union Chemical Laboratories, ITRI of Rep. of China and Rhone Poulenc Fibres of France through a grant to the Department of Materials Science and Engineering. This support is gratefully acknowledged.

Special appreciation is extended to Rhone Poulenc Fibres of France for providing the pneumatic drawdown device and polyester polymers in addition to the financial support. Allied Fibers and Plastics is most appreciated for supplying high molecular weight polyester polymer. Thanks are also extended to all the faculty members and students in the Polymer Engineering and Textile Science programs who made my stay at the University an enjoyable and stimulating experience.

Upmost thanks are extended to Dr. S. J. Wang of Chung Shan Institute of Science and Technology, in Taiwan, Republic of China for helping with the computer simulation work, Dr. K. Koyama of Yamagata University,

Japan for his suggestion in building a small heater for the infrared microscope, Mr. C. Y. Lin for his assistance in online measurements, my colleagues at Union Chemical Laboratories for their continuous encouragement, and the Machine and Electronic Shops in Dougherty Engineering Building for construction, installation and maintainance of the equipment used in this research.

Finally, the author expresses his deepest appreciation to his wife and parents. Without their continuous encouragement and confidence this work would not have been possible.

ABSTRACT

High speed melt spinning of linear, branched, and high molecular weight poly(ethylene terephthalate) (PET) polymers using a pneumatic drawdown device was carried out in this study. Characterization of the structure of final spun fibers of each polymer and the structure development along the spinline for different mass throughputs and take-up velocities were studied.

The final spun fibers were characterized with various techniques: birefringence, density, wide angle x-ray scattering (WAXS), differential scanning calorimetry (DSC), shrinkage, and tensile testing. A filament cutting technique was utilized and on-line temperature and birefringence measurements were performed to study the PET structure development along the spinline.

A sharp diameter thinning (necking) phenomena was clearly observed on the spinline for linear and high molecular weight samples at high take-up speeds. After necking, the fiber exhibited almost constant diameter and a semi-crystalline structure. Mechanisms for necking formation were considered in this study.

A computer simulation was also performed in this research. The computer simulation results agreed

qualitatively with the the experimental dataal data but quantitative agreement with the experimental data was not achieved. The changes of fiber structure from fully amorphous to semi-crystalline, however, could be simulated on the spinline.

TABLE OF CONTENTS

CHAPTER PAGE

CHAPTER PAGE

LIST OF FIGURE

FIGURE PAGE

FIGURE PAGE

FIGURE PAGE

FIGURE PAGE

CHAPTER 1

INTRODUCTION

For centuries, nature was the only source of fiber for textiles. The quality and quantity of natural fibers strongly depended upon the environment. Since first being manufactured on a wide scale in the 1950's , synthetic fibers were readily accepted by consumers because of their durability, blendability with natural fibers, better wrinkle recovery, and ease of maintenance.

There are several advantages of manufacturing synthetic fiber:

(1) It is fast, automatic, and independent of weather conditions.

(2) The quality and quantity can be carefully controlled.

(3) The fiber properties can be designed and modified in the manufacturing processes.

For example, in the polymerization process, controlled degrees of polymerization, incorporation of functional groups, addition of certain additives or copolymerization with other monomers can improve fiber raw material properties. In the fiber spinning process, controlling the fiber diameter, changing the shape of

fiber cross-section by utilizing spinneret holes of different shapes, i.e. circular, triangular, pentalobal, etc., or production of bicomponent fibers etc., can be used to improve luster, stiffness, and resilience of the fiber. It is highly likely that in the future fiber producers will be able to manufacture fibers which possess the luster of silk, the wettability of cotton, and the bulk of wool.

Today man-made fibers are used not only in apparel and home furnishings but also in (1) medicine; artifical arteries and disposible surgical products, in (2) transportation; radial tires and road construction materials, in (3) environmental applications in air filters and (4) erosion control composites and in (5) a growing number of products for aerospace uses (56).

There are three basic processes used in the manufacture of man-made fibers: (1) wet spinning, (2) dry spinning, and (3) melt spinning. Wet spinning involves conversion of fiber raw material into a solution, and extrusion of this solution through a spinneret into a coagulating bath, where additional chemical reactions convert the material back into the desired fibrous form. In dry spinning, the polymer is dissolved in a volatile solvent to form a spinning dope. The dope is forced through a spinneret into a chamber

containing warm gases (usually air). In the chamber, the warm air causes the solvent to evaporate and the solidified polymer forms fibers. In melt spinning, the polymer is melted and the molten polymer is pumped through a spinneret by a metering pump. The extruded polymer melt is solidified by cooling air and wound up by a take-up device. Of these, melt spinning is the simplest and most economical method and requires no chemical change of any kind in the process. The first successful melt spinning process was performed with nylon 66 by Carothers (20) of E.I.du Pont de Nemours and Company in 1931 and was commerciallized in 1939 (60).

In a conventional melt spinning process, take-up velocities are usually below 1500 m/min. At low take-up velocities, molecular orientation is insufficient to impart the required properties of textile fibers. Because the spun fiber is weak and unstable, it can not be directly used for weaving or knitting. A drawing process is necessary as a post spinning operation since sufficient orientation can not be imparted during the spinning operation. The drawing process gives the fiber the necessary tenacity and elastic modulus for use in the textile industry.

Extensive research was done and numerous papers were published concerning the relationship between

molecular orientation and physical properties of the fiber. They concluded that molecular orientation plays a very important role in determining the fiber physical properties. With increasing molecular orientation, the birefringence, crystallinity, density, and tenacity increase while fiber elongation decreases.

Fiber producers have found that the stability of fiber improved with increased take-up speed in the spinning process (55,88). They observed that in spinning poly(ethylene terephthalate) (PET), partially oriented yarn (POY) formed at a take-up speed of about 3000 m/min, resulted not only in increased production rates but also improved the stability of yarns which had better storage properties (55,88).

From the economic point of view, both increasing take-up speed and reducing the number of processing steps will decrease production costs. If fiber producers can produce fully oriented fibers directly from the melt spinning process by increasing the take-up speed to certain limits, they can eliminate the sequential drawing process. The fully oriented fibers, produced by high speed spinning, may then only require twisting into plied yarns and possible texturizing before being woven or knitted. In the spunbonding nonwoven industry, efforts are made through air

attenuation and drafting techniques to achieve as high a degree of orientation as possible to improve the mechanical properties of these structures (56).

Recently, 6000 m/min take-up devices have been commercialized (33). The structure and physical properties relationships of PET fibers spun at high speeds behave differently from the partially oriented fibers. The effect of high spinning speeds on the fiber structure and physical properties has been studied by many researchers (2,35,36,51-53,66,71,82,83,87-100,117, 118,128,129).

However, there has been very little information reported on the relationships between the structure and physical properties of linear, branched, and high molecular weight PET polymers under high speed spinning. Furthermore, the fiber structure development along the spinline under high speed spinning was still unclear.

The purpose of this study was to examine the structure and physical property relationship of three different PET polymers: linear, branched, and high molecular weight, under different mass throughputs and take-up velocities. Furthermore, structure development along the spinline was investigated by measuring fiber diameter, birefringence, and temperature during spinning of these three different polymers. A computer

simulation was also performed to simulate the structure development along the spinline of PET during high speed spinning. Based on these studies, we have developed a more fundamental understanding of these polymers under high speed spinning.

CHAPTER 2

LITERATURE SURVEY

2.1 General Background

The first fundamental research on PET fibers was done by the Carothers team for E. I. Du Pont de Nemours and Company from 1928 to 1937 (60,74,75,127). However, the polycondensation of linear PET is more difficult than for polyamides, and this delayed the development of PET in synthetic fiber production. In 1941, J. R. Winfield and J. T. Dickson of Calico Printer's Association Ltd., successfully introducted PET fiber in Great Britain (60). In 1947, both the Imperial Chemical Industries Ltd. (ICI) and Du Pont Company purchased the rights to manufacture PET fibers. Du Pont's PET fiber was marketed under the tradename "Dacron"® while ICI called the same fiber "Terylene"®. Because of their ease of maintenance and excellent crease resistance properties, PET fibers were widely accepted by consumers.

2.2 Basic Structure of Poly(ethylene terephthalate)

The Textile Fibers Products Identification Act (60) defines poly(ethylene terephthalate) fiber as

"a manufactured fiber in which the fiber forming

substance is any long chain synthetic polymer composed of at least 85 percent by weight of an ester of a substituted aromatic carboxylic acid, including but not restricted to substituted terephthalic units,

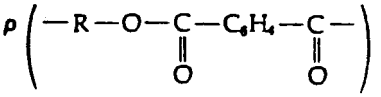

and parasubtituted hydroxybenzoate units,"

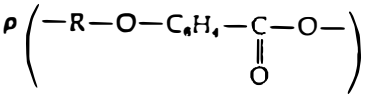

Basically, the chemical structure of PET fiber is a linear polymer with a repeat unit of oxyethylene oxyterephthaloyl (75):

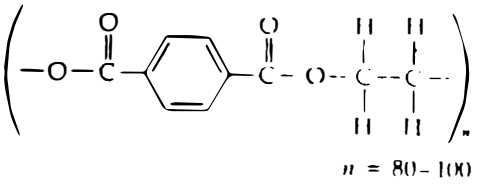

n = 80-100

The crystal lattice of PET is triclinic (24) as shown in Figure 2.1. The unit cell parameters are a=4.56Å, b=5.94Å, c=10.75Å, α =98.5°, β =118°, γ =112° (24). The polymer chain lies along the c axis and the c repeat distance consists of one structural unit (24). The molecular chains were found to be roughly planar with aromatic rings nearly parallel to (100) planes (24).

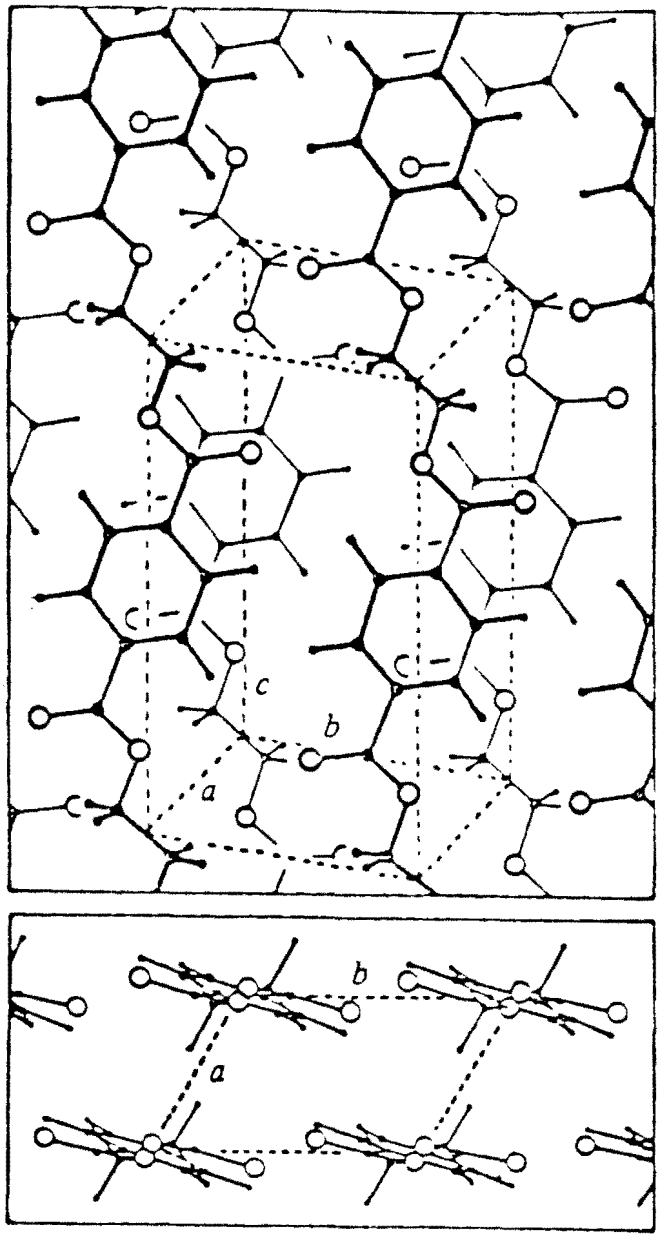

Figure 2.1. Schematic of molecular packing in poly(ethylene terephthalate).

2.2.1 Density

Based on the unit cell determined by Daubeny, Bunn, and Brown (24), The crystalline density of PET is 1.455 g/cm^3. For completely amorphous PET, the density is 1.335 g/cm^3(24). There have been other reported values of the crystalline density, i.e., 1.501 g/cm^3 (120), 1.495 g/cm^3 (67), and 1.515 g/cm^3 (29). These are based on redeterminations of the crystal unit cell dimensions. In this research, we used the Daubeny value due to its widespread acceptance in the literature.

2.2.2 Crystallinity

Due to low intermolecular force between molecules, the crystallization rate of PET is low and crystallization time is long under quiescent crystallization (51,74,81,127).

In the melt spinning process, below 3500 m/min, PET fibers do not crystallize in the spinline and an amorphous structure is observed. Shimizu et al. (87,92,93,95), Heuvel et al. (51), and Perez et al. (82) reported that at take-up speeds above 4500 m/min, PET polymers crystallized in the spinline. The crystallinity of PET fiber increased as the take-up speed increased. This is apparently due to enhanced crystallization kinetics caused by orientation-induced

crystallization. The crystallization kinetics are discussed further in section 2.3.

The crystallinity can be determined and calculated from density measurement, differential scanning calorimetry (DSC) techniques, x-ray diffraction methods, infrared absorption or nuclear magnetic resonance. Typical crystallinity values range from zero for quenched amorphous samples to about 55% crystalline for well crystallized samples (23,48).

2.2.3 Thermal Properties

The glass transition temperature (Tg) of PET usually ranges between 67 C^{O} to 75 C^{O} (17,18). The glass transition is an important phenomenon occurring in amorphous material or the non-crystalline regions of a semi-crystalline polymer. Above Tg the polymer exhibits the behavior of a rubbery material (low modulus, high extensions, etc.) while below Tg the polymer exhibits the properties of a glassy material (high modulus, low extension, stiffness, etc.). Amorphous PET crystallizes in the range of 95 C^{O} to 145 C^{O} (15). In general, the higher the orientation the lower is the crystallization temperature. The equilibrium melting temperature of crystalline PET is about 255^{O}.

2.3 Crystallization

The crystallization phenomena can in general be devided into two processes: nucleation and crystal growth. The nucleation is the initiation of a very small amount of crystalline material emerging from the parent phase by a fluctuation process (14). Crystal growth in polymers also generally proceeds by a nucleation mechanism: namely, by surface necleation on the growth plane.

Both nucleation and crystal growth are dependent on crystallization conditions such as time, temperature, pressure, mechanical forces, and pretreatment (14,58).

There are three different types of nucleation occurring in crystallization from the polymer melt:

(1) Heterogeneous nucleation, i.e. nucleation due to the presence of a second phase and occurring at the interface with it. The second phase may be impurities or nucleating agents on which crystallization takes place.

(2) Homogeneous nucleation, i.e. nucleation in the absence of a second phase. The spontaneous aggregation of polymer chains in a manner which is reversible by thermal motion. Until a critical size is reached, the subsequent addition of chains is irreversible, the growth may be consider to have commenced.

(3) Orientation-induced nucleation, i.e. nucleation is enhanced due to some degree of alignment by orientation of the polymer molecules. Regions of chain alignment are easily converted to a nuclei embryo and crystallization take place.

Binsbergen (14) reported that when polypropylene is oriented by shear stress or tensile stress as low as about 0.1 kg/cm^2, nucleation is induced at a much lower degree of supercooling than is required for normal crystallization. The nucleation lines are parallel to the direction of stress direction. The density of nucleation lines increases with increasing orientation.

2.3.1 Crystallization Kinetics

Numerous investigation have been made of the crystallization kinetics of polymer materials. Most of these studies focus on crystallization under isothermal conditions.

(1) Isothermal crystallization kinetics

The degree of phase transformation from amorphous phase to crystalline phase is related to time by the Avrami equation (81):

$$\chi_{(t)} = 1 - \exp(-kt^n) \qquad (2.1)$$

where

$\chi_{(t)}$: the degree of phase transformation

k : the crystallization rate constant containing nucleation and growth rate

n : Avrami index

(2) Non-isothermal crystallization

Crystallization of polymer melts, in practical processing operations, proceeds non-isothermally over a wide range of temperature. The overall crystallization rate constant, which contains contributions from nucleation and growth processes depends on the temperature.

$$K = K(T) \tag{2.2}$$

Nakamura et al. (81) expressed non-isothermal quiescient crystallization as:

$$\chi_{(t)} = 1 - \exp\left(-\int_0^t K(T)\, d\tau \right)^n \tag{2.3}$$

where

n : Avrami index determined from the data of the isothermal crystallization

$$K(T) = k(T)^{1/n}$$

(3) Crystallization kinetics in melt spinning process

In the melt spinning process, temperature is a function of time along the spinline and resulting time dependence of K can be written as:

$$K = K(T(t)) \tag{2.4}$$

Polymer crystallization in the melt spinning process is also very sensitive to molecular orientation in the amorphous phase. Ziabicki (127) determined the kinetic function of non-isothermal and oriented condition in melt spinning process as:

$$K(t) = K_o(T)\exp(A \cdot f^2) \qquad (2.5)$$

where

$K_o(T)$: the crystallization rate in an isotropic unoriented system

f : orientation factor

A : material constant

Ishizuka and Koyama (58) studied the crystallization kinetics of polypropylene in melt spinning. They reported crystallization kinetics for a heterogeneously nucleated system as:

$$-\ln\left(-\frac{\chi}{\chi_\infty} \right) = \frac{1}{\chi_\infty} \cdot \frac{\rho_c}{\rho_l} \cdot k_f \sum_{i=0}^{p} \chi \left\{ \sum_{j=i}^{p} G_i(T_{(u)} \Delta N_a(u)) \Delta t \right\}^n$$

$$N_i(T_{(\tau)} \Delta N_a(\tau)) \qquad (2.6)$$

where

χ_∞ : the maxium crystallinity

ρ_c : density of crystalline phase

ρ_l : density of liquid phase

k_f : shape factor which depend on the dimensionability of the growth

ΔN_a : orientation of the amorphous phase

N_i : temperature and orientation dependent rate of nucleas formation

G_i : time, temperature, and orientation depend linear growth rate

(4) Crystallization kinetics in PET melt spinning

Due to low kinetic crystallizability of PET polymers, at low spinning speeds, PET polymers do not crystallize in the spinline and an amorphous fiber structure is observed in the fibers. However, at high spinning speeds, PET polymers do crystallize in the spinline. Shimitzu et al. (87,92,93,95), Henvel et al. (51), and Perez et al. (82) reported that at take-up speeds above 4500 m/min, PET polymers crystallized in the spinline and crystallinity increased as take-up speeds increased. This is apparently due to enhanced crystallization kinetics caused by orientation-induced crystallization.

Kikutani (66) reported the crystallization kinetics of PET polymers as:

$$\frac{\chi_c}{\chi_\infty} = 1 - \exp\left(-\left(\int_0^t K(T(t) \cdot \Delta N) d\tau \right)^n \right) \qquad (2.7)$$

where

χ_c : crystallinity

χ_∞ : maxium crystallinity

ΔN : total fiber birefringence

This crystallization kinetic equation was used to simulate the spinline behavior of PET polymers in Chapter 4.4.

2.4 Dynamics of Low and Moderate Speed Melt Spinning

Melt spinning is the fundamental operation in the manufacture of fibers from PET polymer. The process involves melting the polymer and extruding it through spinneret(s) into a gaseous medium and stretching it by a take up device. The fiber structure changes along the spinline with the rate of deformation and the rate of cooling. The study of spinning dynamics has become the key point of the melt spinning process. A complete series of studies (both theoretical analysis and experimental Investigation) of the spinline problem began with the work of Ziabicki and Kedzierska (122-124) and Kase and Matsuo (61-65). More detailed review have

been given by Dees (25,26), White (114), and Tsou (109). A brief summary of the important features of the problem is given in the following paragraphs.

The problem involves mass balance, force balance, energy balance, and structure development along the spinline. These balances must be solved simultaneously to interpret this complex melt spinning process:

(1) Mass balance

In steady state melt spinning, the mass balance may be expressed as

$$\rho A V = W = \text{constant} \qquad (2.8)$$

where

ρ : fiber density

A : fiber cross-section area

V : fiber velocity

W : mass throughput

(2) Force balance

The gradient of axial force along the spinline, dF/dx, results from several contributions,

$$\frac{dF}{dx} = W \frac{dV}{dx} - \pi \alpha \frac{dR}{dx} - \rho g R^2 + \pi D \tau_f \qquad (2.9)$$

and after intergration (base on pure elongational flow)

$$F_{(x)} = F_{(0)} + W\,(V_{(x)}-V_{(0)}) + \pi\,\alpha\,(R_{(0)}-R_{(x)}) - \pi\,\rho\,g\int_0^x R^2 dx + 2\,\pi\int_0^x R\,\tau_f\,dx \qquad (2.10)$$

where

$\frac{dF}{dx}$: gradient of axial force along the spinline

$V_{(x)}$: current axial velocity of the filament at the distance x from spinneret

$V_{(0)}$: extrusion velocity

$R_{(x)}$: current radius of the filament

$R_{(0)}$: radius of the orifice

α : surface tension

τ_f : shear stress on the filament surface resulting from air drag (skin friction)

The individual terms in equation (2.3) describe the contribution of rheological force, inertia, surface tension, gravity, and air drag forces:

$$F_{(x)} = F_{rheo(x)} = F_{rheo(0)} + F_{in} + F_{surf} - F_{grav} + F_{air} \qquad (2.11)$$

The effects of surface tension, $F_{surf}= \pi\alpha(R_0-R_x)$ and gravity, $F_{grav}= \pi\rho g\int_0^x R^2 dx$ are generally small compared to the other term, except for the low speed spinning of very thick filaments where Fgrav and Fsurf can become appreciable. Otherwise these two factors contribute less than 1% of the total tension and can be neglected for both low and high speed spinning (126).

(3) Energy balance

Heat transfer from the spinline to the cooling medium (air) provides another important factor in spinning dynamics. The melt viscosity of fiber depends upon the temperature of the fiber which in turn depends on the cooling rate of the fiber. As the temperature of the fiber decreases (causing an increase in the viscosity) the rheological force exerted on the molecules, which causes the deformation, increases.

The energy balance can be approximated as,

$$W\, C_p \frac{dT}{dx} = - h\, \pi\, D\, (\, T - T_s\,) \qquad (2.12)$$

where

$\frac{dT}{dx}$: cooling rate

h : heat transfer coefficient

T_s : cooling air temperature

C_p : heat capacity of polymer

2.5 Dynamics of High Speed Melt Spinning

As opposed to low speed spinning, the increase in the elongation rate in the threadline induces a much higher degree of molecular orientation at high spinning speeds. From the thermodynamics point of view the increased orientation decreases the free energy of

molecules, thus creating a more stable phase (27). Strain induced crystallization occurs in the spinline and a high birefringence is obsevred for PET fiber at spinning speeds over 4500 m/min (51-53,66,76,82,91, 95-97,116,117). The latent heat released by crystallization may influence the viscosity of the polymer, causing changes in the spinline behavior and structure development of PET that are quite different from that of low and moderate speed spinning.

Kikutani (66) combined strain hardening, birefringence, and crystallization kinetics with the conventional mass, force, and energy balances as below:

(1) Force balance equation

$$\frac{dF}{dx} = W \left(\frac{dV}{dx} - \frac{g}{V} \right) + \pi D \tau_f \qquad (2.13)$$

(2) Rheological equation

$$\frac{dV}{dx} = \frac{F \rho V}{\eta W} \qquad (2.14)$$

(3) Strain hardening equation

$$\eta = 1.3 \exp\left(\frac{4400}{T + 273} \right) \exp\left(2^{18} \chi_c^{16} \right) \qquad (2.15)$$

(4) Energy balance equation

$$\frac{d\chi_c}{dx} = \frac{Cp}{\Delta H} \frac{dT}{dx} + \frac{4h}{\Delta H D \rho V} \left(T - T_s \right) \qquad (2.16)$$

(5) Crystallization kinetics

$$\frac{\chi c}{\chi_\infty} = 1 - \exp\left(-\left(\int_0^\tau K\left(T(\tau)\ \Delta N \right) d\tau \right)^n \right) \qquad (2.17)$$

(6) Birefringence equation

$$\frac{d\Delta N}{dx} = \frac{Cop}{V}\frac{dV}{dx} - \frac{\Delta N}{V\ \tau_f} \qquad (2.18)$$

The notations are listed in Appendix A.

From this model, the spinline problem can be simulated for PET high speed spinning. More detail will be given in Chapter 4.4.

2.6. Fiber Formation Process in Low and Moderate Speed Melt Spinning

When molten polymer is extruded from the spinneret(s), the orientation, which is created by shear flow within the spinneret channel is relaxed by die swell and the polymer becomes unoriented (27). The molecular orientation by shear flow is not an effective contribution to the final fiber orientation. The extruded polymer is then deformed by the take-up force. Fiber molecules are stretched from a random conformation to an oriented conformation. This orientation actually is a balance between the orientation induced by the deformation of the melt stream and the relaxation due to thermal motion of the molecules before the glass transition point is reached.

In other words, the structure development along the spinline depends upon the spinline stress and the amount of supercooling. The physical properties of the fiber depend upon the formation of the fine structure along the spinline.

The spinline problem was studied by Ziabicki and Kedzierska (122-124,126) and Kase and Matsuo (61-65). They reported velocity and diameter distributions along the spinline as a function of the spinning conditions. Ziabicki and Kedzierska were the first to publish x-ray patterns and birefringence data of melt spun fibers and showed that the orientation of the molecules increased with take-up stress. Henson and Spruiell (49) and Nadella et al. (79,80) also studied the spinline stress for polypropylene fibers under low spinning speed. They concluded that the spinline stress dominated the structure development process in melt spinning. Abbot and White (1) studied the effect of spinning speed, flow rate and melt temperature on the orientation and crystallization of melt spun polyethylene. They reported that the mechanical properties increased with increased crystalline orientation.

In general, PET exhibits a rather low crystallization rate, short relaxation time and low

viscosity (66,103,126,128). At low and moderate spinning speeds (below 3500 m/min), the rate of crystallization is sufficiently slow and the rate of cooling is sufficiently high to prevent crystallization from occurring. X-ray (51,66), density (51,66,96), DSC analysis (51,83,92), and shrinkage data (36,92) showed that fiber spun at these conditions exhibited an amorphous structure or a mesophase (oriented amorphous structure) (2).

Nakamura, Watanabe, Katayama, and Amano (81) pointed out that at high take-up velocities and spinline stress, PET will crystallize due to enhanced crystallization rate, which is apparently due to molecular orientation produced in the polymer melt.

2.7. Fiber Formation Process in High Speed Spinning

The morphology of fiber structure is determined by the conformation of fiber molecules. Highly oriented fiber molecules strongly influence the morphology of the fiber and its physical properties. Thus, the structure development and physical properties of high speed melt spun fibers has become a topic of both theoretical and practical importance for many fiber research laboratories.

Shimizu et al. published a series of papers on the

high speed spinning of several polymers (81-94). They have studied polypropylene (PP), poly(ethylene terephthalate) (PET), nylon-6, nylon-66, and poly(ethylene -1, 2-diphenoxyethane-p, p'-dicarboxylate) at spinning speeds up to 9000 m/min.

Their results revealed that most high speed spun fibers show characteristic structure and properties compared with conventional drawn yarns. For example, high speed spun PP fibers (79,80) exhibited a remarkable increase in crystallinity and in both crystalline and amorphous orientation resulting in a hard elastic structure. In nylon-6 (92), the content of α and γ phase was controlled by the spinning speed and the γ -phase increased with take-up speed. For nylon-66 (93) the α-phase predominated at every spinning speed and the crystal size along the fiber axis increased with the spinning speed. Heuvel and Huisman (52) reported high crystallinity and orientation were observed with increasing take-up speeds for nylon-6 fibers. They also reported an increase in γ -phase with an increase in the take-up speed and proposed that γ -phase was mainly generated from orientation induced nuclei and α -phase grew slowly after moisture pick up at take up speeds above 2500 m/min.

Lecluse (71) reported the effect of take-up speed

and water diffusion on the structure of nylon-66 fibers. She reported that the higher the spinning speed, the lower the ratio of α to γ phase along the spinline and after a critical speed of about 3000 m/min to 4000 m/min only the γ-phase may be observed along the spinline.

Suryadevara and Spruiell (107) studied the effect of molecular weight on the structure and properties of high speed melt spun nylon-6. They reported an increase in spinline stress with increasing take-up speed and molecular weight. The total crystalline fraction and phase fraction increased and the α-phase fraction decreased with increasing take-up speed. The fiber modulus and tensile strength increased with increasing molecular weight and take-up speed.

Ishibashi et al. (57) investigated the molecular weight effect on the melt spinning of nylon-6. On-line temperature and diameter measurements were carried out. They found that the temperature and diameter profiles were independent of the number average molecular weight over the range 18,500 to 24,000 grams/mole.

2.7.1 Fiber Formation Process in High Speed Spinning of Poly(ethylene Terephthalate)

Shimizu and coworkers have performed a series of studies on high speed spun PET. In 1977, they reported

changes in PET fiber structure and physical properties with take-up speeds up to 9000 m/min (89). At spinning speeds over 5000 m/min, they observed a large increase in the density and crystallinity. The crystallization peak occurring heating of as spun samples also vanished in DSC traces.

In 1978, they reported the effect of melt draw ratio and flow rate on the high speed spinning of PET (92). They concluded that the take-up speed played the dominant role in the fiber structure formation. Increasing the melt draw ratio or decreasing the mass flow rate increased both the fiber crystallinity and orientation. They reported that high molecular weight polymers crystallized at lower speeds and increasing the viscosity increased the spinline stress which accelerated the orientation and crystallization process.

In 1981, Shimizu et al. (96) observed radial variations across high speed spun fibers. They reported that the fiber structure developed to a highly oriented state. After increasing the take-up speed above 7000 m/min, the density and birefringence began to decrease and the degree of crystallinity, measured by heat of fusion, levelled off. They observed an almost fully oriented crystalline region. A skin and core structure was observed at high take-up speeds and the degree of

molecular orientation and crystallinity were higher in the skin than in the core. The difference in the birefringence between the skin and core increased with increasing take-up speed.

In 1982, Shimizu (97) reported on the structure development in high speed spinning. He observed a sharp diameter thinning (necking) on the spinline at take-up speeds above 5000 m/min for PET fibers. The orientation induced crystallization corresponded to birefringence values above 60×10^{-3}.

In 1983, Shimizu et al. (98,99) reported again on the formation of fiber structure in high speed spinning. The spinning stress played a very important role. Among the spinning stresses, the air drag and inertia stresses became the dominate stresses. Their examination concluded that the inertia stress played an important role in the formation of fiber structure, while the air drag had only a small effect on it.

In 1984, Shimizu et al. (101) reported on the effect of take-up speed on the unit cell parameters and superstructure of PET fibers. They summarized that the crystallite size in the lateral directions as well as chain direction increased with spinning speed. In contrast, the imperfection parameter along the chain direction decreased with increasing spinning speed. In

the range of spinning speeds from 5000 m/min to 6000 m/min, the interface between the crystalline and amorphous phases in the microfibril was highly inclined with respect to the plane perpendicular to the fiber axis. In the range from 8000 m/min to 9000 m/min, this inclination is rather small, and many voids existed between the microfibrils.

In 1978, Heuvel and Huisman (51) reported that increasing the take-up speed to 3500 m/min only increased the orientation without any indication of crystallization. At take-up speeds above 4000 m/min, extremely fast strain-induced crystallization occurred. At higher spinning speeds (above 5000 m/min) very well-developed crystals were detected. They also proposed molecular arrangements in the fibers at various take-up speeds Figure 2.2.

In 1979, Perez and Lecluse (82) reported on crystallization induced by orientation when the take-up speed exceeded 3500 m/min. The necking phenomena was observed on the spinline at take-up speeds of 5400 m/min. A sudden increase in birefringence was observed in this region. The fiber had an amorphous structure before necking and a fully crystallized structure after necking. Their results were similar to Shimizu's.

In 1982, Perez (83) reported the effect of the

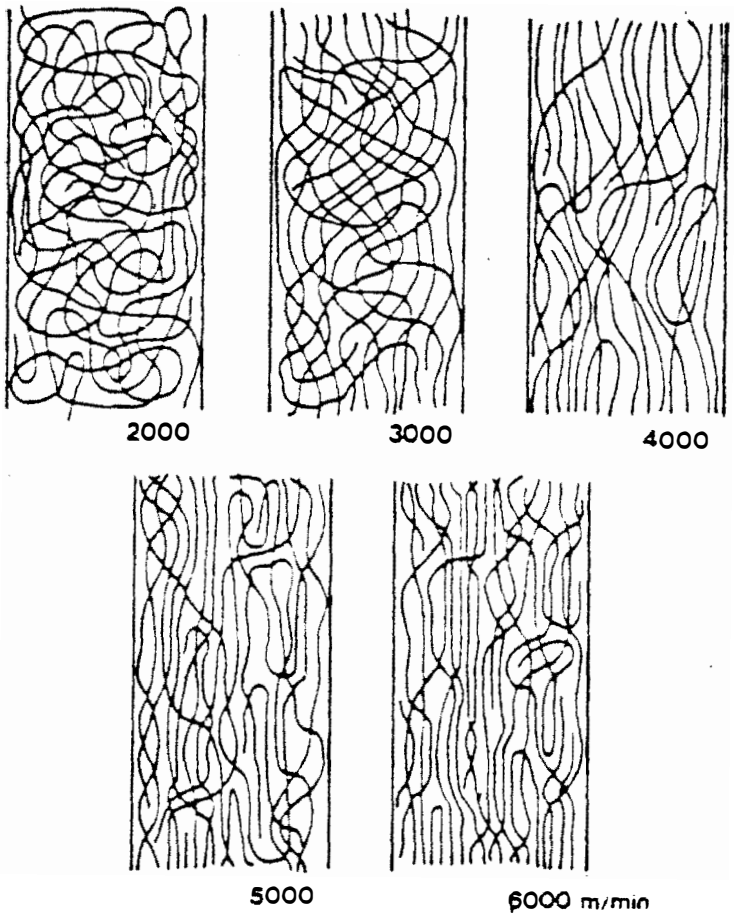

Figure 2.2. Proposed molecular arrangement in fibers at different take-up speeds. (ref. 51).

rheological properties of PET on structure development in high speed spinning. He compared the rheological properties of branched and linear PET in shear on a cone and plate mechanical spectrometer and observed the branched PET had higher normal stresses and a pseudo-plastic behaviour. An increase in molecular weight and branching led to higher relaxation times. He concluded that the high sensitivity of the spinline profile and of the structures induced was directly related to the rheological behaviour of the polymer. The viscoelastic behavior of PET controls the critical state of stress-inducing crystallization. The mechanical behavior of high speed spun fibers depended upon the degree of orientation and had a small effect on crystallinity. He also reported that necking phenomena were not so obvious in branched PET high speed spinning.

Yasuda (118) reported on the structure developement and physical properties of high speed spun PET fibers. He presented a correlation of take-up velocity with the birefringence and crystallinity differences between the center core and outer skin of the fiber at high speeds and proposed that this difference results from lower temperature and higher stresses in the skin portion.

Matsui (76) studied the PET fiber formation process on the spinline. He reported diameter and birefringence

profiles obtained by cutting the fiber on-line and temperature profiles obtained by using a contact type thermocouple. He divided the spinline into three regions: a flow deformation region, orientation induced crystallization region, and a plastic deformation region. He discussed the deformation process in each of these regions. Most of the fiber structure developed within the orientation induced crystallization region. He also observed that fiber diameter variations decreased at the higher speeds because the spinline is more stable at the higher stress levels.

In 1983, George (37) et al. also reported that the PET crystallization process is extremely rapid, occurring over a few centimeters of the spinline. At high speeds, the "freeze point", which was defined as the point at which velocity reached its final value, was reached at 200 ^{o}C. A minimum stress of 0.08 g/denier or a minimum level of orientation must be reached before crystallization can be initiated. Garg (35) reported similar results.

In general, based on density, differential scanning calorimetry (DSC), birefringence, wide angle x-ray scattering (WAXS), and small angle x-ray scattering (SAXS), the fine structure of high speed spun PET fibers exhibit high molecular orientation, birefringence and

crystallinity, more perfect crystalline structure, a skin and core structure and many voids within the microfibrils. The physical properties of high speed spun fibers exhibit high tenacity, birefringence, and melting point, and low shrinkage and elongation.

On-line studies disclosed a necking phenomena that was observed at take-up speeds above 4500 m/min. A fully developed crystalline structure was observed after necking and an amorphous structure was observed before necking. Based on these results the crystallization process is evidently an orientation induced crystallization process produced by high stresses in the spinline.

CHAPTER 3

EXPERIMENTAL MATERIALS, EQUIPMENT, AND PROCEDURES

3.1 Materials

Three different samples of poly(ethylene terephthalate) (PET) were used in this study. Linear PET with an intrinsic viscosity (I.V.) of 0.58 ml/g and a branched PET with an I.V. of 0.54 ml/g were supplied by Rhone Poulenc Fibres of France. Linear high molecular weight PET with an I.V. of 0.91 ml/g was supplied by Allied Fibers and Plastics.

3.2 Melt Spinning Equipment

The melt spinning experiments were performed using a screw extruder manufactured by Fourne Associates of West Germany and a pneumatic drawdown device supplied by Rhone Poulenc Fibres of France. A Schematic of the extruder and drawdown device is shown in Figure 3.1.

3.2.1 Fourne Screw Extruder

The Fourne Screw Extruder used has a 13 millimeter diameter screw which receives polymer pellets by gravity feed from a seven liter capacity nitrogen purged hopper. The extruder supplies molten polymer at pressure of 1.0 to 3.0 x 10^3 psi to a gear pump (Zenith) which provides a constant mass flow to the spinneret. The discharged

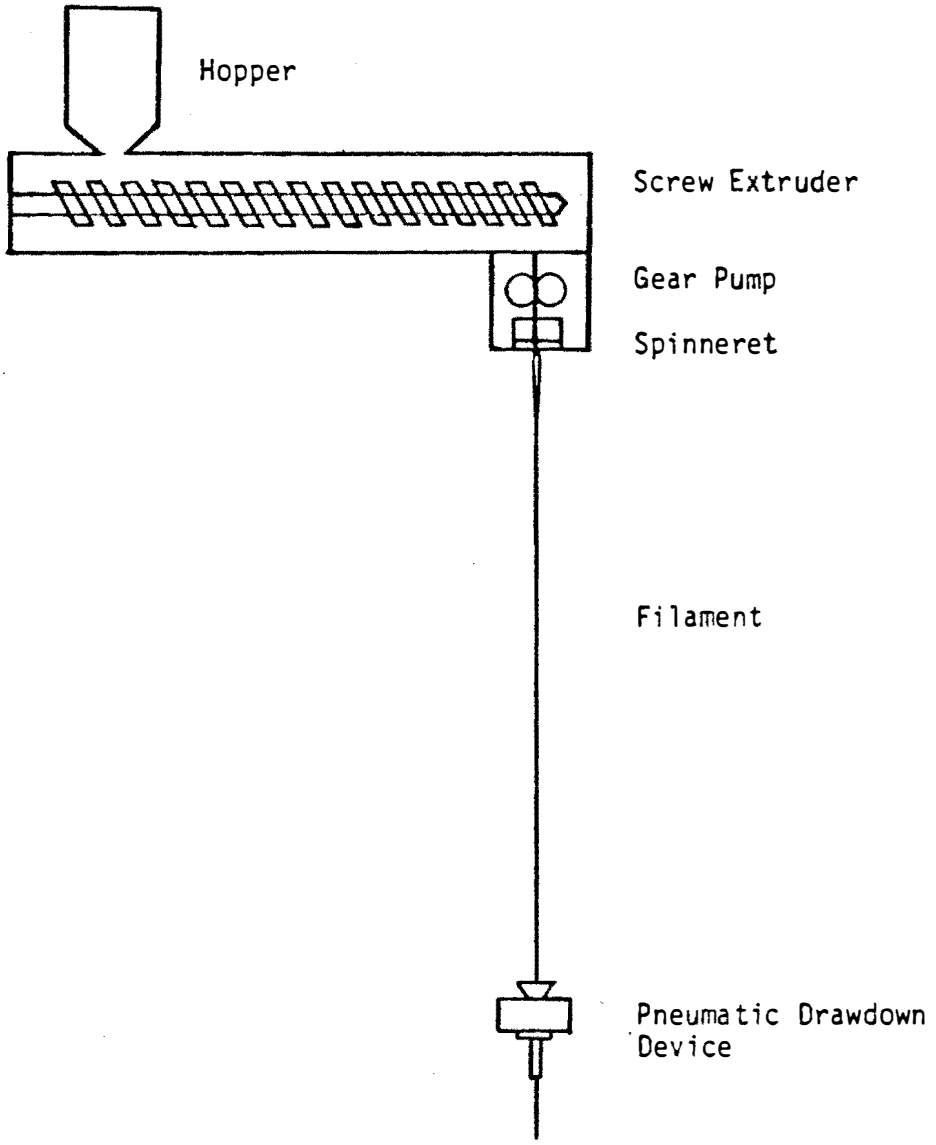

Figure 3.1. Schematic of screw extruder and pneumatic drawdown device.

polymer stream from the gear pump passes through a 325 mesh filter screen and through a single capillary die which has a diameter of 0.762 millimeter and a L/D ratio of 5.0.

The extruder and spinning head assembly is wrapped with electric band heaters arranged to provide four separate heating zones. Four controllers are used to maintain the desired temperature in each of these four zones.

Two platinum-resistance thermocouples are inserted into the polymer stream to measure the polymer temperature in the discharge stream. The temperatures are indicated on a meter on the control panel. The melt pressure is indicated by a Dyanisco pressure gauge. The gear pump speed is manually adjusted by means of a variable speed gear box to obtain the desired flow rate of the polymer melt. Once set, the flow rate remains constant.

The entire assembly of the extruder and spinning block is mounted on a vertical steel column. It can be moved up and down along the column by a motor. Further details of the various parts of the extruder and its operating and maintenance instructions are given in reference 26.

3.2.2 Pneumatic Drawdown Device

A pneumatic drawdown device was supplied by Rhone Poulenc Fibers of France. A schematic of this device is shown in Figure 3.2.

The device has a pressure indicator near the air inlet. Pressurized air was used to produce a suction force on the filament near the entrance of the device. The filament take up velocity can be adjusted by changing the pressure of the compressed air source. The actual take up velocity was calculated based on the fiber diameter, density, and mass throughput.

The final filaments were collected in a large cardboard box. The pneumatic drawdown device did not require special maintenance, and was easily wiped clean after each spinning run.

3.3 Fiber Characterization Apparatus

3.3.1 Polarizing Microscope

Fiber diameter and birefringence readings were made with a Leitz polarizing microscope (Ortholux) equipped with a Baush and Lomb filar micrometer eye piece and a 10 order Berek compensator. The retardation "R" was obtained by adjusting the compensator with crossed polars. The birefringence "Δn" was calculated from the following equation:

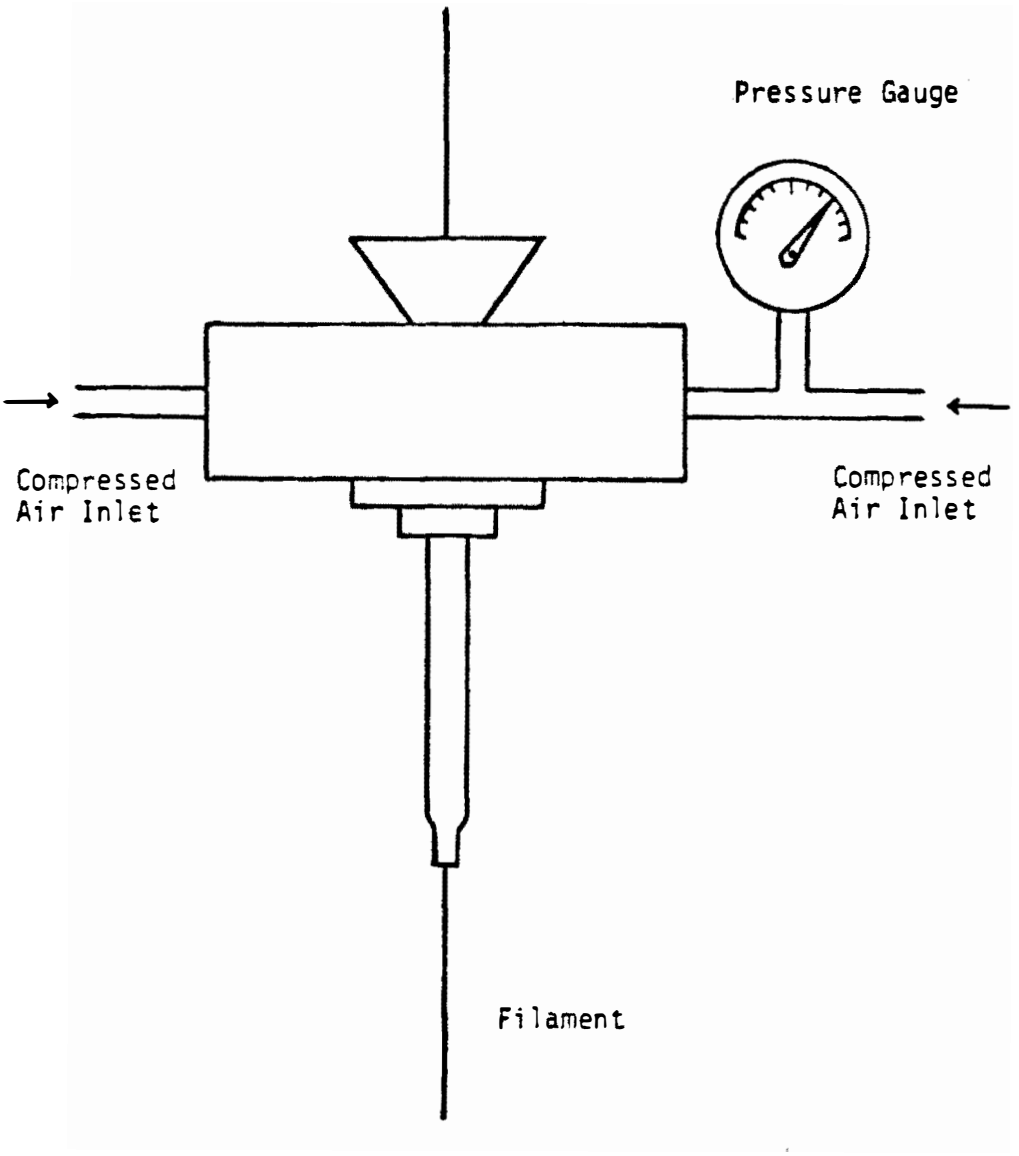

Figure 3.2. Pneumatic drawdown device.

$$\Delta N = \frac{R}{D} \qquad (3.1)$$

where

ΔN : fiber birefringence

R : retardation reading

D : fiber diameter

The compensator constant for the 10 order Leitz Berek compensator was found to be 2.065.

The amorphous orientation factors were determined from the equation

$$\Delta N = \chi \, \Delta^0_{cr} \, f_{cr} + (1 - \chi) \Delta^0_{am} \, f_{am} + \Delta N_{form} \qquad (3.2)$$

where

ΔN : total measured birefringence

χ : total crystalline fraction

Δ^0_{cr} : intrinsic birefringence of the crystalline phase

f_{cr} : crystalline orientation function

Δ^0_{am} : intrinsic birefringence of the amorphous phase

f_{am} : amorphous orientation function

ΔN_{form} : form birefringence

The crystalline orientation function was obtained from wide angle x-ray scattering (WAXS) results.

3.3.2 Density Column

The density of the fiber was determined from a density gradient column. Low and high density mixtures of distilled water and sodium bromide were mixed to produce a solution which had a density ranging from 1.300 g/c.c. to 1.450 g/c.c.. Beads of known density were placed in the column to calibrate it. The density column was maintained at 23 ^{o}C $\pm$ 0.5 ^{o}C by means of circulating water from a constant temperature water bath. A more complete description of the preparation of the column is given in reference number 26. Density readings of fiber samples were taken at least 24 hours after samples were put into the column.

Density values were used to calculate percent crystallinity according to the equation:

$$\chi_{cr} = \frac{\rho - \rho_{am}}{\rho_{cr} - \rho_{am}} \frac{\rho_{cr}}{\rho} \times 100 \qquad (3.3)$$

where

χ_{cr} : the weight fraction of crystallinity

ρ_{cr} : density of crystalline phase

ρ_{am} : density of amorphous phase

ρ : density of the sample

3.3.3 Wide Angle X-Ray Scattering (WAXS)

Wide angle x-ray film patterns were obtained using a Philips Norelco x-ray generator. A nickel filtered

CuKα radiation source of wavelength 1.542 Å was used. The x-ray unit was operated at 30kV and 20mA. In a Statton camera, the fiber sample bundle was fixed on a sample holder which attached to the beam collimator. The distance from sample to film was 3.0 cm. At least 14 hours exposure time was allowed before developing the film.

3.3.4. Rigaku X-Ray Diffraction System

A Rigaku D/max-IIIA x-ray diffractometer system equipped with a fiber specimen attachment and a control/data processing unit (5072 D1) was used to obtain 2θ scans of the fiber samples. A PDP-11 microcomputer was connected to the system to record data from the intensity measurements.

A bundle of carefully aligned parallel fibers was used to obtain 2θ and azimuthal scans to evaluate the orientation factors. To obtain the crystalline orientation factors, the 2θ value for a (hkl) plane was determined and the diffractometer was set at this 2θ value. The sample was automatically controlled by the control/data processing unit which scanned from 0 to 90 degrees in steps of one degree. The data were recorded on the PDP-11 microcomputer. The background intensity was obtained by measuring the scattered intensity at the

same (2θ) planes of PET spun fibers spun at take-up velocities around 3500 m/min. The net intensity (measured intensity minus the background intensity) was used in calculating the average of $\cos^2\phi$ ($2\theta=25.7^{o}$) and $\cos^2\phi$ ($2\theta=17.5^{o}$). The calculation of $\cos^2\phi$ was performed utilizing the following equation:

$$\overline{\cos^2\phi_{hkl}} = \frac{\int_0^{\pi/2} I_{hkl}(\phi)\cdot\cos^2\phi\cdot\sin\phi\ d\phi}{\int_0^{\pi/2} I_{hkl}(\phi)\cdot\sin\phi\ d\phi} \qquad (3.4)$$

where $I_{hkl}(\phi)$ is the intensity of the diffracted beam from the (hkl) plane making an angle with the fiber axis.

Perez (78) reported (based on Wilchinsky's method) that for PET fiber

$$(\cos^2\phi_{100}) = (\cos^2\phi_{u,z}) \qquad (3.5)$$

$$(\cos^2_{010}\phi) = \cos^2\delta\cdot(\cos^2\phi_{u,z}) + \sin^2\phi\cdot(\cos^2\phi_{v,z}) + 2\sin\phi\cdot\cos\phi\cdot(\cos\phi_{u,z}\cdot\cos\phi_{v,z}) \qquad (3.6)$$

where

z axis : the fiber axis

u,v axis: perpendicular to each other and to z axis

δ : the angle between the normal to plans (100) and (010)

and

$$(\cos^2\phi_{u,z}) + (\cos^2\phi_{v,z}) + (\cos^2\phi_{c,z}) = 1.0 \quad (3.7)$$

This results in

$$(\cos^2\phi_{c,z}) = 1 - (0.651(\cos^2\phi_{100,z}) + 1.349(\cos^2\phi_{010,z})) \quad (3.8)$$

and crystalline orientation factor was calculated as:

$$f_{cr} = \frac{1}{2}(\overline{3\cos^2\phi_{c,z}} - 1) \quad (3.9)$$

and amorphous orientation factor was computed from equation 3.2.

3.3.5 Instron Tensile Tester

The mechanical properties of the spun fibers were measured by using a table model Instron Tensile Tester at 21°C ± 2°C and 65% ± 2% RH. A gauge length of 10 cm was selected (7).

3.3.6 Scanning Electron Microscope

An AMR 900 scanning electron microscope was used to observe the peeled fibers. The sample was coated by a thin gold-palladium alloy film.

3.3.7 Differential Scanning Calorimetry (DSC)

A Perkin Elmer (DSC-2C) differential scanning calorimeter equipped with a microcomputer was used to determined the thermal properties of the spun fibers. The fiber samples were cut into small pieces and placed in a standard aluminum sample container consisting of a pan and lid. A specially designed crimper was used to crimp the pan and lid. Each sample (about 10.0 mg) was placed in the sample holder of the DSC and scanned between 330^{O}K and 550^{O}K at a rate of 10^{O}K/min. The DSC was calibrated using an indium standard (Tm=429.71^{O}K) before the measurements on the PET fibers. The crystallinity was evaluated from the equation:

$$\chi_{DSC} = \frac{\Delta H_{exp}}{\Delta H_{100\% \text{ crys.}}} \times 100 \qquad (3.10)$$

where χ_{DSC}: crystallinity percentage from DSC.

ΔH_{exp} : heat of fusion of sample

$\Delta H_{100\% \text{ crys.}}$: heat of fusion of 100% crystallized sample

ΔHexp was computed from heat of fusion in the crystalline melt peak minus heat of fusion in the crystallization peak.

3.3.8 Infrared Microscope

A Barnes Infrared Microscope model RM-2B was used to determine filament temperature along the spinline. A small heater with a black surface was designed to mount in front of the infrared microscope (Figure 3.3). The distance between the heater surface and the microscope lens (15X) was 3.0 cm. The heater temperature was controlled between 30 ^{O}C to 300 ^{O}C by a Leeds and Northrup Electromax III controller. This system, combined with a recorder, permitted noncontact measurement of the fiber temperature on the spinline. More details of operating the infrared microscope are given in section 3.4.4.

3.4. Procedure

3.4.1 Drying Of PET Chips

A batch of PET chips (about 1,800 g) was first dried in a conventional hot air circulation oven (Fisher Model 300) at a temperature of 105 ^{O}C for at least four hours. Then the chips were dried in a laboratory type vaccum oven (National Appliance Company Model 5831) at a temperature of 105 ^{O}C and at an absolute pressure of 0.5 inches of mercury for twenty four hours. After drying, the chips were stored in glass jars sealed under prepurified nitrogen until ready for use.

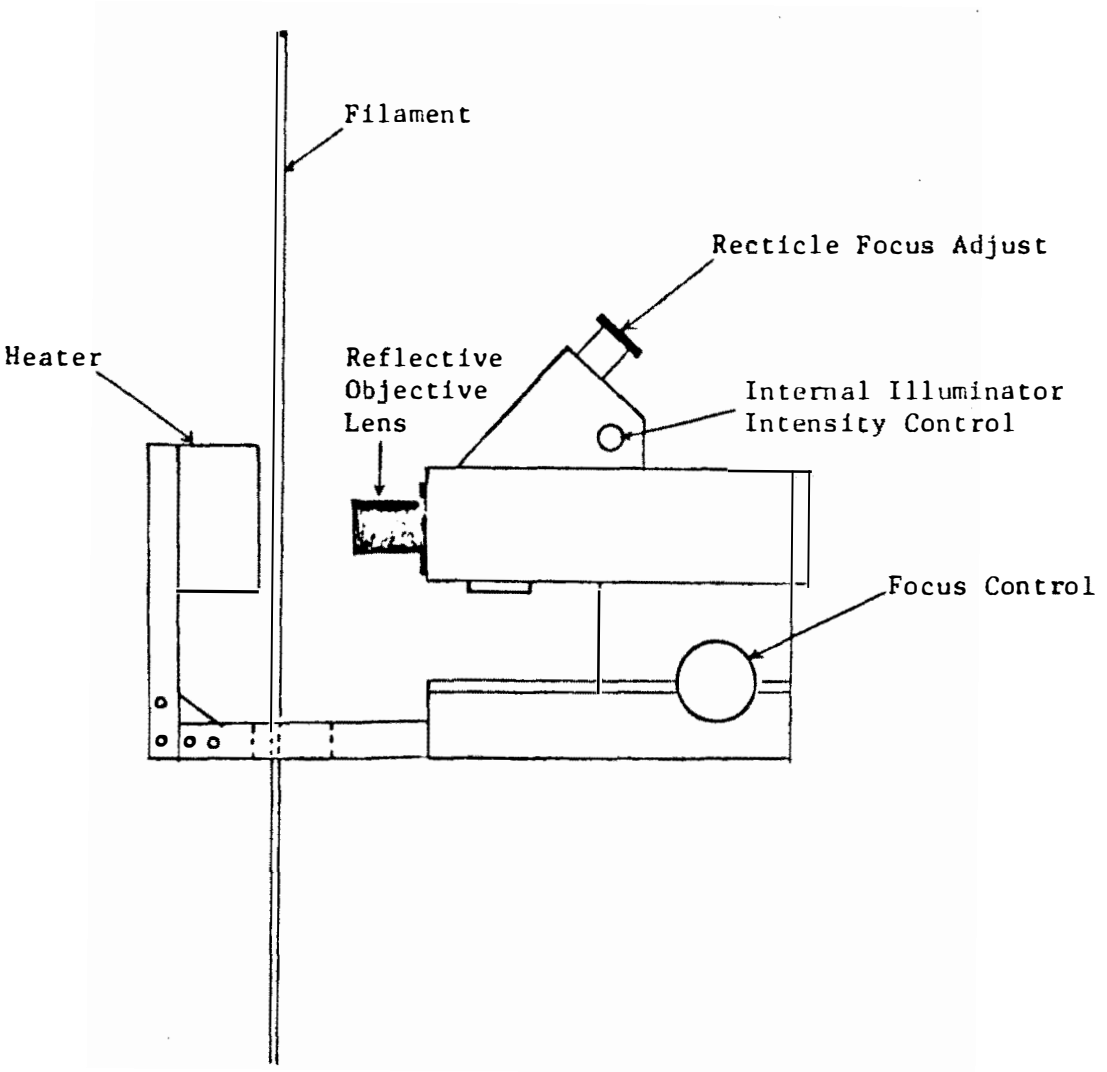

Figure 3.3. Barnes RM-2B microscope unit and temperature adjustable heater.

3.4.2 Melt Spinning Procedure

The extruder was preheated for at least two and one-half hours before operation. The procedure for starting up the extruder was then followed according to the operating manual (26).

Both the linear and branched PET were melt spun at 290 ^{O}C. For high molecular weight PET it was necessary to increase the melt temperature to 310 ^{O}C. After carefully adjusting the throughput to the desired rate, the filament was drawn down by the pneumatic drawdown device. The spin length, the distance between the spinneret and the drawdown device, was adjusted by moving the spinning head assembly up or down along the support column. The take up velocity increased with increasing air pressure in the aspirator or decreasing the spin length. The air pressure within the aspirator ranged from 5 to 90 psig. The filament exiting the drawdown device was collected in a large collection bin.

3.4.3 Cutting Of Filament Along The Spinline

A two-clamp, hand controlled cutter (see Figure 3.4) with a compressed spring was designed for cutting filament on the spinline. The length of filament segment removed from the spinline was 8.0 cm.

Extreme care was exercised during the cutting of

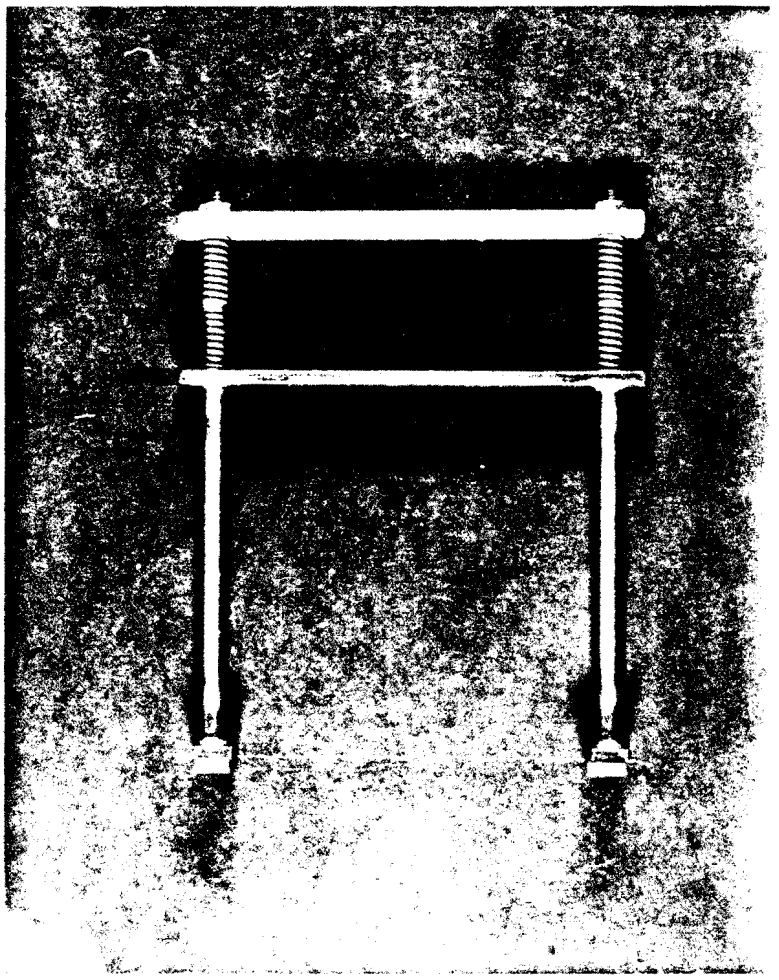

Figure 3.4. Two clamps hand control cutter.

the running filament. The cut sample was not allowed to stretch in the cutting process. A very tiny filament loop accumulated on the lower clamp is prefered (see Fig.3.5). Filament samples which were cut less than 50 cm from spinneret were rapidly quenched in a cold water pan to minimize polymer melt deformation.

3.4.4 On-line Temperature Measurement

An infrared microscope (IR microscope) with a small heater was mounted along the spinline (see Figure 3.4). The heater was set to the desired temperature. The remainder of the procedure was as follows:

(1) Turn the emissivity control, the ambient control and meter range selector switch fully counterclockwise (ambient control to its switch off position).

(2) Turn the zero control to position 500.

(3) Block the entrance aperture of the objective with a material at ambient temperature; such as a piece of rough surface cardboard.

(4) Set the objective select switch to select the proper position for the power of the objective being used.

(5) Turn the emissivity control to position 1.0.

(6) Turn the meter range selector switch to the

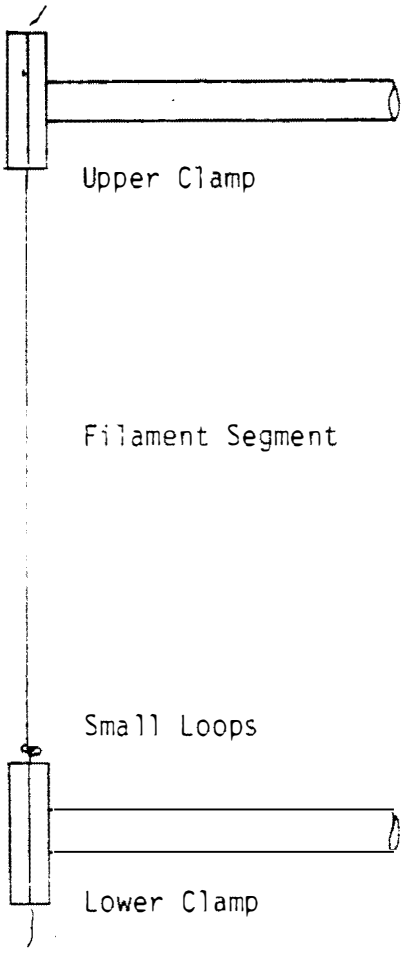

Figure 3.5. On-line cut filament segment.

desired radiometric position X1 or X10, according to the expected radiance.

(7) Adjust the zero control so that the output meter indicates 0.0 on the radiometric scale.

(8) Remove the cardboard. Read out the IR radiation of the heater (background temperature) from the output meter.

(9) At a chosen position along the spinline, focus the filament within the IR microscope focusing point and read out the difference between fiber temperature and heater set temperature.

(10) Change the location along the spinline and repeat measurement between filament and heater temperature until no difference can be determined between filament and heater set temperature.

(11) Measure the distance from spinneret and record temperature from the heater controller.

3.4.5 On-line Birefringence Measurement

The polarizing microscope was set at the appropriate position and angle to the spinline. Guilding the filament was accomplished by using a v-groove arc type aluminum guide within the microscope's viewpoint. A schematic of the online birefringence measurement is shown in Figure 3.6 and the guide is shown in Figure 3.7.

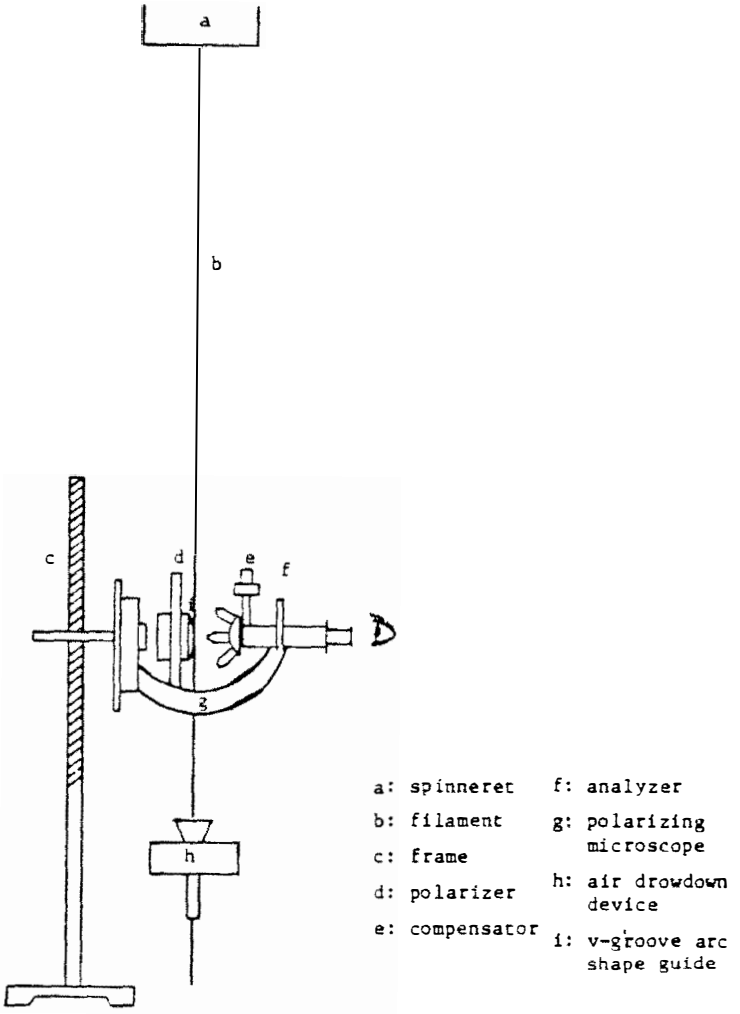

Figure 3.6. Schematic of on-line birefringence measurement.

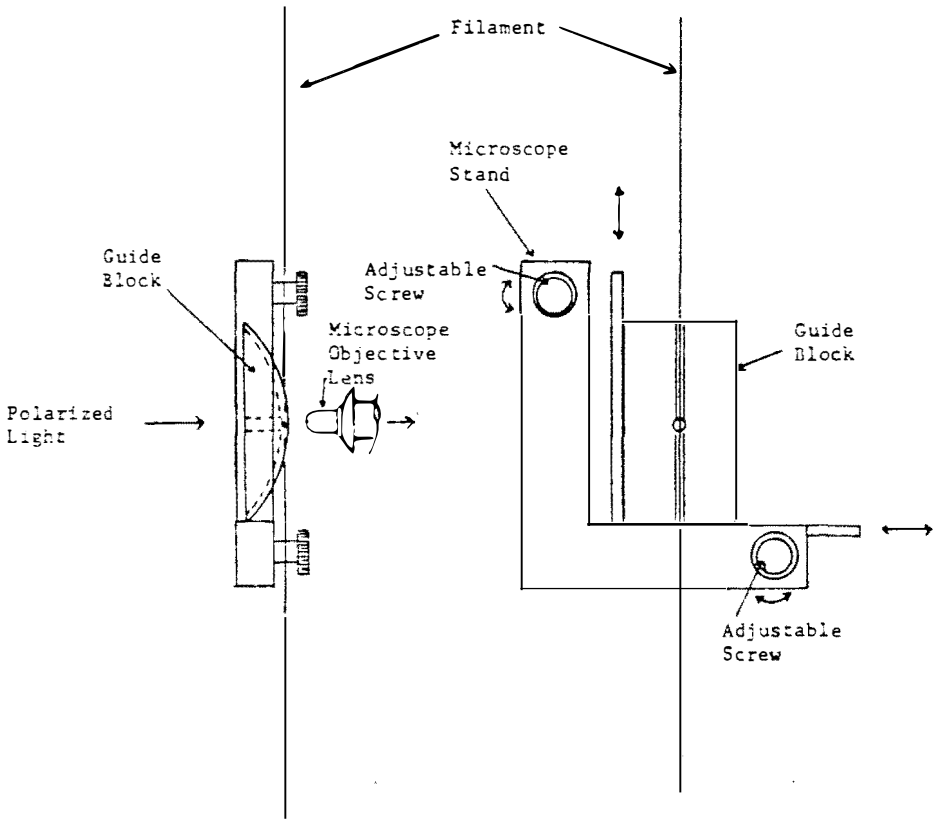

Figure 3.7. Schematic of v-groove arc type guide.

Quickly measure the filament diameter by using the Bausch and Lomb filar microscope eye piece. After the diameter reading, turn the 10 order Berek compensator to measure the black fringe of the filament from both the negative and positive side. The birefringence was calculated by dividing the measured retardation by the fiber diameter from equation 3.1. There was some unavoidable error introduced by the friction between the filament and the guide. The filament diameter from the reading was an average filament diameter of five measurements.

3.4.6 Shrinkage Measurement

A 500 ml beaker containing distilled water was heated to the boiling point. Fiber samples were cut into 10.0 cm (L_0) lengths and placed in the boiling water for 3 minutes. After taking the samples out of the water, the final fiber length (L_1) was measured. The percent shrinkage was calculated as:

$$\text{Shrinkage } (\%) = \frac{L_1 - L_0}{L_0} \times 100 \qquad (3.10)$$

CHARPTER 4

STRUCTURE DEVELOPMENT OF HIGH SPEED SPUN FIBERS

4.1 Characterization Of High Speed Spun Fibers

Fiber structure and properties are two interrelated aspects. Fiber properties are a result of fiber structure which is controlled by processing conditions and resin properties. The elucidation of fiber structure has been based on many sources of information, which include: optical properties, thermal analysis, density, electron microscopy, x-ray diffraction, and general physical properties.

Unfortunately, no single technique can elucidate all fiber structure. But, taken together, these techniques do provide substantial information about the structure and morphology of the fibers.

4.1.1. Birefringence

Polarized light can be used to determine fiber birefringence which yields information on molecular orientation. Figure 4.1 presents the total birefringence versus take-up velocity. The results show that the fiber birefringence increases with take-up velocity. The birefringence of linear PET rapidly increased at 3000 m/min and reached a value of 140 x

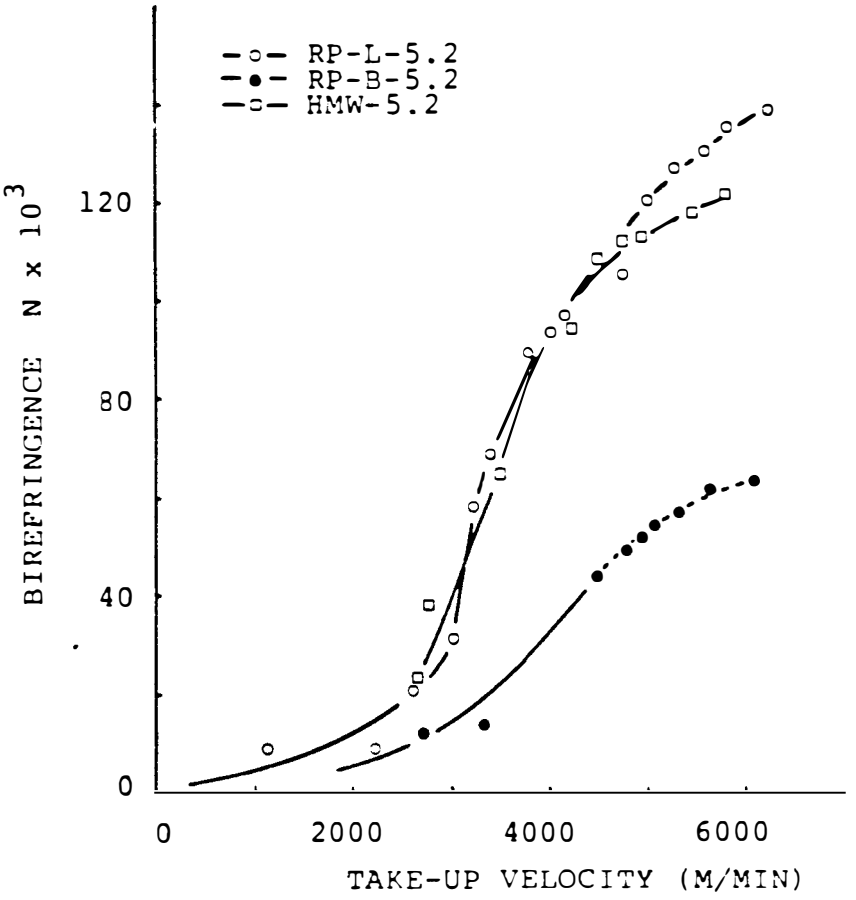

Figure 4.1. Total fiber birefringence vs. take-up velocity.

10^{-3} at 6000 m/min. For branched PET the increase was not so rapid. It reached a value of 45 x 10^{-3} at 4500 m/min and 60 x 10^{-3} at 6000 m/min. The dotted line in Figure 4.1 represents the occurrence of broken filaments on the spinline. For high molecular weight PET, the initial rate of increase is similar to the linear PET, but the birefringence begins to levels off at 5000 m/min and reached 120 x 10^{-3} at 6000 m/min. Similar results were observed by Perez (82), and Shimizu et al. (90,92,96,97).

The birefringence increased smoothly from low to high speed without clearly showing the transition from amorphous to crystalline state. This may be attributed to increased molecular orientation as take-up speed increased. When highly oriented amorphous molecules transferred to the crystalline structure the total orientation of the filament did not change much as the total birefringence of the fiber was measured.

The entanglements of the molecular chain in the high molecular weight sample prevented this sample from reaching as high a degree of ultimate crystallinity as the lower molecular weight sample at high take-up velocities (see crystallinity measurements below). Thus, the overall birefringence was lower than linear PET at high take-up velocities.

4.1.2 Density And Crystallinity

Molecular arrangements within the fiber create a complex fiber structure. Based on a two phase, amorphous and crystalline model, the crystallinity of fibers can be interpreted by x-ray diffraction, density, DSC, etc.,. Among these the density measurement is the simplest and most convenient method.

Increasing the take-up velocity results in an increase in the density of the fibers. When the polymer crystallizes, the density of the fiber increases sharply. Figure 4.2 shows that the onset of crystallization occurs around 4000 m/min for the linear polymer of lower molecular weight. The high molecular weight sample, generally showed the highest density at take-up velocities below 4500 m/min. But entanglements apparently result in lower ultimate crystallinity and prevent further density increases at speeds from 5000 m/min to 6000 m/min. Because the branched chains restricted the molecules from crystallizing within the fiber, the density of the branched sample increased slowly as the take-up velocity increased.

Generally, the fiber crystallinity was calculated from density data by equation (3.3). Figure 4.3 shows the crystallinity values resulting from this calculation. Linear PET crystallinity increased rapidly

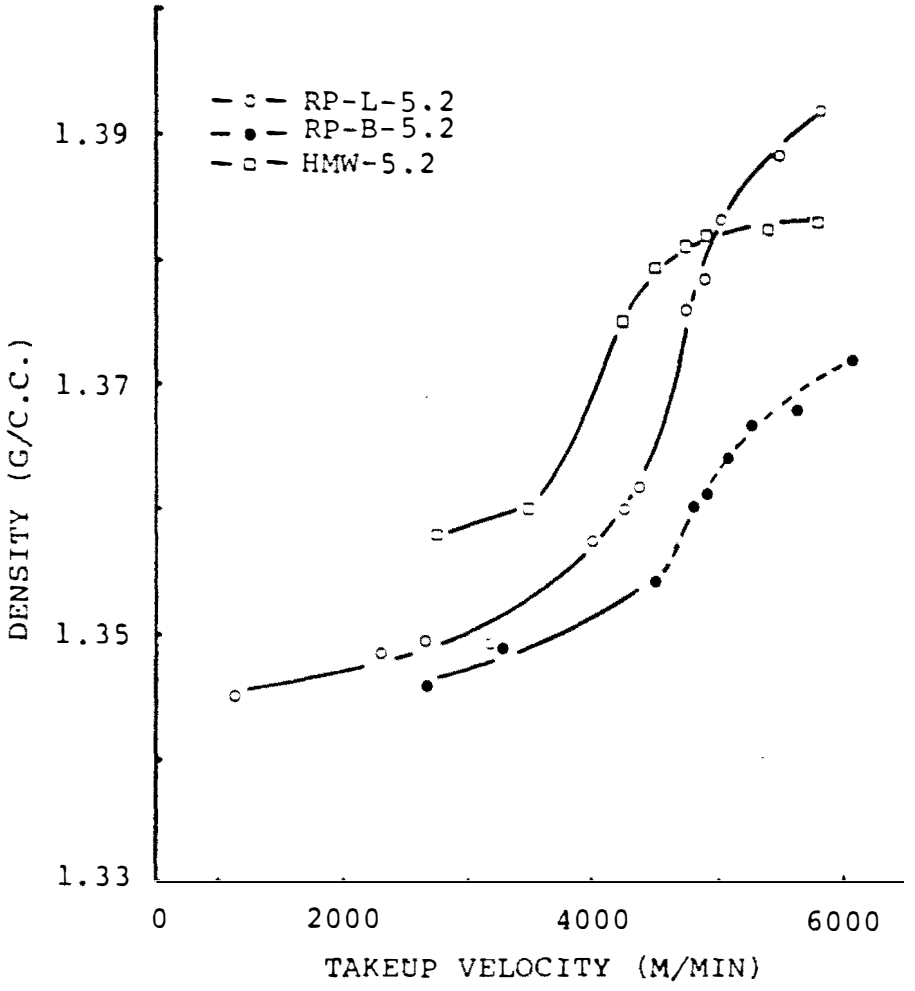

Figure 4.2. Fiber density vs. take-up velocity.

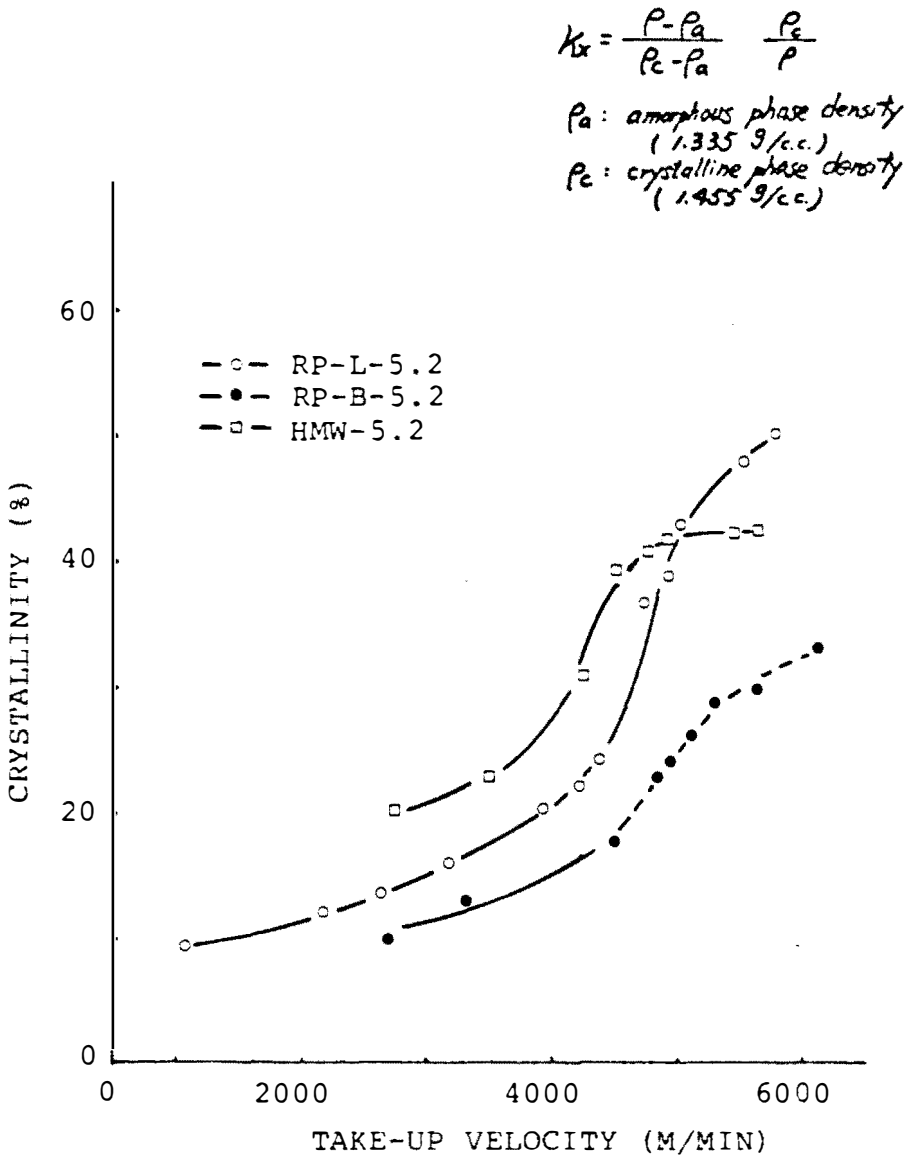

Figure 4.3. Fiber crystallinity vs. take-up velocity.

when the take-up velocity exceeded 4000 m/min. The high molecular weight fibers had a higher crystallinity content compared with the linear and branched PET fibers at take-up velocities below 5000 m/min and levelled off after 5000 m/min. It is proposed that the stress build up in the spinline of high molecular weight sample is higher than linear and branched PET at the same take-up velocity. Even at low take up velocities, the higher stress build up on the spinline results in a higher density and crystallinity for the high molecular weight samples. At higher take-up velocities the entanglements between molecules restricted any further crystallization so that the crystallinity levelled off. The branched sample exhibited the lowest crystallinity. These results revealed that the branched polymer did not easily crystallize.

4.1.3 Differential Scanning Calorimetry (DSC) Analysis

In Figure 4.4 a typical PET polymer DSC trace is presented. The glass transition (Tg) can be seen at about 350 ^{O}K, followed by a crystallization exotherm peak around 378 ^{O}K, and finally a melting endotherm at about 528 ^{O}K. From Figures 4.5, 4.6, and 4.7, it is concluded that by increasing the take-up speed, the fiber changed from an amorphous to a crystalline structure. The glass

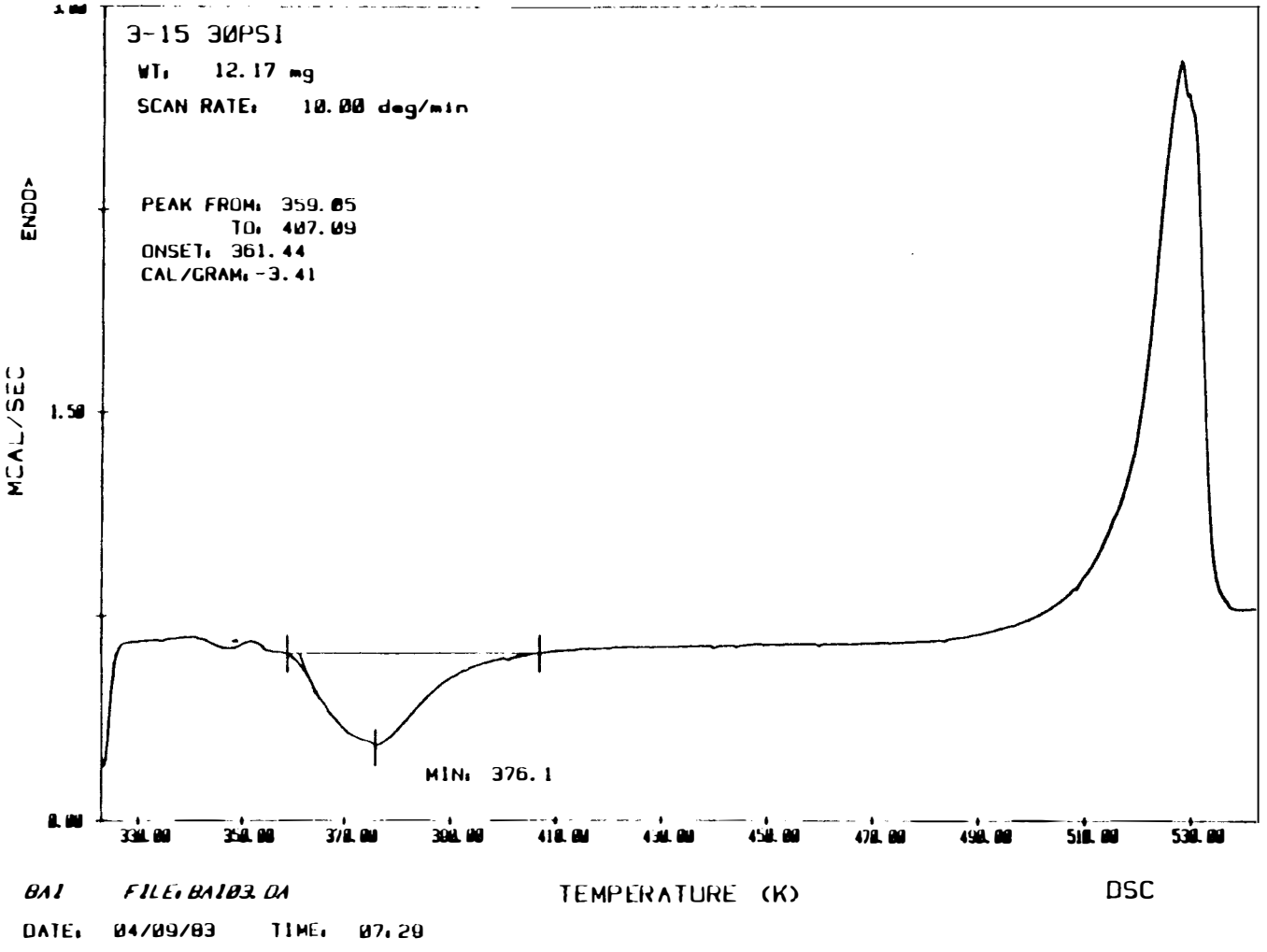

Figure 4.4. Differential scanning calorimetry spectra of poly(ethylene terephthalate) fiber.

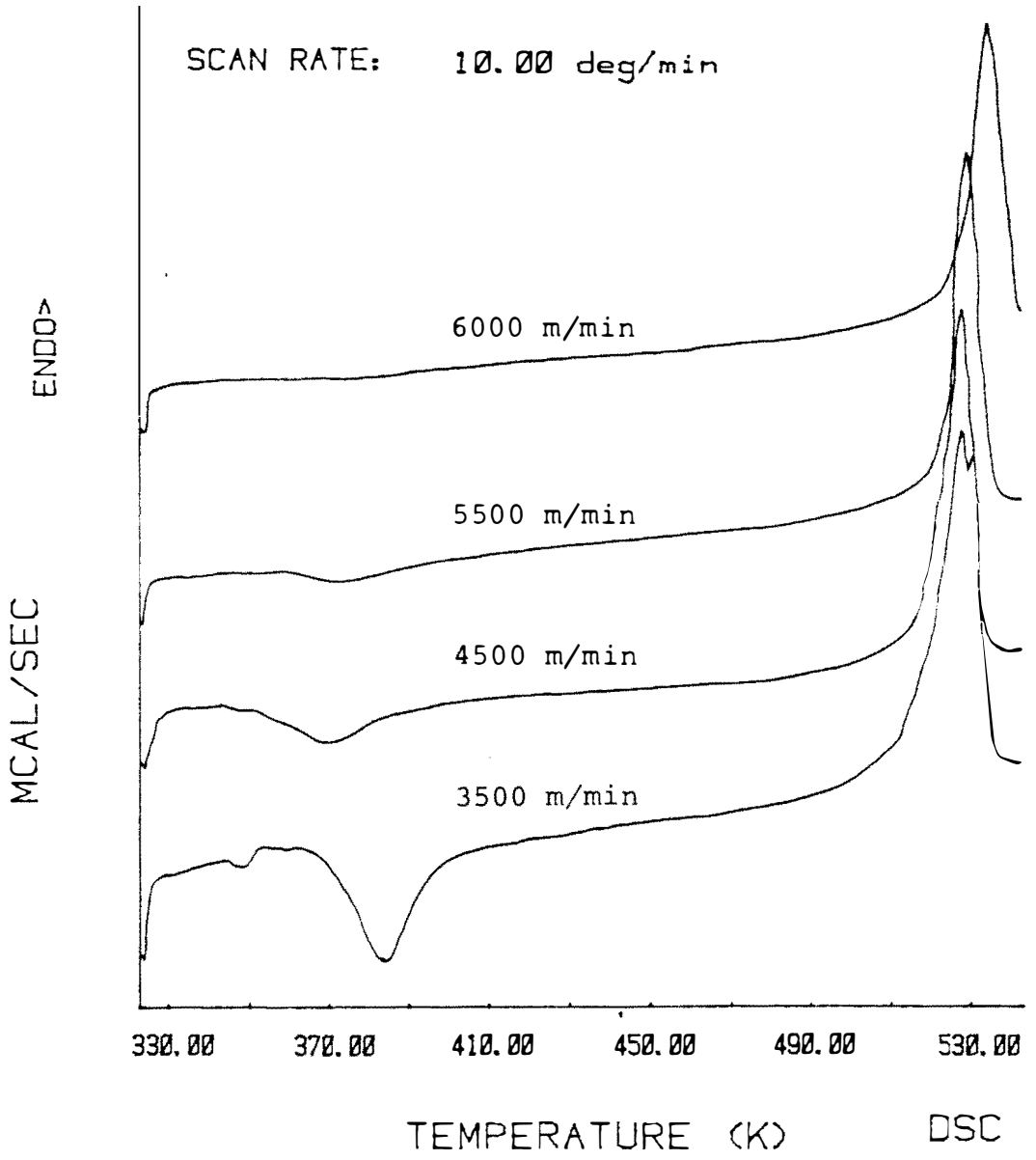

Figure 4.5. Differential scanning calorimetry spectra of linear PET fiber at different take-up speeds.

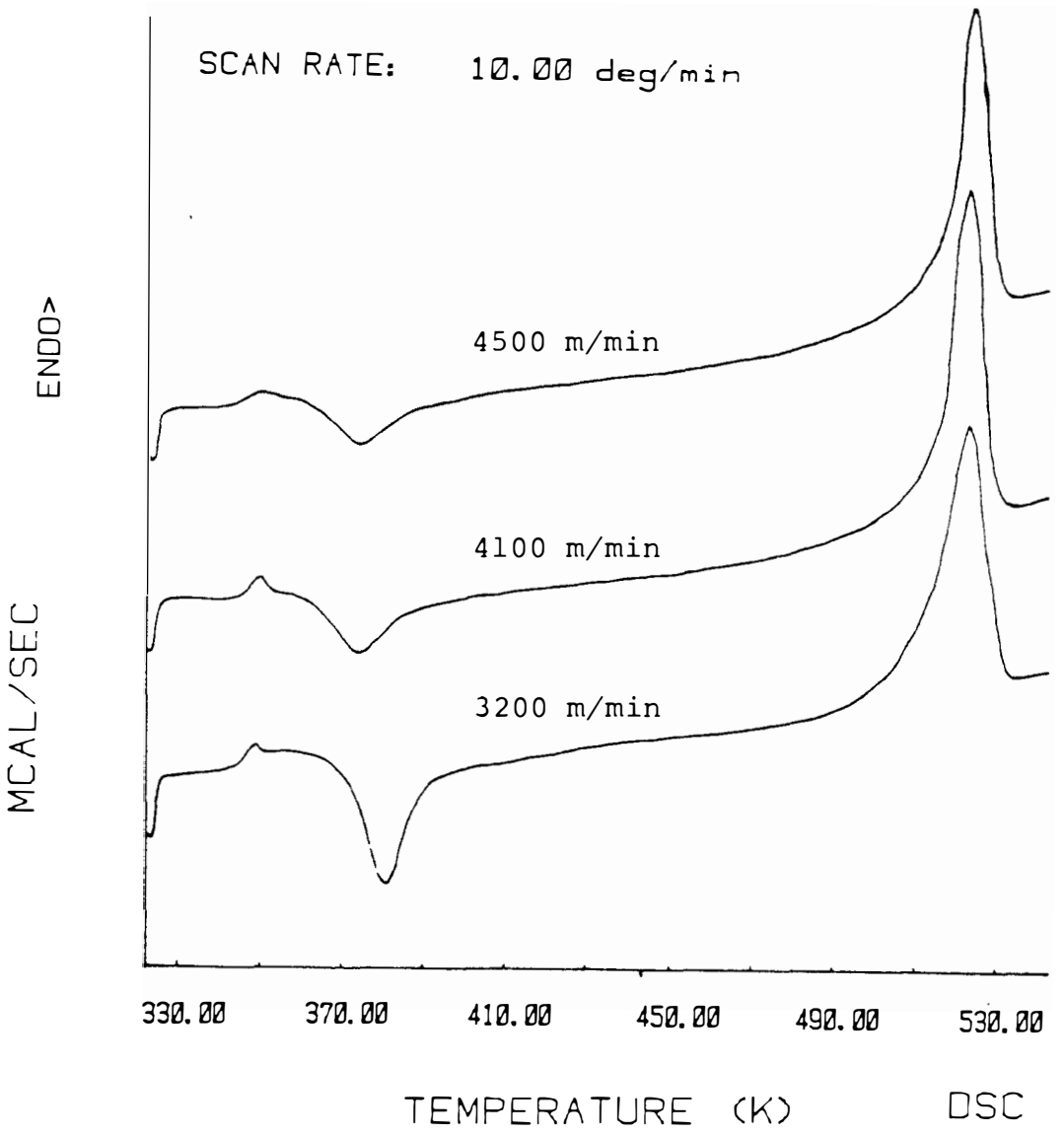

Figure 4.6. Differential scanning calorimetry spectra of branched PET fibers at different take-up speeds.

HMW-5.2

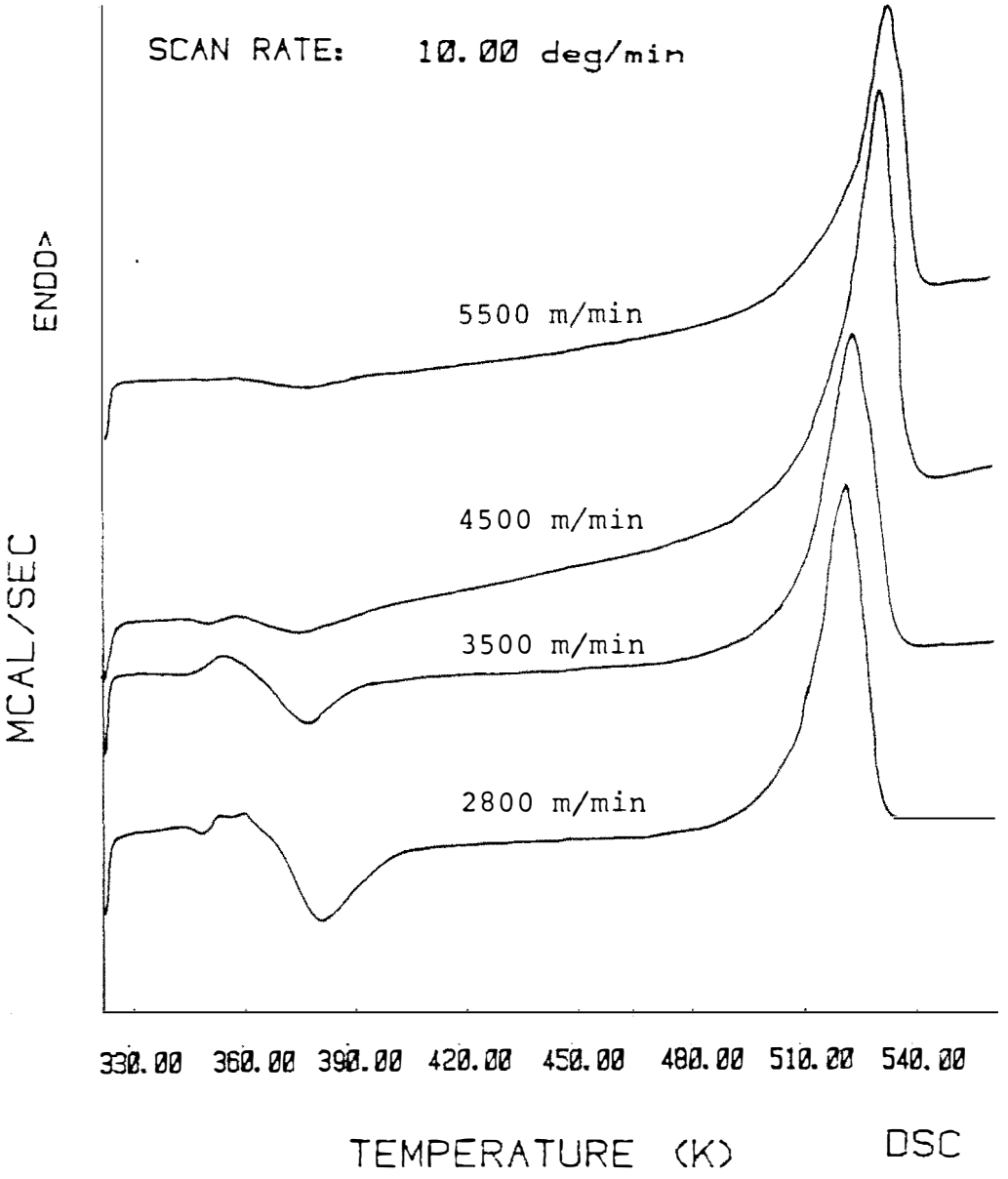

Figure 4.7. Differential scanning calorimetry spectra of high molecular weight fibers at different take-up speeds.

transition temperature was observed for fibers spun below 4500 m/min but it could not be seen at take-up speeds above 5000 m/min. The crystallization peak in heating also vanishes at the higher take-up velocities.

Figure 4.8 clearly shows that the crystallization peak decreases as take-up velocity increases. Figure 4.9 shows that melting temperature increases with take-up velocity. Figure 4.10 shows that the crystallinity computed from the DSC scan increases with take-up velocity.

From the DSC analyses, it was concluded that the structure of PET fibers changed from an amorphous to a crystalline state when the take-up velocity increased from low to high spinning speeds. Also the perfection of the crystalline region increased as the take-up velocity increased. Together with the density results these show that PET begins to crystallize on the spinline at speeds in the range 4000 to 4500 m/min. These results are similar to those of Perez (82), Heuvel and Huisman (51), and Shimizu (90,92,96,97).

4.1.4 Tensile Properties of Melt Spun Fibers

The mechanical properties of textile fibers are probably the most critical parameters in determining the end-use performance properties. The individual fiber

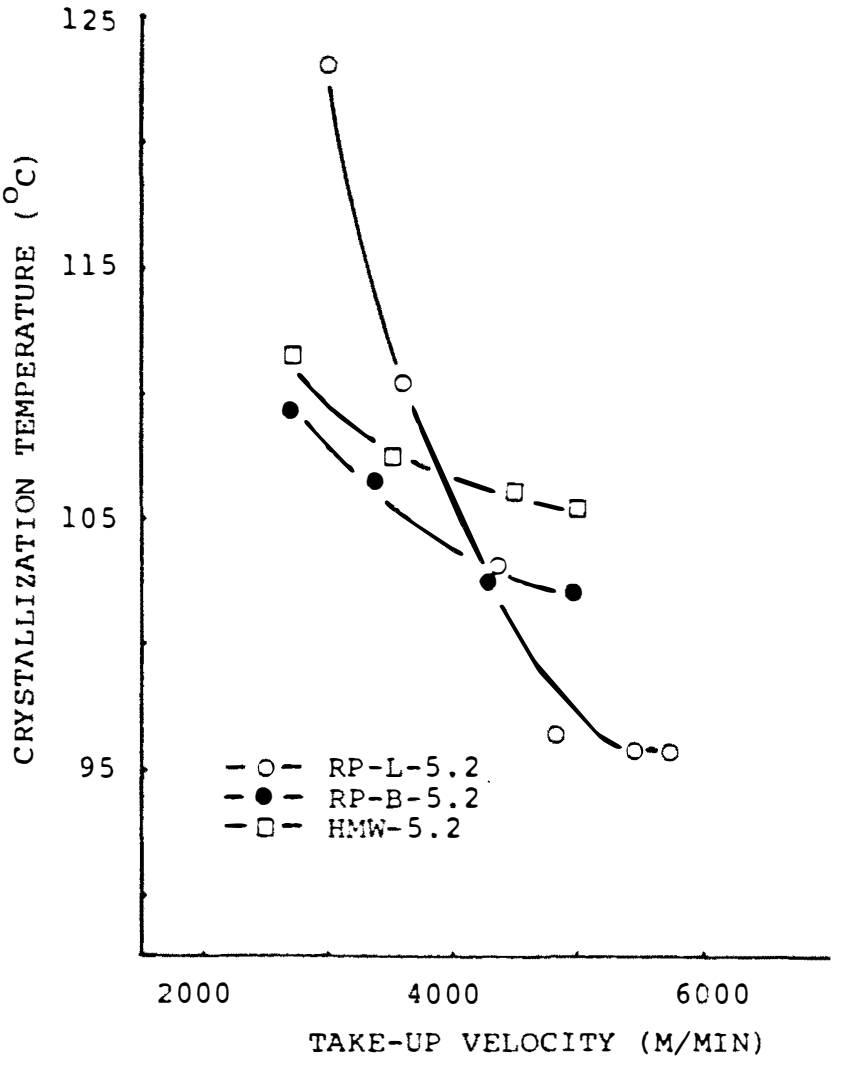

Figure 4.8. Crystallization temperature measured at the exothermal peak vs. take-up velocities.

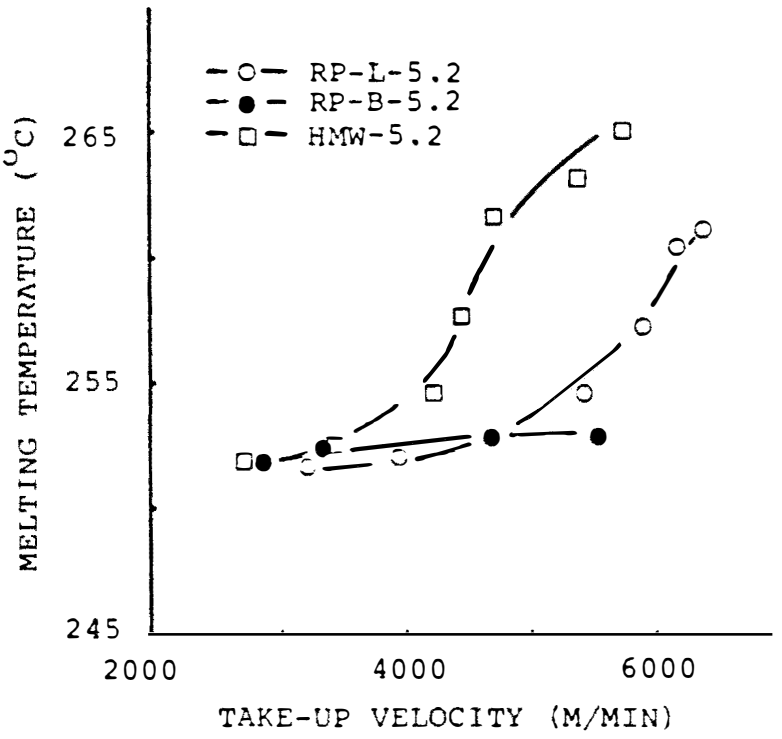

Figure 4.9. Melting temperature at the endothermal peak vs. take-up velocities.

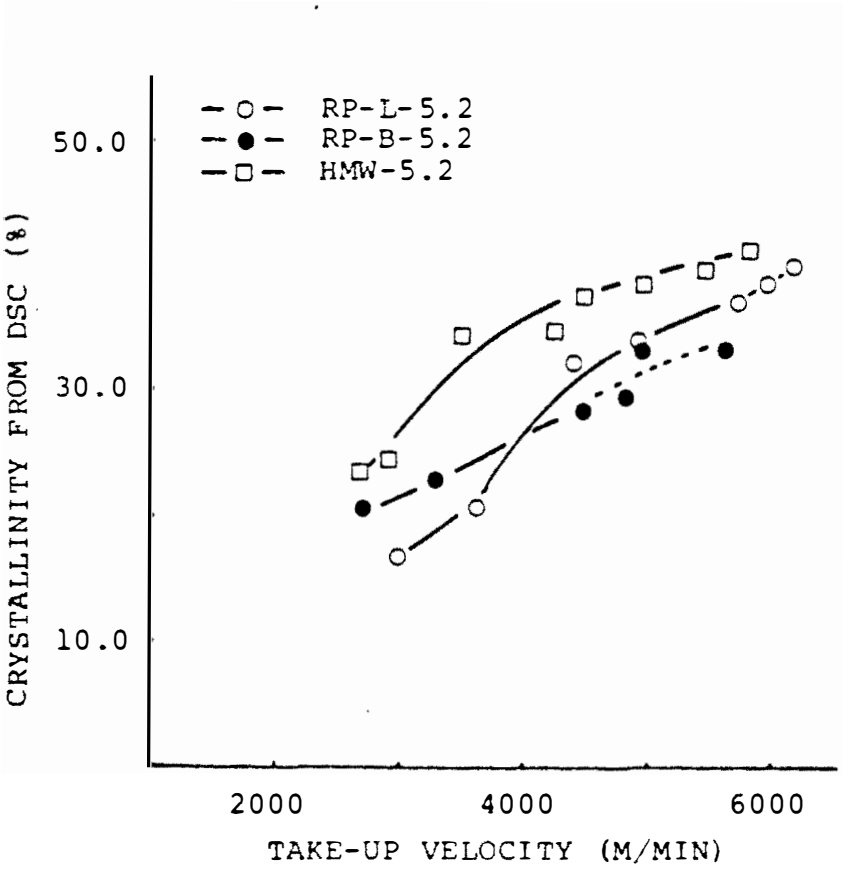

Figure 4.10. Crystallinity from DSC measurement vs. take-up velocities.

properties are directly related to yarn and fabric properties. Therefore, the inherent fiber structure arrangement is closely related to mechanical properties of textile fibers.

The tensile properties of high speed spun fibers were determined in a constant elongation rate Instron machine. The load-elongation curves are shown in Figures 4.11, 4.12, and 4.13.

Generall, the low take-up velocity fibers exhibited yield point and natural draw ratio in the load-elongation curves. Increasing the take-up velocity decreased the fiber elongation and natural draw ratio. The natural draw ratio was sensitive to the degree of preorientation (i.e. the molecular orientation in the polymer before any elongation). The high speed spun fibers did not exhibit natural draw ratio or yield point. In fact they showed behavior similar to drawn fibers. The fiber tenacity increased with take-up velocity (Figure 4.14).

The true tenacity (based on final diameter) did not change significantly as take-up velocity increased (Figure 4.15). The high molecular weight samples exhibited the highest tenacities and the branched samples exhibited the lowest tenacities.

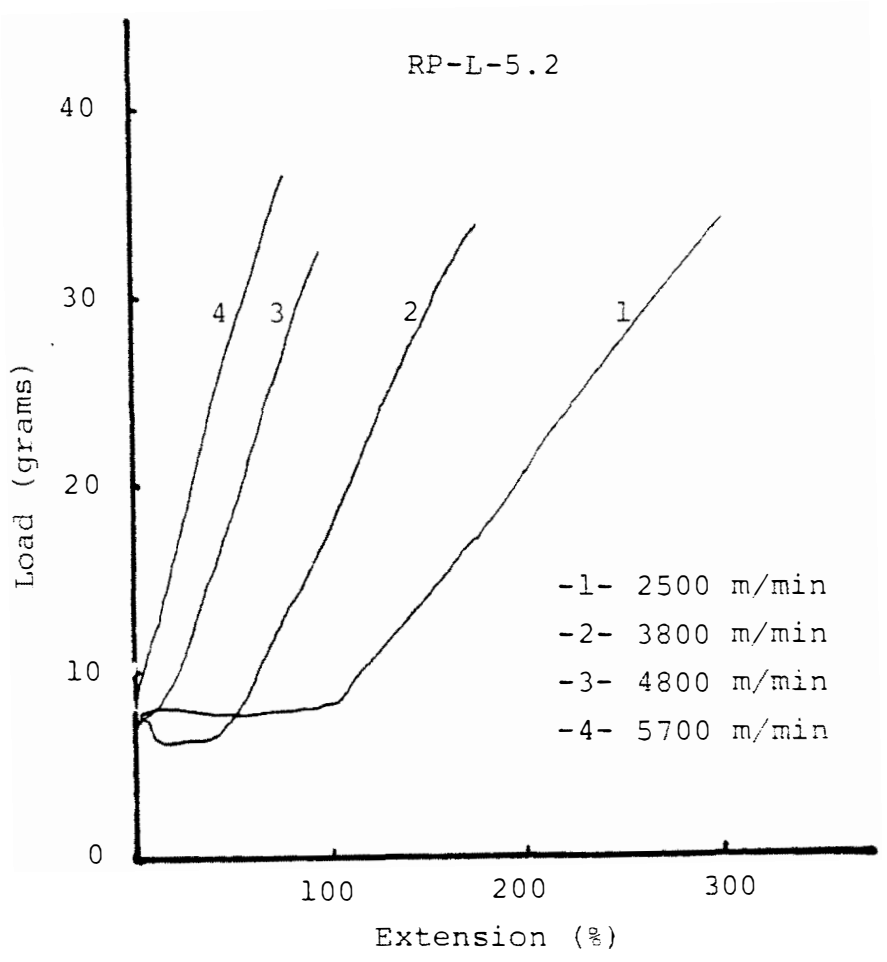

Figure 4.11. Load extension curves of linear PET fibers spun at different take-up velocities.

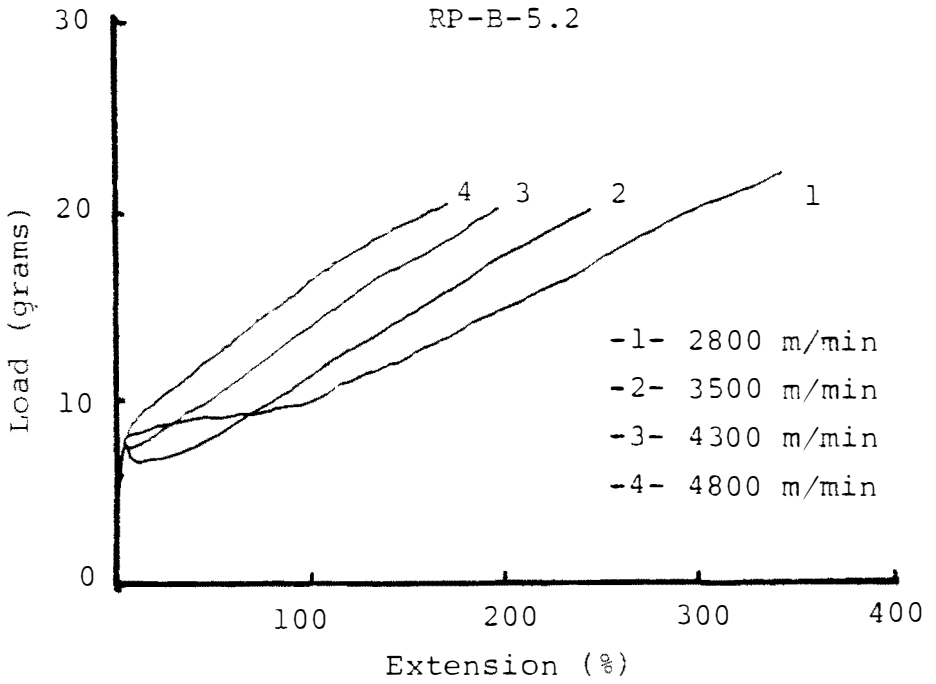

Figure 4.12. Load extension curves of branched PET fibers spun at different take-up velocities.

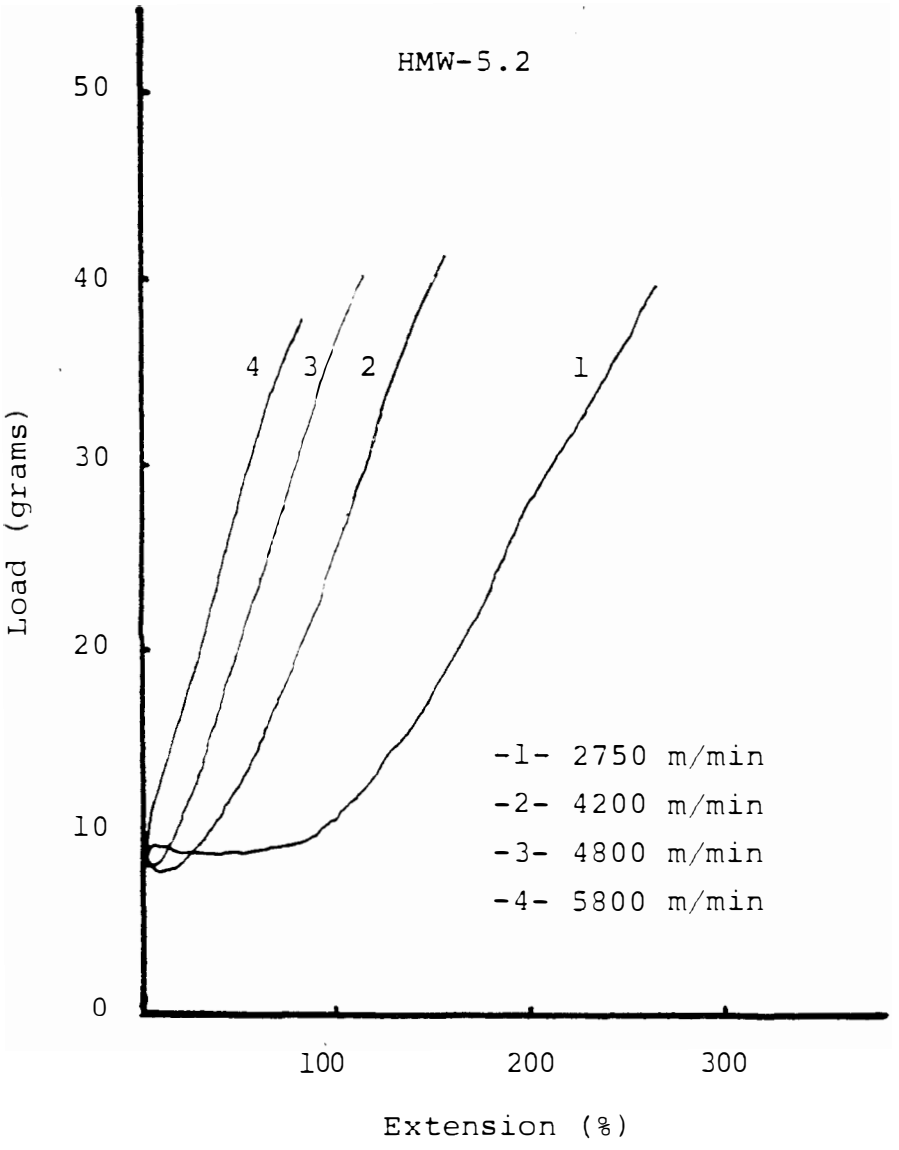

Figure 4.13. Load extension curves of high molecular weight fibers spun at different take-up velocities.

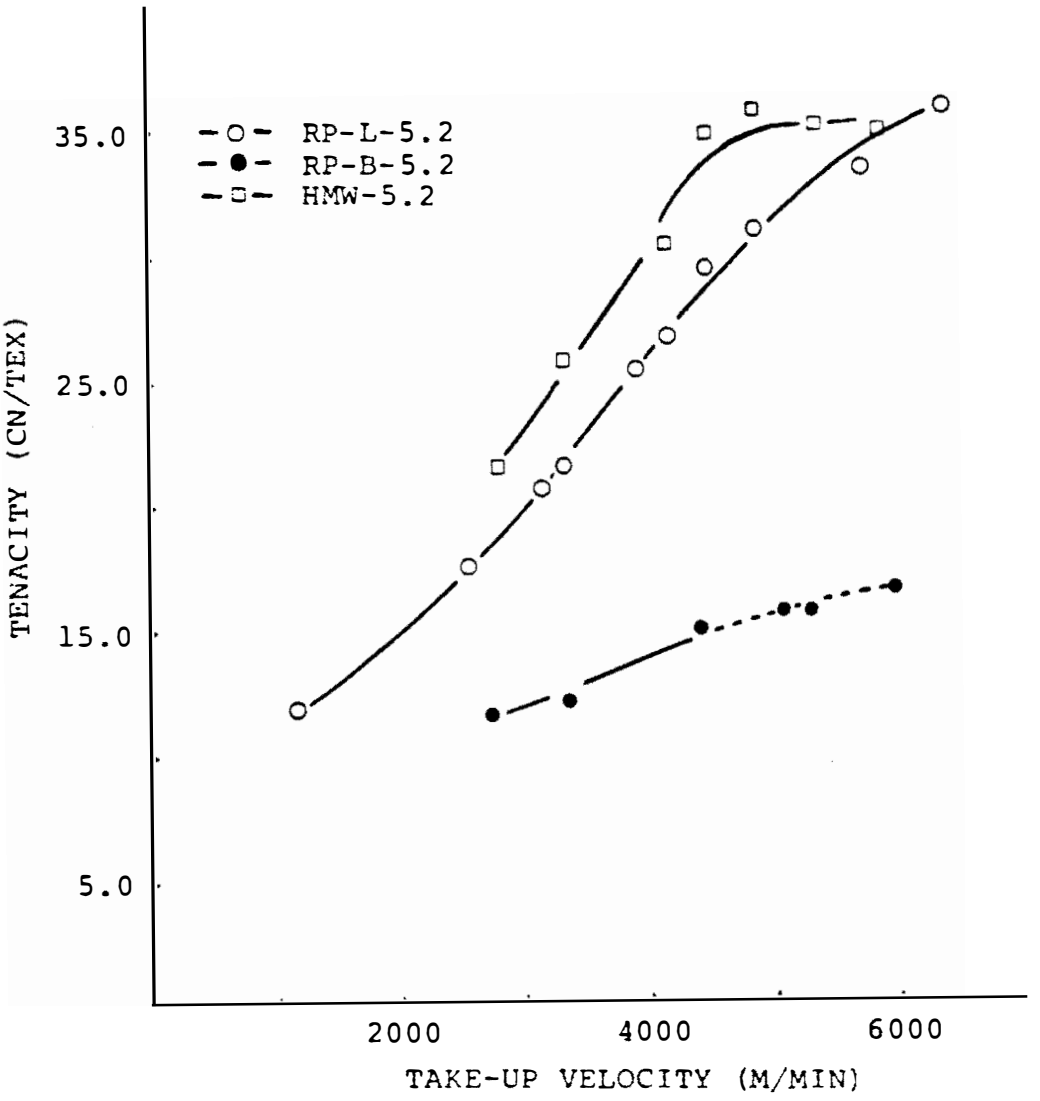

Figure 4.14. Tenacity of fibers at different take-up vleocities.

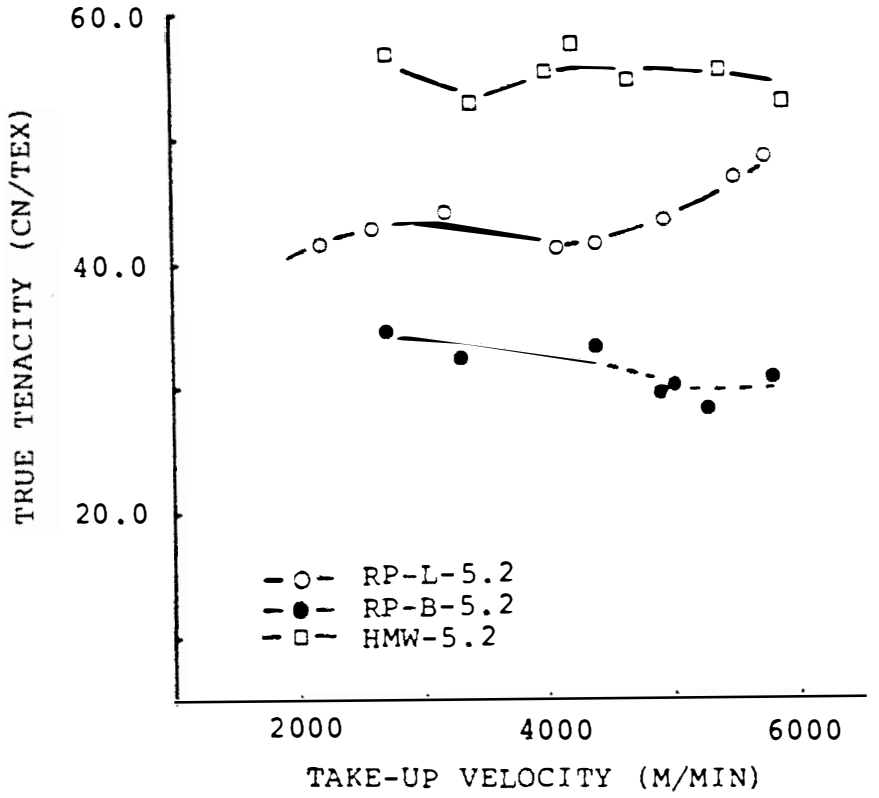

Figure 4.15. True tenacity of linear, branched, and high molecular weight fibers at different take-up velocities.

4.1.5. Shrinkage

Figure 4.16 shows the relationship between shrinkage in boiling water and take-up velocity. Below 3500 m/min, the fiber exhibited large shrinkages. Above 4500 m/min, the shrinkage decreased to less than 3%. Below the glass transition temperature, the oriented molecules are "frozen" in. When heated in the boiling water, the oriented molecules relaxed back to their original conformation. If the fiber had crystallized, the crystals would have prevented the oriented amorphous parts from relaxing back. Thus, at high speeds the shrinkage values were low. These results also indicate that the onset of crystallization was approximately 4500 m/min. Above 5000 m/min, heat stability increased. The lower throughput fibers resulted in higher shrinkages than high throughput fibers, probably because of the cooling effect. The fiber cooled faster and the crystallization process was not complete at lower throughput.

4.1.6 Scanning Electron Microscopy (SEM)

The morphology and structure of fibers are usually determined by a combination of microscopic observation and diffraction techniques. The high resolution of scanning electron microscopy can allow one to directly

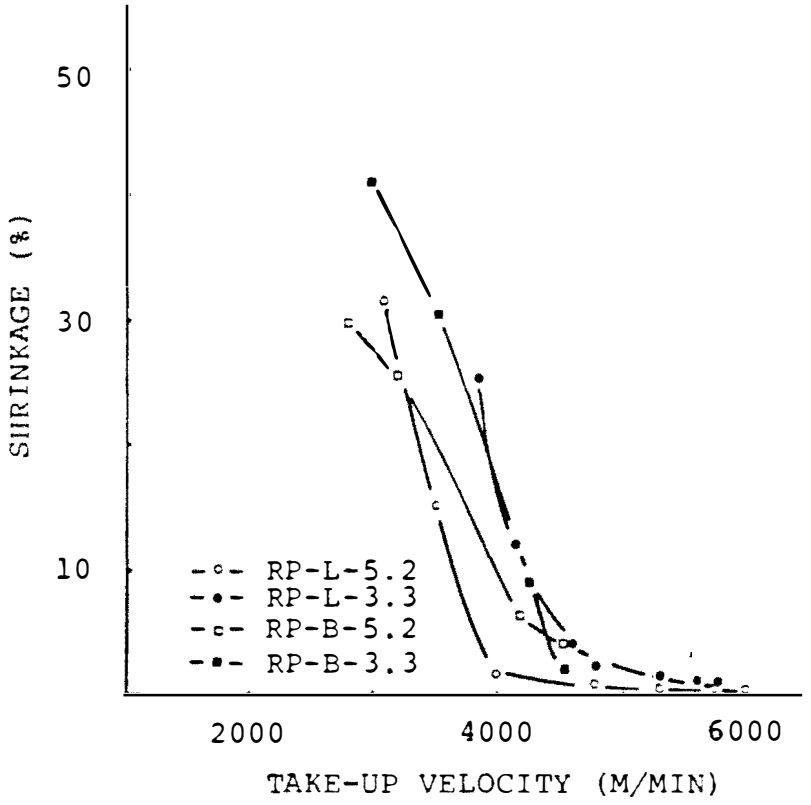

Figure 4.16. Relation between shrinkage and take-up velocities.

observe the surface characteristics of fibers as well as peeled fibers and fracture surfaces. The fibrillar superstructure can be observed in peeled fibers. The peeling operation consisted of cutting the fiber about half way through its diameter and then pulling this cut segment down along the fiber axis in order to display its interior structure.

Figure 4.17 shows a SEM photomicrograph of the surface of the peeled interior of a low speed spun fiber. It can be seen that such a fiber does not exhibit a fibrillar structure. A highly fibrillated structure was observed in high speed spun fiber (Figure 4.18). The SEM results suggest that the high speed spun fibers had highly fibrillated structures and the fibrils were parallel to the fiber axis.

4.1.7 Wide Angle X-Ray Scattering (WAXS)

From a macroscopic point of view, a crystallized material can be identified by WAXS examination. The degree of crystalline orientation can be qualitatively described from the diffraction arc shape on film diffraction patterns. The arc becomes sharp and short when the crystalline orientation is high.

From Figures 4.19 and 4.20, the WAXS patterns show a transition from an amorphous to a partially

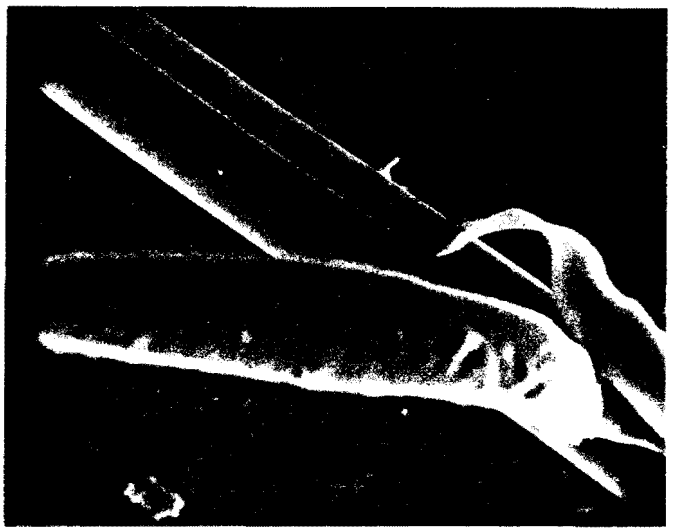

500X

TAKE-UP SPEED 2500 m/min

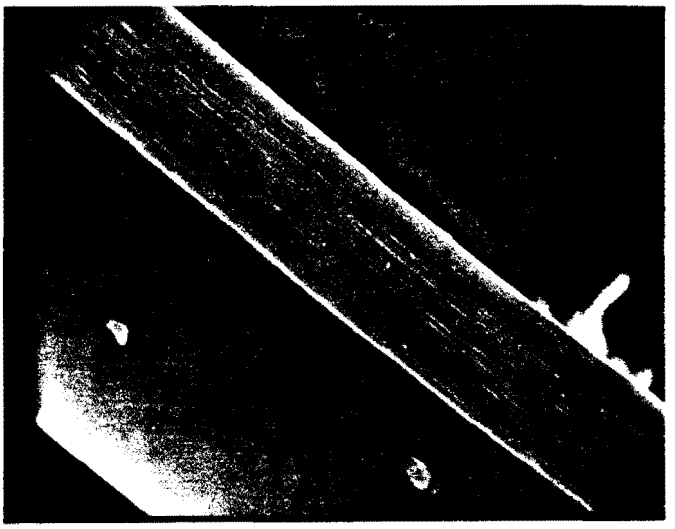

2000X

Figure 4.17. Photographs of peeled fiber from linear PET with a take-up velocity of 2500 m/min.

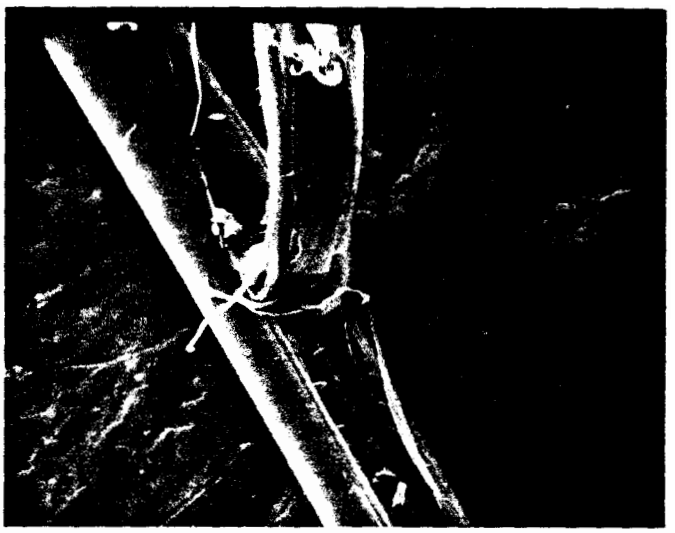

500X

TAKE-UP SPEED 5800 m/min

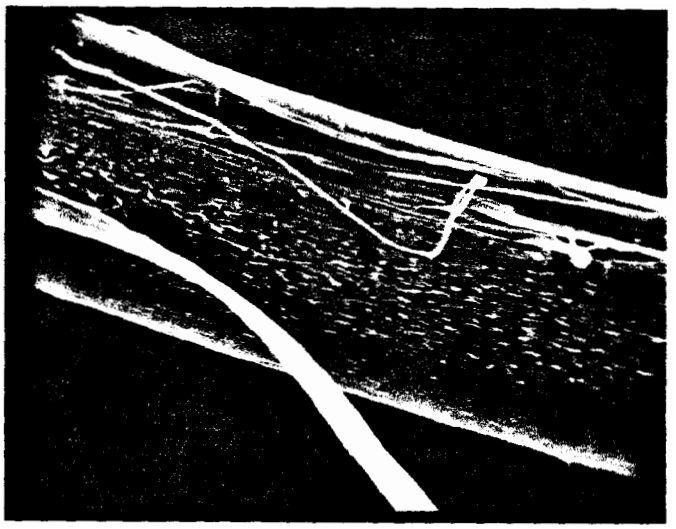

2000X

Figure 4.18. Photographs of peeled fiber from linear PET with a take-up velocity of 5800 m/min.

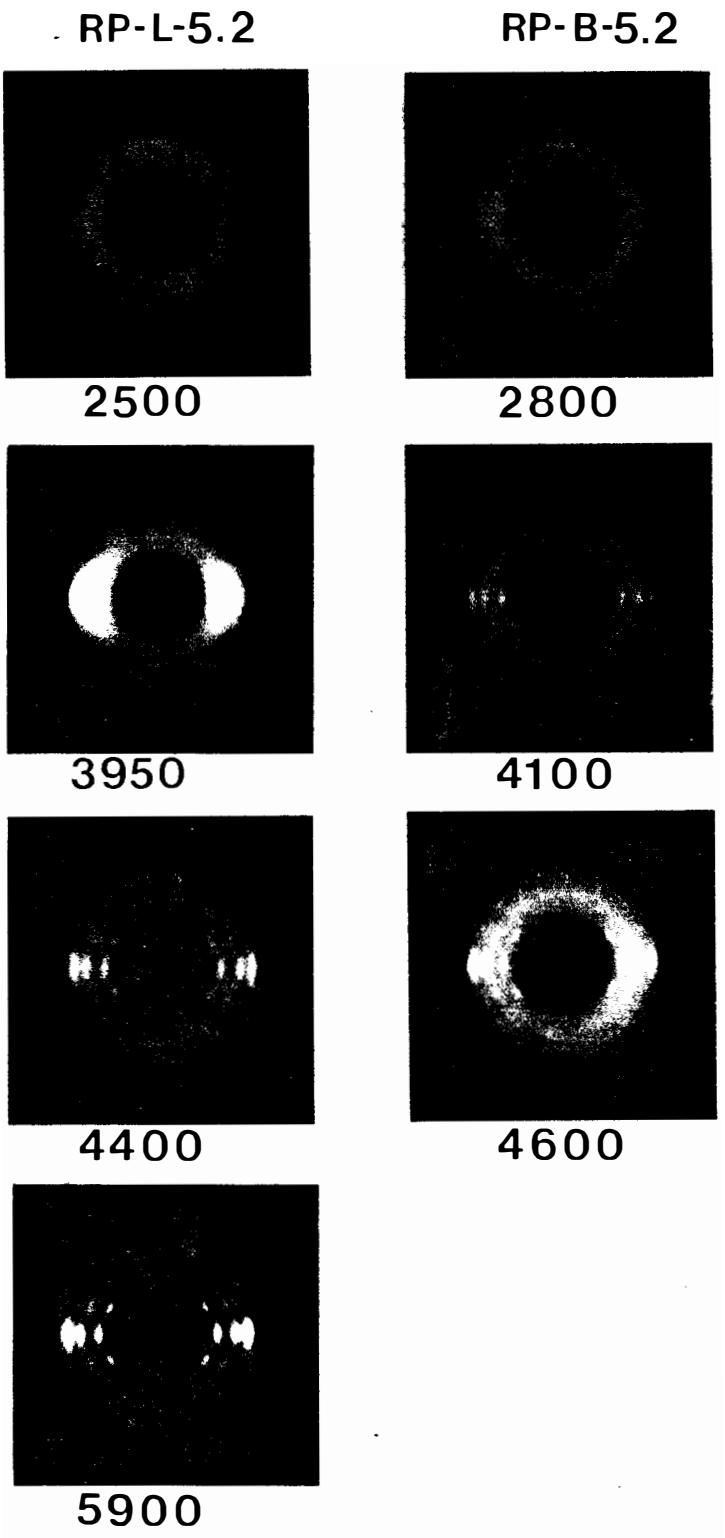

Figure 4.19. Wide angle x-ray scattering patterns of linear and branched PET at different take-up velocities.

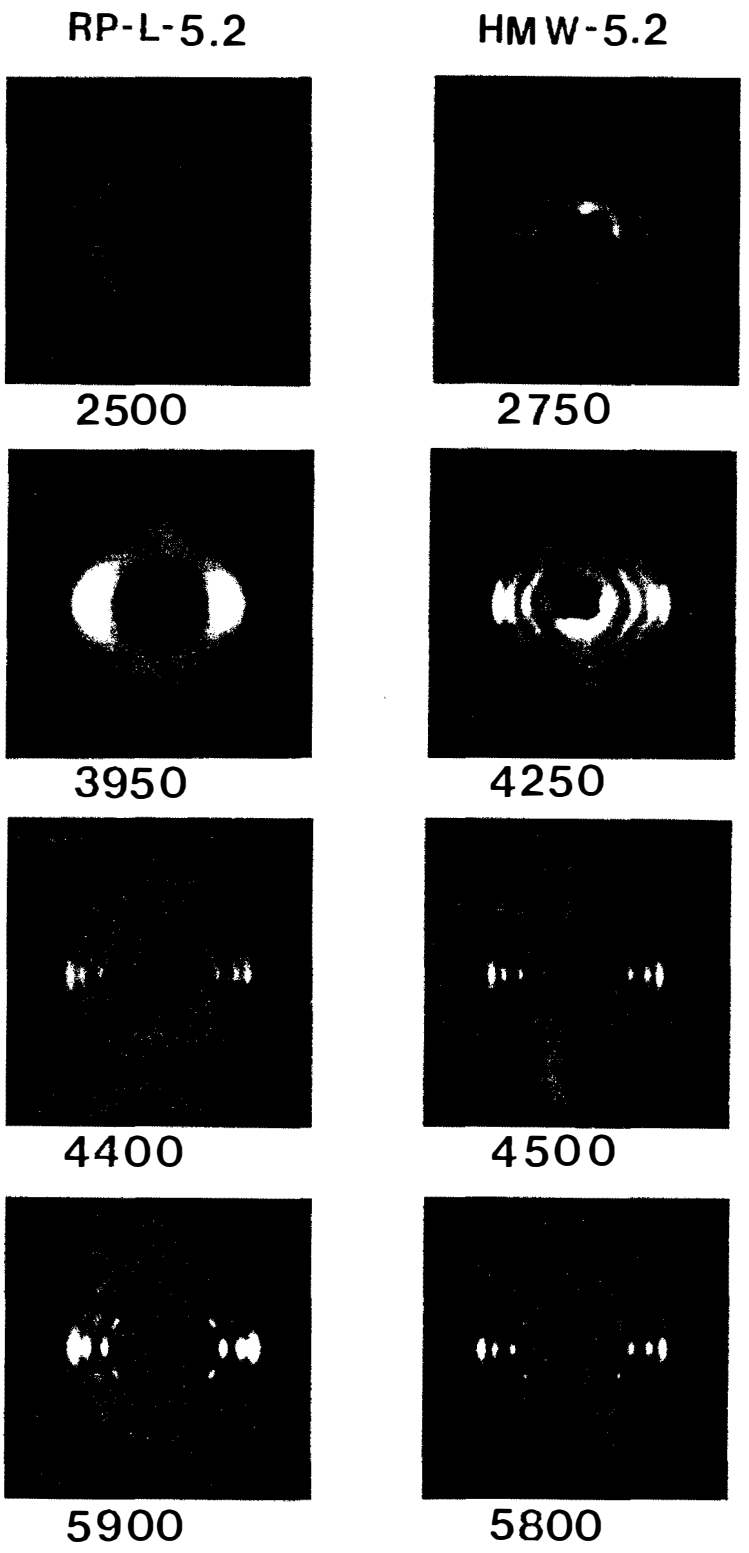

Figure 4.20. Wide angle x-ray scattering patterns of linear and high molecular weight PET at different take-up velocities.

crystalline fiber structure around 4000 m/min for the linear and branched PET. X-ray patterns for the high molecular weight fiber exhibited crystalline reflections at lower take-up velocities than for the other polymers. They exhibited highly oriented structures at high speeds.

Below 4000 m/min, linear and branched PET did not crystallize on the spinline. The observed crystalline diffraction at low take-up speeds for the high molecular weight PET was a result of the high stress levels, caused by the high viscosity, which produced some stress-induced crystallization at lower take-up speeds.

4.1.8 Orientation Factors

Quantitative determination of the crystalline orientation factors was obtained by measurement of the intensity of scattered radiation from several sets of crystalline planes. For PET fiber, the (100) and (010) planes were chosen (82). Amorphous orientation factors can be calculated from equation 3.2.

The chain axis (c-axis) crystalline orientation factor for PET fibers are plotted against take-up velocity in Figure 4.21. All three polymers exhibited high crystalline orientation factors at take-up velocities above 4500 m/min. The amorphous orientation

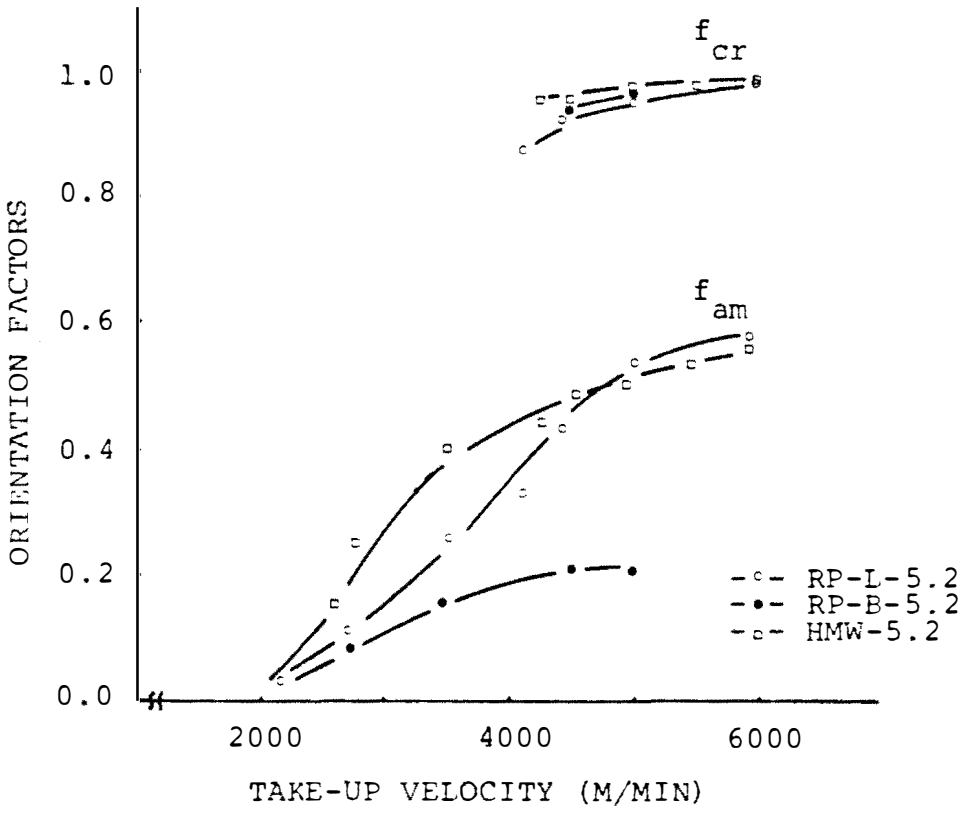

Figure 4.21. Crystalline orientation factor and amorphous orientation factors vs. take-up velocities.

factor increased with take-up velocity. The high molecular weight fibers exhibited high amorphous orientation factors at lower speeds and increased slowly with spinning speed. Branched PET exhibited the lowest amorphous factors.

The observed high crystalline orientation and somewhat lower amorphous orientation factors may be the result of high molecular orientation prior to crystallization. Abhiraman (2) reported the crystallites, which originated from highly oriented amorphous molecules, were highly oriented since orientation induced crystallization occurred on the spinline at high spinning speed. Thus, a high degree of crystalline orientation (fcr) would result even at low take-up velocity, but the amorphous orientation (fam) would be relatively low even at high take up velocities.

Most physical properties of fibers are strongly influenced by the orientation in the amorphous region or the average orientation. Compared with previous fiber tenacity results, increasing the orientation of molecules also increased fiber tenacity.

4.1.9 Relationship between Density, Birefringence, and Wide Angle X-Ray Scattering

From figure 4.22 which displays density, birefringence and combined WAXS film patterns, it was obvious that there was a linear relationship between density and birefringence in linear PET samples. At lower birefringences, an amorphous WAXS pattern was observed and the density increased slowly. But the slope of density and birefringence increased when birefringence exceeded 45 x 10^{-3}. Similar results were reported by Shimizu et al. (90,92). The WAXS patterns showed an oriented crystalline structure in this region. It is interesting that the density increased more rapidly with birefringence in the branched PET samples than in the linear PET samples (see Figure 4.23). The branched PET also showed an orientation induced crystallization when the birefringence exceeded 45 x 10^{-3}.

4.2 Cutting of Filament on the Spinline

4.2.1 Fiber Diameter and Birefringence Profile

The development of fiber structure along the spinline is an interesting subject among fiber researchers. Usually diameter and birefringence profiles can be determined by using a combination of

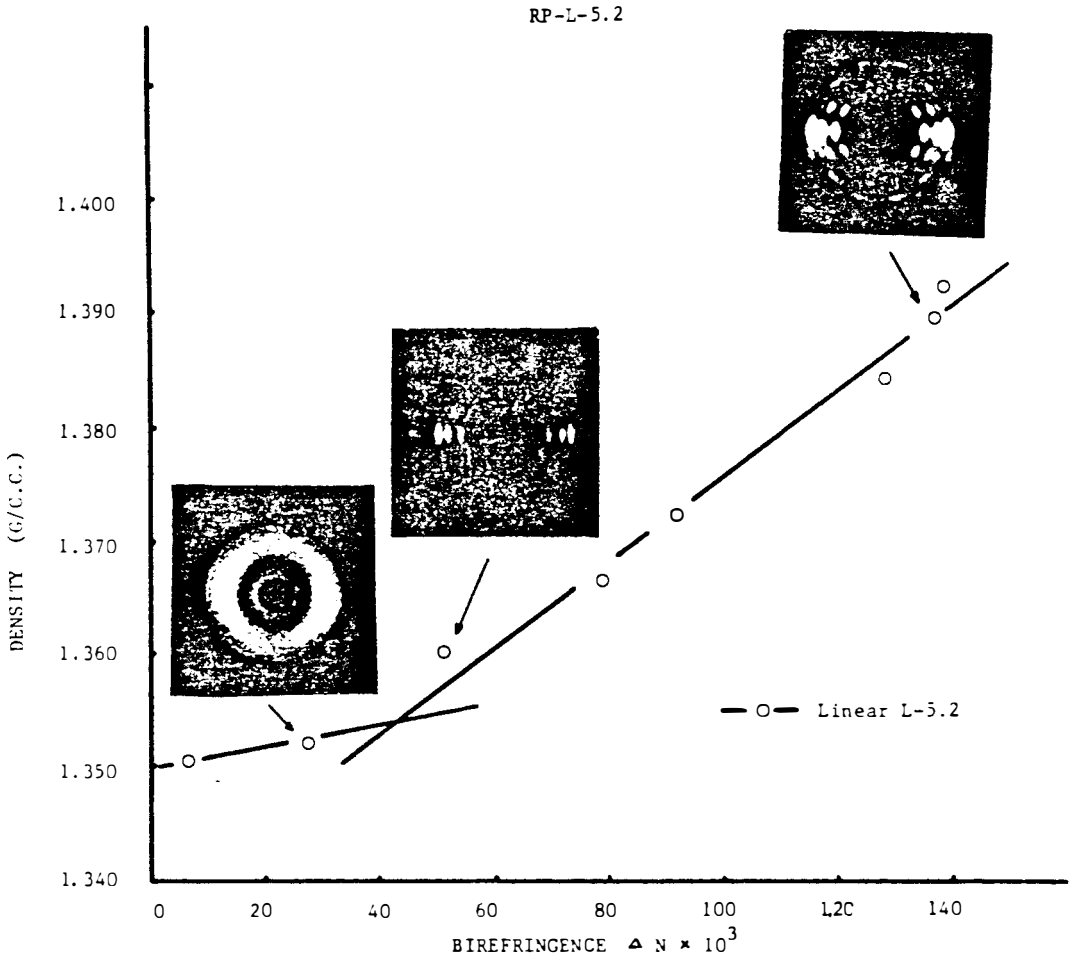

Figure 4.22. Relationship between birefringence, density, and wide angle x-ray patterns of linear PET.

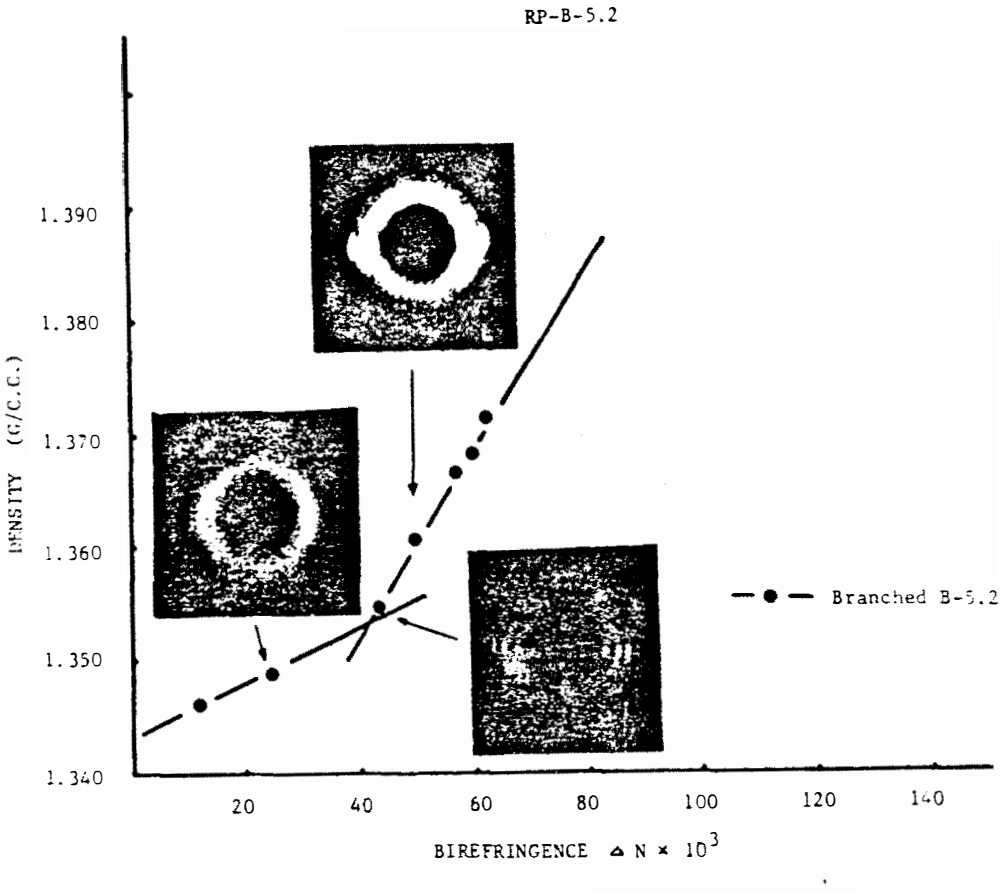

Figure 4.23. Relationship between birefringence, density, and wide angle x-ray patterns of branched PET.

photographic and microscopic techniques on rapidly quenched samples which are cut from the spinline (127).

A spinline cutting technique was developed in this research (see Chap. 3.4.3) to determine fiber diameter and birefringence profiles at different take-up velocities. Although there is an error introduced by the temperature change of the filament segments, the online cut samples can be accurately measured for filament diameter and birefringence profiles.

Figures 4.24 and 4.25 show the diameter and birefringence profiles of linear PET at different take-up velocities and throughputs. The diameter decreased in a non-linear manner when the filament was drawn down from the spinneret. At low take-up velocities, no sharp diameter thinning (necking) phenomena was observed on the spinline, and birefringence values on cut segments were very low. A necking phenomena occurred when the take-up velocity exceeded about 4600 m/min. The necking occurred between 100 to 150 cm below the spinneret depending on the take-up velocity and spinline length. With increasing take-up velocity and decreasing spinline length, the distance between neck and spinneret decreased (see Figure 4.26). The diameter of the filament after necking was almost the same as the diameter of the final fibers.

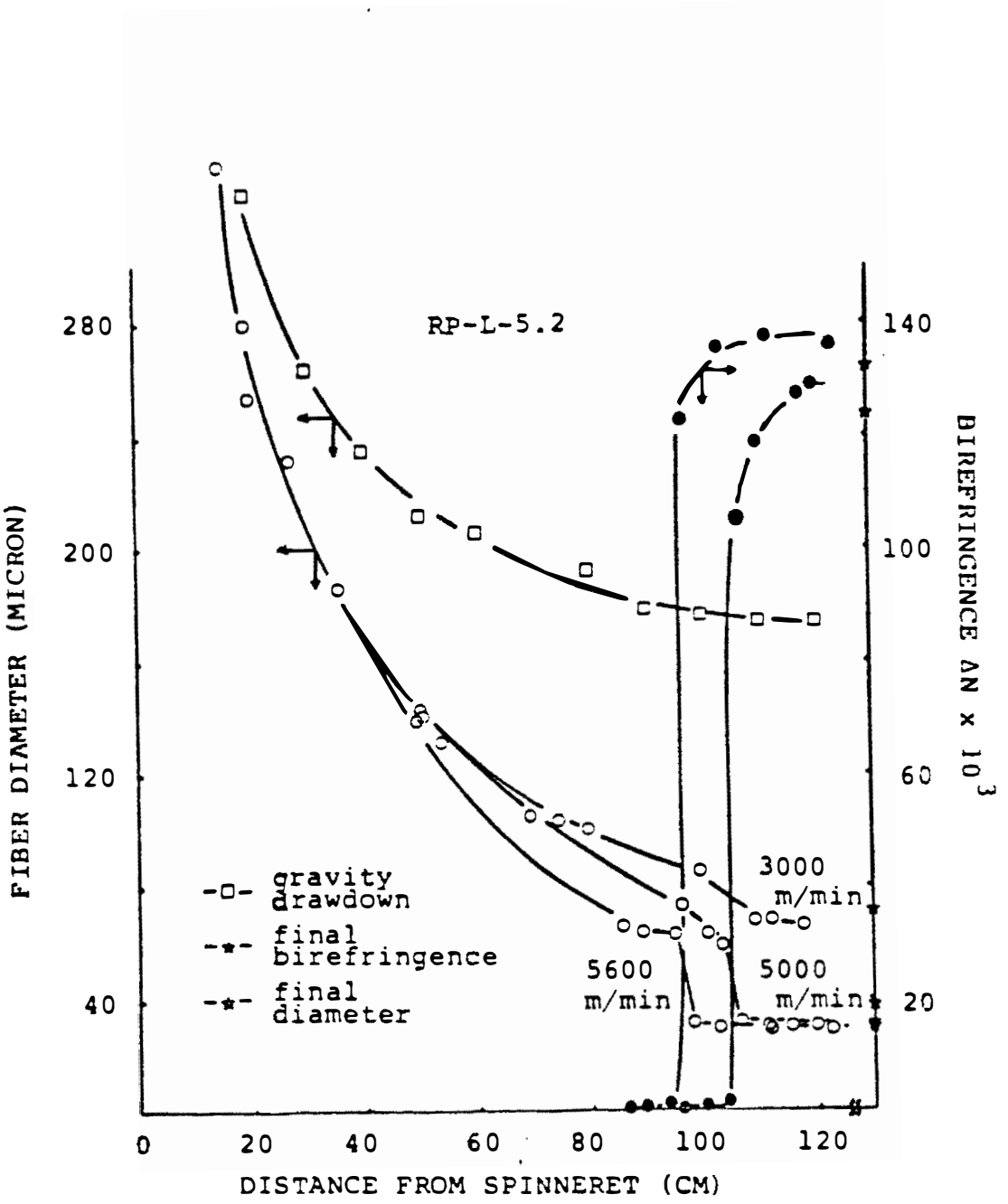

Figure 4.24. Diameter and birefringence profile along tne spinline for linear PET (cut sample with a mass throughput of 5.2 g/min).

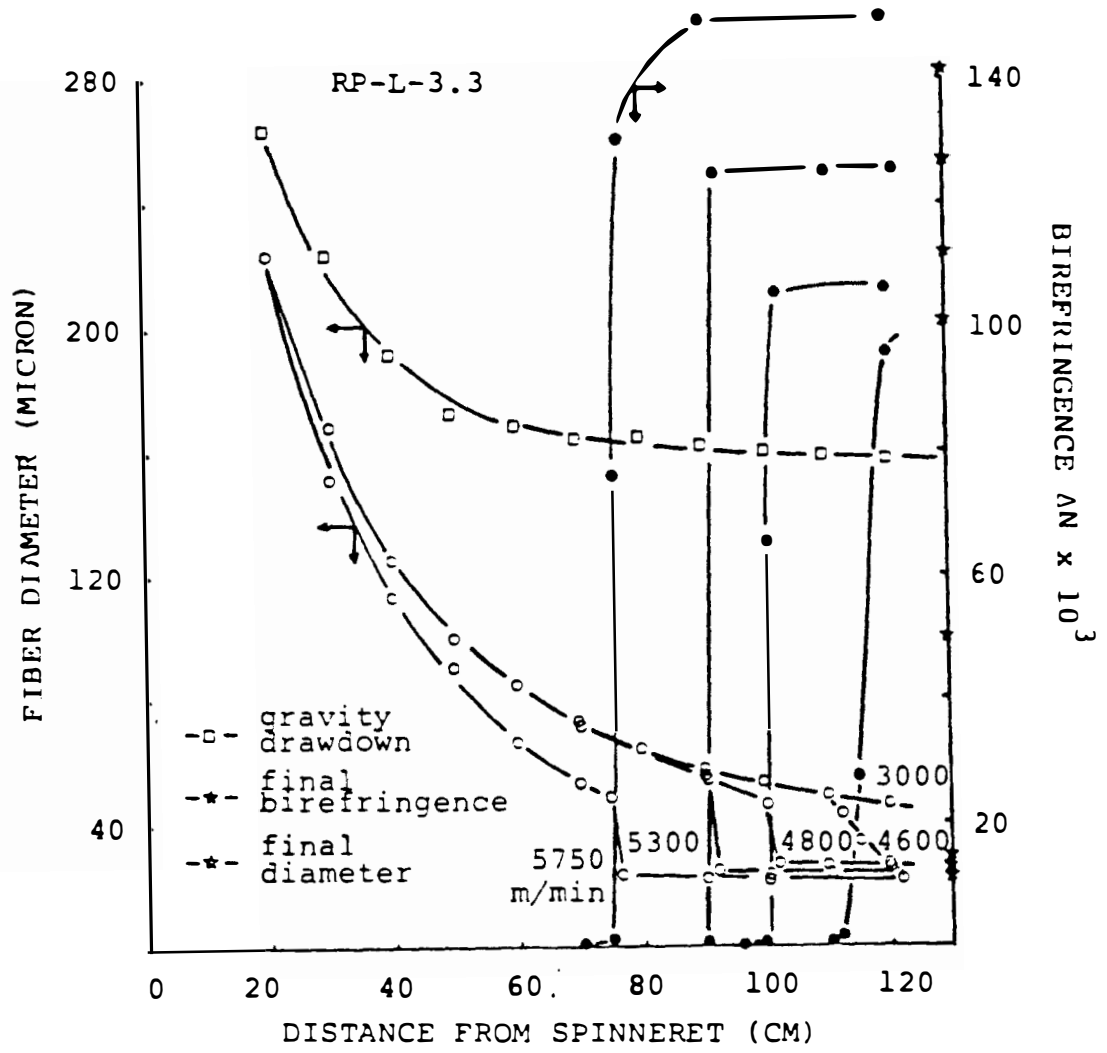

Figure 4.25. Diameter and birefringence profile along the spinline for linear PET (cut sample with a mass throughput of 3.3 g/min).

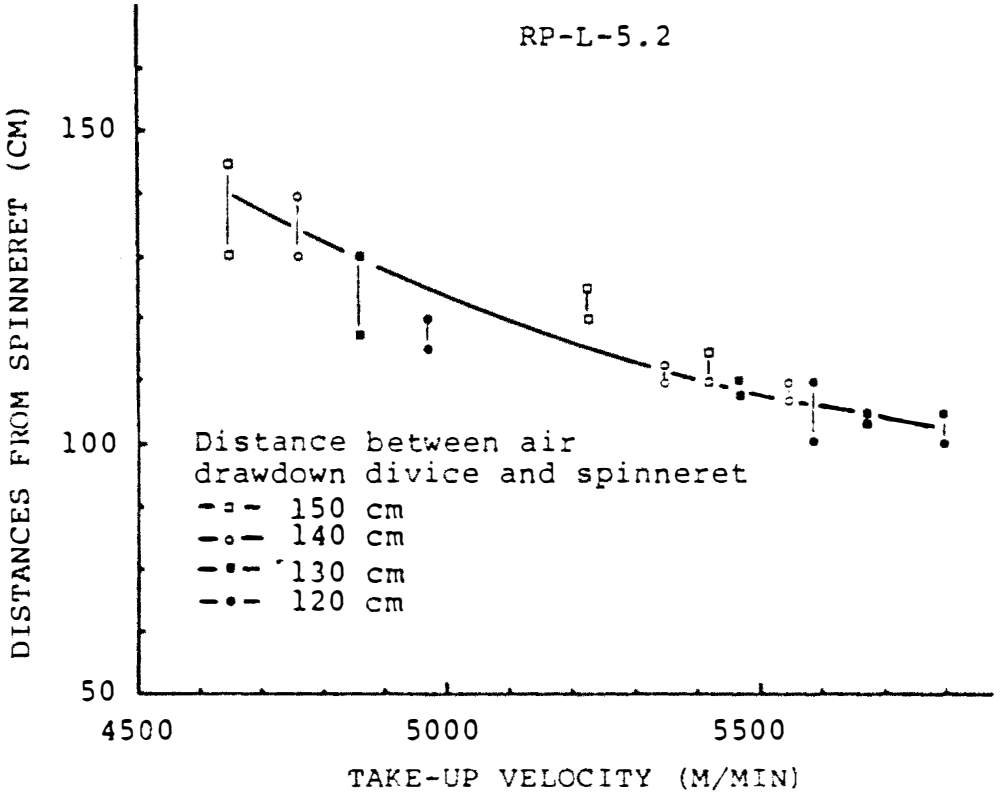

Figure 4.26. Distance of necking position from the spinneret vs. take-up velocities.

The birefringence measurements made from the cut segments at high take-up velocity fibers showed very low values before necking and sudden increase in birefringence after necking. The birefringence almost reached the final birefringence of high speed spun fibers after necking. Decreasing the mass throughput, moved the necking position toward the spinneret. Increasing take-up velocities and decreasing mass throughput resulted in an increase of spinning stress in the threadline. This caused necking to occur closer to the spinneret.

A comparison between linear and branched PET showed that for the branched PET samples, the birefringence increased with take-up velocity, but the branched sample increased more slowly than the linear one (see Figure 4.27 and 4.28). The necking phenomena was not clearly observed in branched cut samples.

High molecular weight PET also exhibited the necking phenonema on cut samples at high take-up speeds. The distance of the neck from the spinneret was shorter than the linear PET sample at the same take-up velocity. The diameter and birefringence after necking was almost the same as the final spun fibers (see Figure 4.29 and 4.30). The lower throughput had higher spinline stress

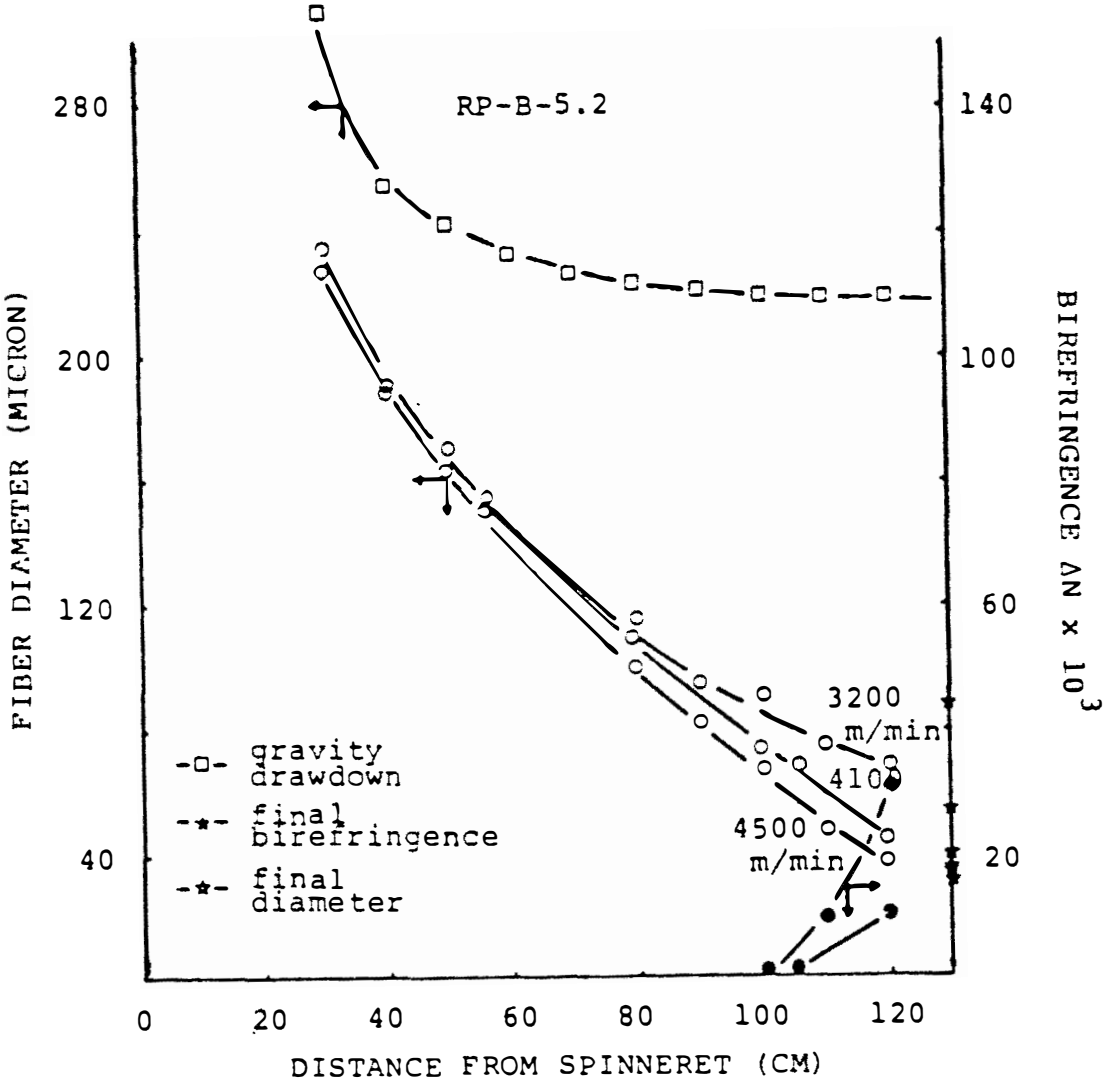

Figure 4.27. Diameter and birefringence profile along the spinline for branched PET (cut sample with a mass throughput of 5.2 g/min).

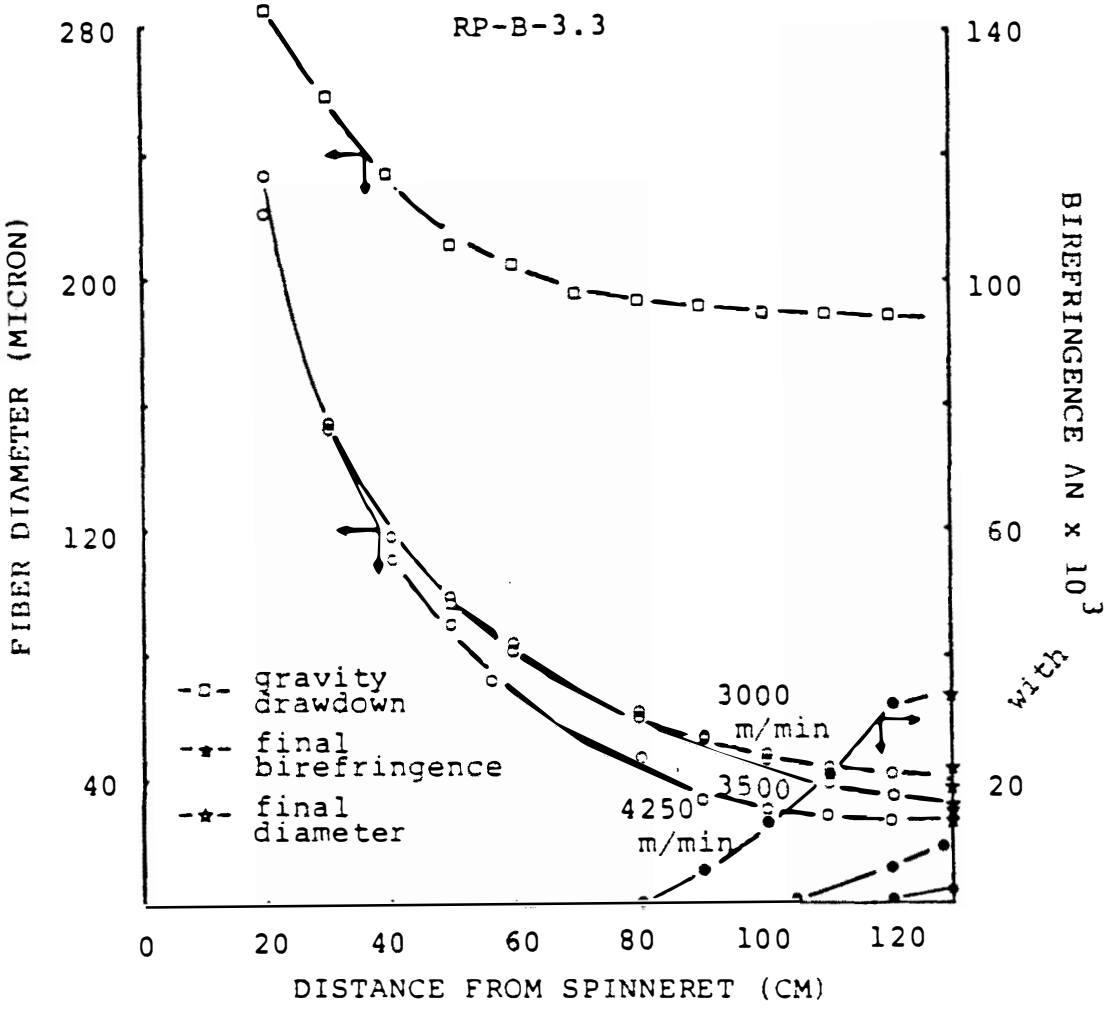

Figure 4.28. Diameter and birefringence profile along the spinline for branched PET (cut sample with a mass throughput of 3.3 g/min).

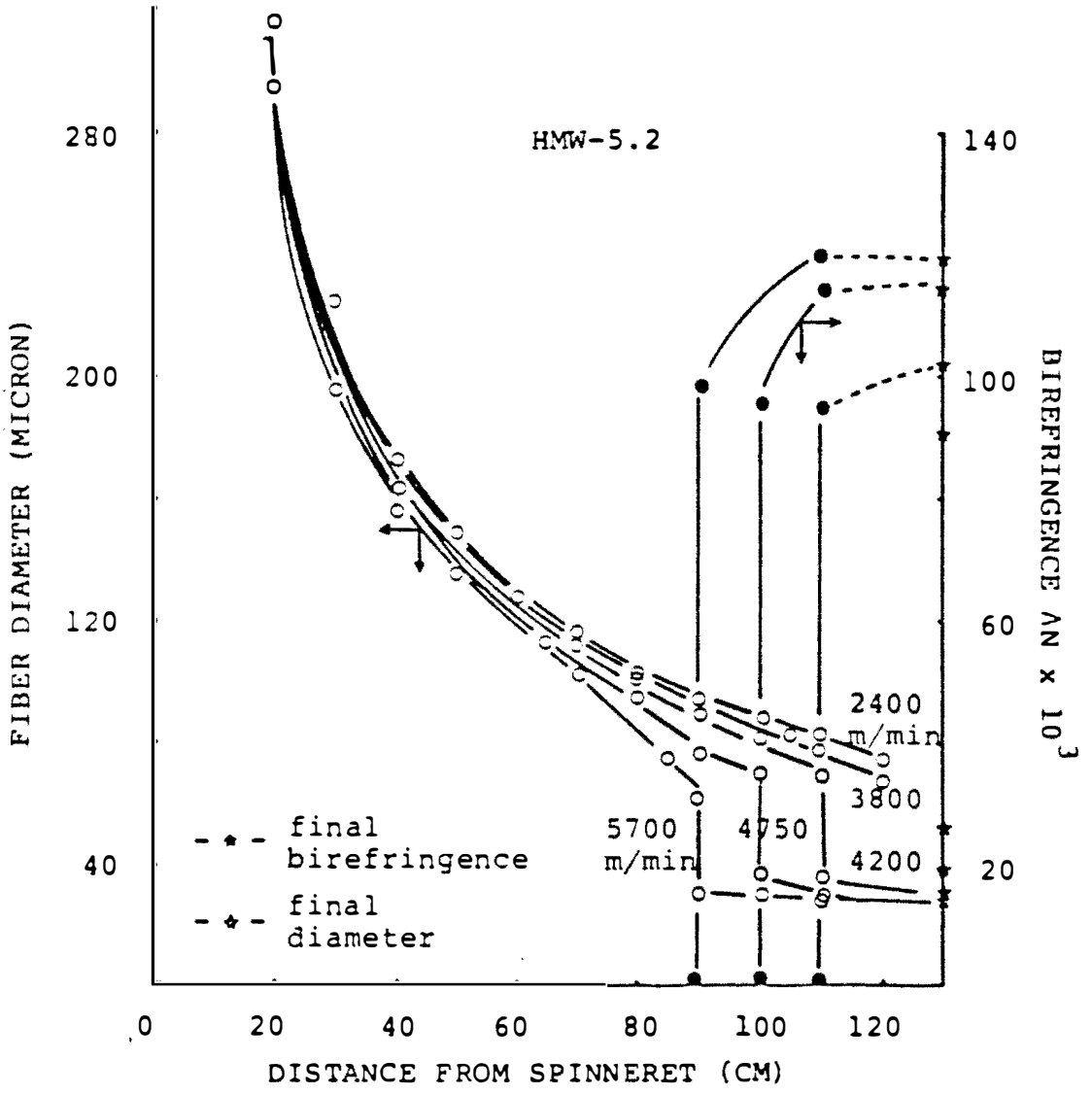

Figure 4.29. Diameter and birefringence profile along the spinline for high molecular weight PET (cut sample with a mass throughput of 5.2 g/min).

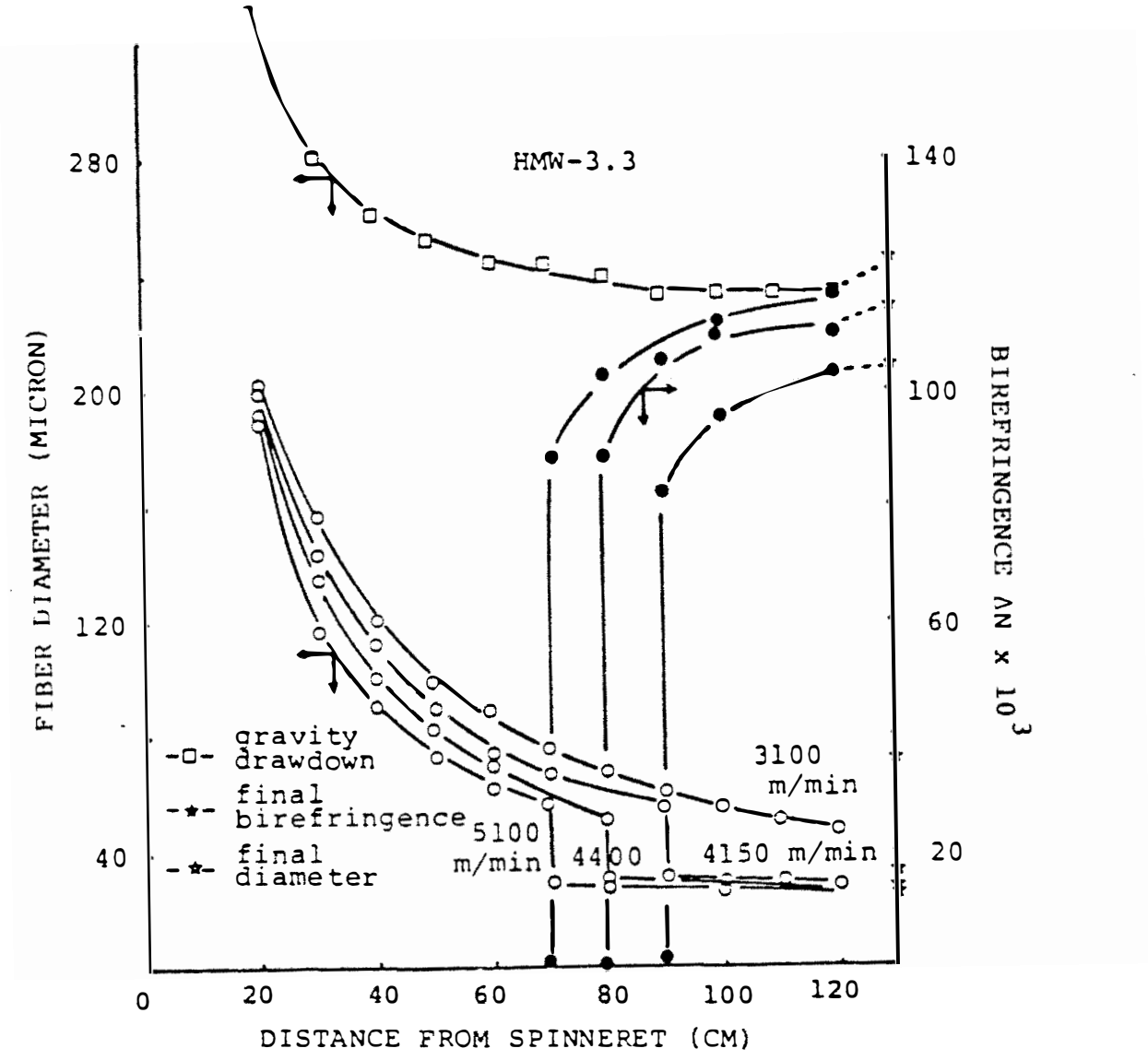

Figure 4.30. Diameter and birefringence profile along the spinline for high molecular weight PET (cut sample with a mass throughput of 3.3 g/min).

and the necking moved to near 70 cm below the spinneret at 5100 m/min take-up velocity. The necking phenomena was observed at 90 cm below the spinneret for 4150 m/min take-up velocity of high molecular weight sample while it was observed at 100 cm below spinneret for 4800 m/min take-up velocity of linear sample at the same mass throughput. This is because of higher spinline stress was built up in the high molecular weight thread line.

4.2.2 Necking On The Cut Sample

When solid polymers are stretched at room temperature, they behave differently. Rubbers can be extended uniformly to several times their original lengths before breaking. Brittle polymers, for example polystyrene and polymethyl methacrylate, also extended uniformly for a few percent of their original lengths before breaking. Ductile polymers, such as polyethylene or polypropylene, can be extended uniformly for a few percent of their original length, but instead of breaking, they form a neck at the weakest point of the specimen. Either due to the decrease in cross sectional area or stress concentration, the neck may get steadily thinner until breaking, or it may stabilize at some point and then the shoulders travel along the length of the specimen. When necking occurs, localized temperature

increase is generated at the neck portion which causes softening of the shoulders resulting in molecular rearrangements in the stress direction (105).

The necking phenomena was also observed in PET filaments in the drawing process. Tompson (103) explained the relationship of drawing tension, temperature, and draw ratio. Generally diameter thinning was observed when PET filaments were drawn at low draw ratios and low tensions. When increasing draw ratios under high tension, a sharp diameter thinning (necking) was observed. This sharp diameter thinning depends on temperature, draw ratio, and tension (stress).

In the melt spinning process, fiber temperature decreased and molecular oreintation, gradually increased as the fiber diameter gradually decreased along the spinline. When the take-up velocity exceeded a certain value, necking was observed on the spinline. Whether necking occurred before or after orientation-induced crystallization is a very interesting question.

Perez et al. (82) reported that when PET (I.V. = 0.66) was spun at a speed of 5400 m/min, there existed a necking zone at a distance of 100 cm from the spinneret in which most of the drawing occurred. A strain rate of 2×10 (sec^{-1}), average temperature of 105 ^{o}C, and a

cooling rate of 26000 ^{o}C/sec coincided with a sudden increase in birefringence. They assumed that the major part of the orientation and crystallization originated in this zone. They examined the fiber structure of the neck and concluded that before necking, the fiber exhibited an amorphous structure and a crystalline structure was observed after necking. They also examined the structure of final spun fiber and proposed that crystallization was induced by orientation when the take-up velocity exceeded 3500 m/min.

Shimizu (97) reported that necking occurred when spinning speeds exceeded 4000 m/min and after necking, the fiber diameter did not change and was equal to its final diameter. He also found that the necking starting position moved closer to the spinneret when the take-up speed increased.

In Matsui's (76) study of the PET fiber formation process in high speed spinning, he observed a sudden diameter change (necking) on the spinline. He reported a rapid crystallization by orientation occurring when fiber birefringence reached 20 x 10^{-3} to 30 x 10^{-3} and heat was generated by crystallization in this region.

Kikutani (66) also reported that a necking phenomena was observed for PET fiber when take-up velocities exceeded 5000 m/min. He reported that the

polymer melt viscosity increased when crystallization occurred.

From the above reports it was understood that rapid diameter thinning (necking) on the spinline is an unusual behavior of PET polymer under high speed spinning. An amorphous structure was observed before necking and a crystalline structure was observed after necking. The diameter and structure of fiber after necking was almost the same as the final spun fiber.

Figure 4.31 and 4.32 show the neck of a linear PET sample at a take-up velocity of 5600 m/min. Figure 4.33 shows the diameter and birefringence profile of the necking zone of linear PET with a mass throughput of 5.2 g/min and a take-up velocity of 5600 m/min. Figure 4.34 shows the diameter and birefringence profile of linear PET with a mass throughput of 3.3 g/min and a take-up velocity of 5750 m/min. From these data, it is seen that once the necking started, both the diameter and the birefringence were almost fully developed within a few millimeters of the neck. The fiber diameter remained almost constant and birefringence almost reached the final spun fiber birefringence after necking.

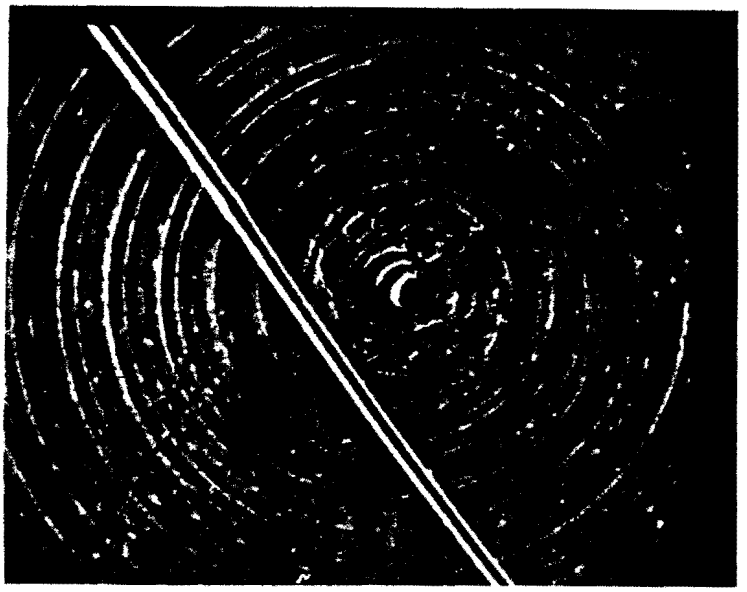

50 X

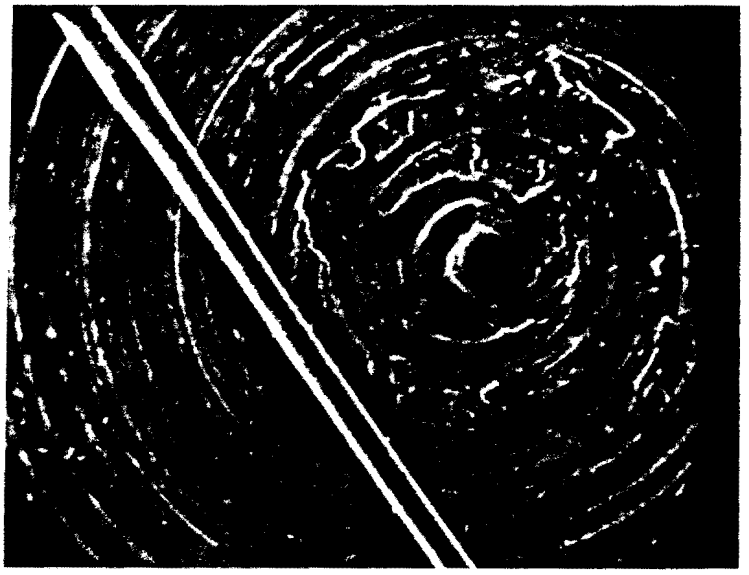

100 X

Figure 4.31. A neck of linear PET cut sample at take-up velocity of 5600 m/min under scanning electron microscope observation.

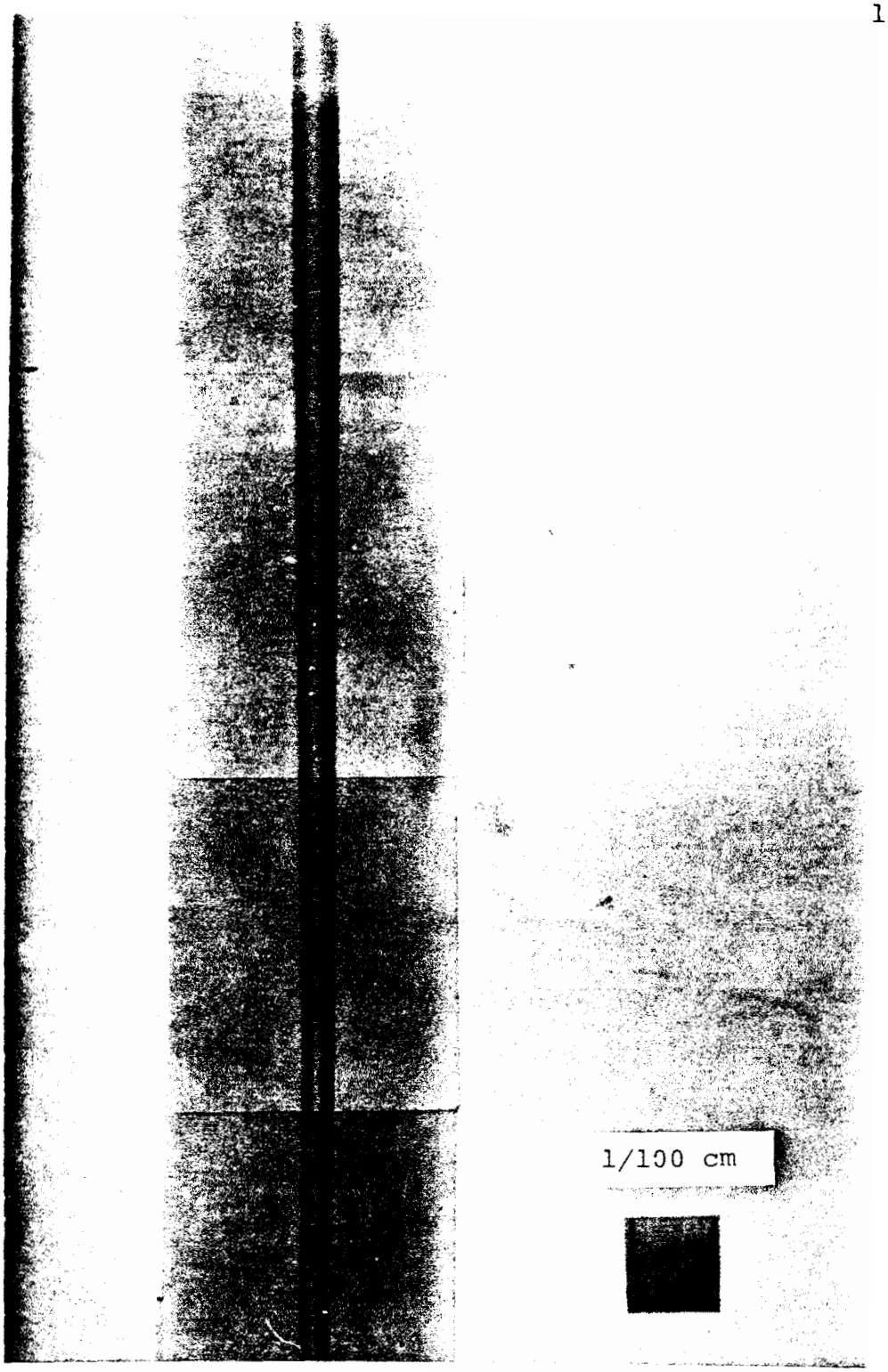

Figure 4.32. A neck of linear PET cut sample at take-up velocity of 5600 m/min under optical microscope observation.

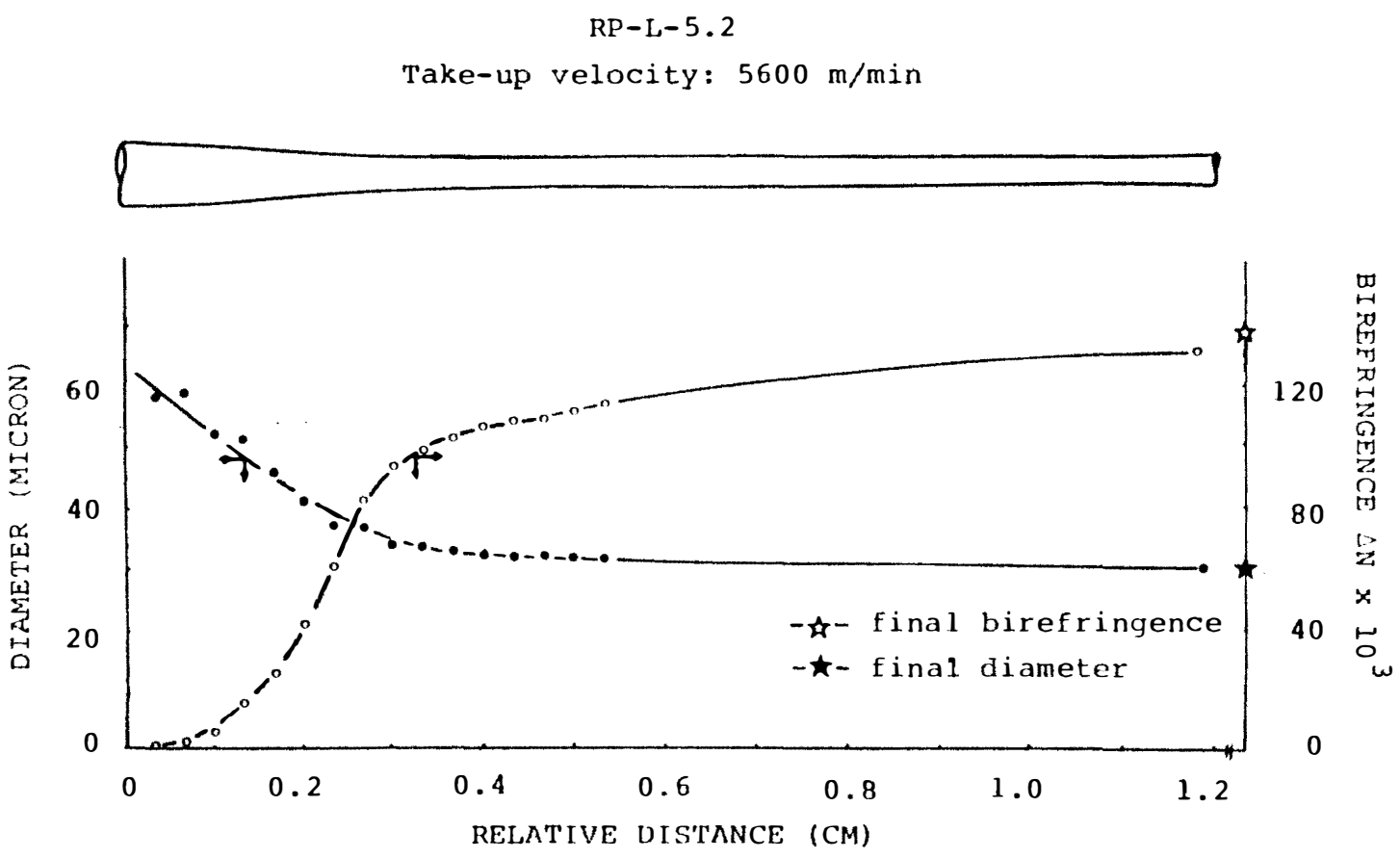

Figure 4.33. Diameter and birefringence profile of a linear PET neck sample at take-up velocity of 5600 m/min and mass throughput of 5.2 g/min.

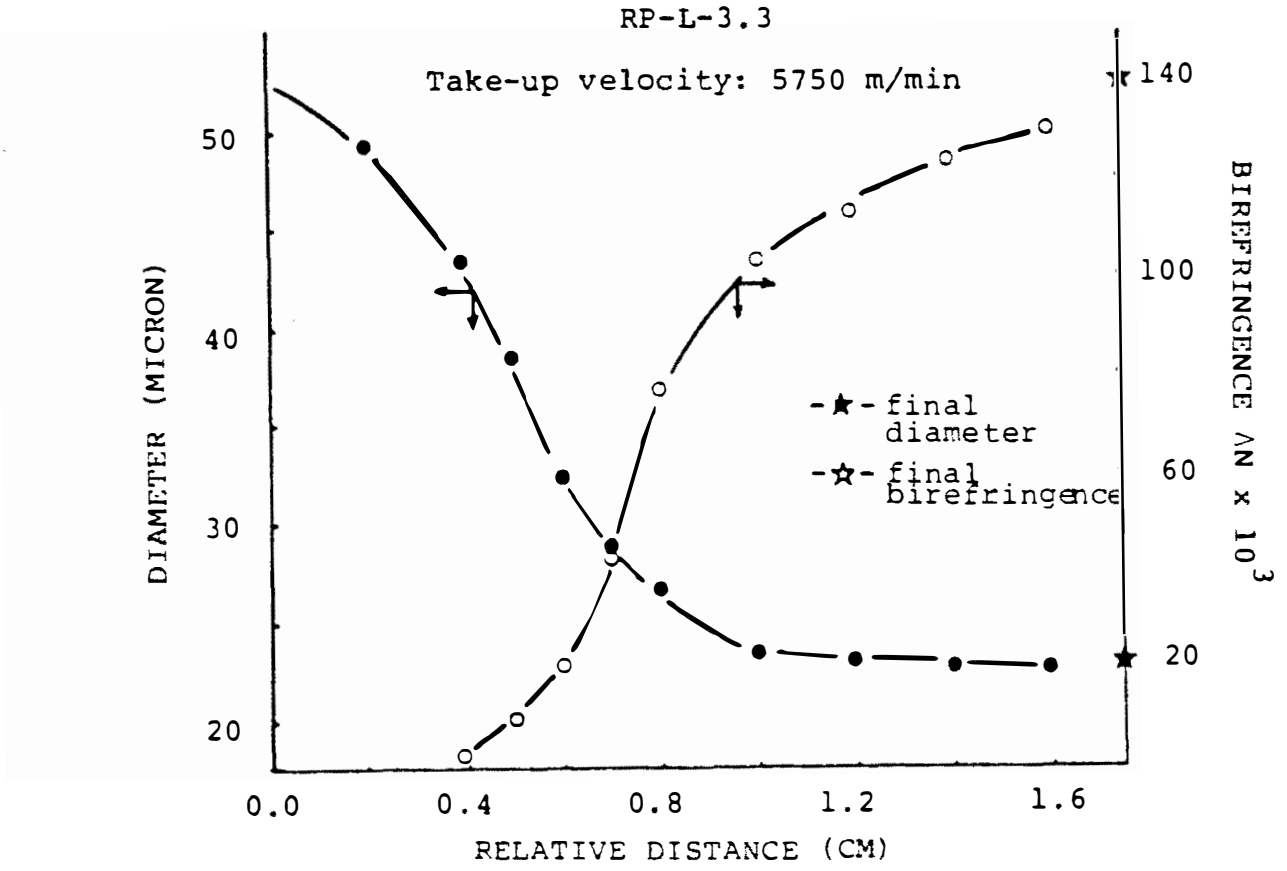

Figure 4.34. Diameter and birefringence profile of a linear PET neck sample at take-up velocity of 5750 m/min and mass throughput of 3.3 g/min.

4.2.3 Wide Angle X-Ray Diffraction of Neck Bundle

In the PET high speed spinning process, necking is an interesting phenomena on the spinline. To further understand the structure change in the neck region, a wide angle x-ray technique was used in this research.

A bundle of sixteen linear PET filaments spun at 5000 m/min was placed in a WAXS sample holder (Figure 4.35 and Table 4.1). The filaments in this bundle were placed parallel to each other with the necks as near to each other as possible. The relative positions of the necks is shown in Table 4.1. By employing WAXS 2θ scanning from 14 to 30 degrees, an amorphous structure was observed above the neck (Figure 4.36). Within the deformation region, there was no detectable crystalline diffraction, but a few millimeters below the neck crystalline diffraction peaks were clearly detected (Figures 4.37 to 4.40). This evidence supports an orientation induced crystallization process in or after the neck region.

4.3 On-line Measurement

4.3.1 Temperature Profile Along the Spinline

The elongational viscosity of a polymer melt is strongly dependent on the temperature. The spinline temperature profile thus became an important subject for

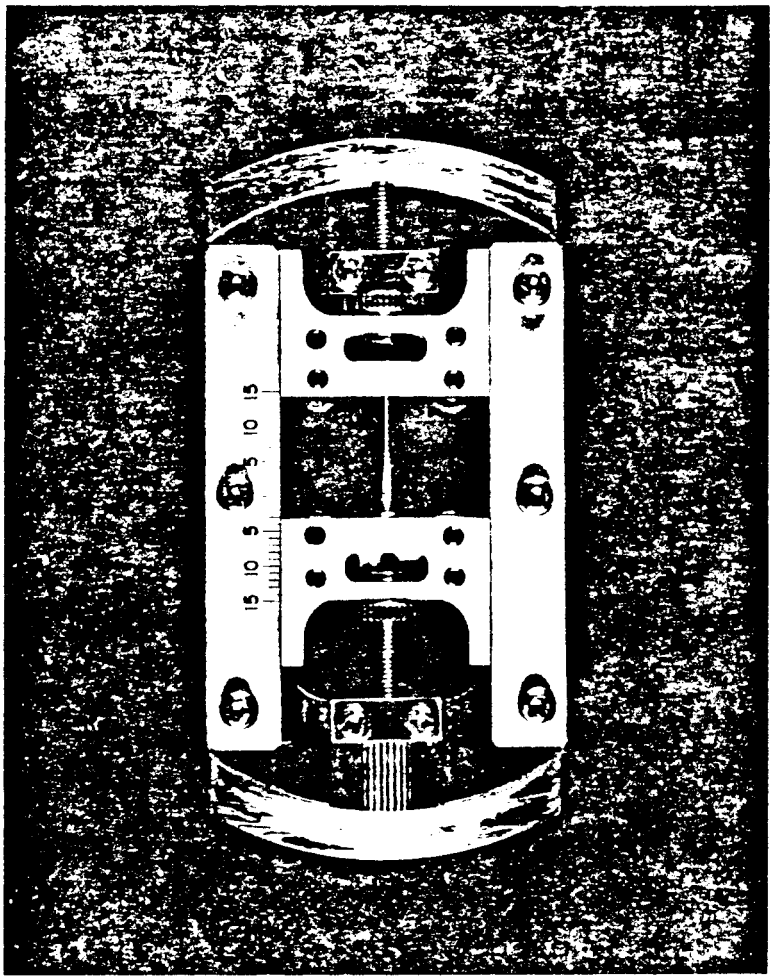

Figure 4.35. A bundle of filaments with neck placed in a sample holder for wide angle x-ray scattering.

Table 1. Relative Position of Neck Samples in the Bundle

Position* (mm)	Diameter (big)	Diameter (small)*
1.29	16	0
3.75	16	0
5.29	11	5
6.29	4	12
7.29	3	13
8.29	0	16

Position*: Relative position of neck samples.

(big)* : Numbers of fiber with big diameter (before necking).

(small)* : Numbers of fiber with small diameter (after necking).

Table 2. Diameter and Birefringence of One Neck Sample in the Bundle

Position* (mm)	Diameter (micron)	Birefringence ($\Delta N \times 10^3$)
1.79	57.4	1.24
3.39	52.9	4.79
4.19	48.2	6.04
4.39	45.0	12.35
4.79	39.0	29.02
5.49	36.5	61.88
6.29	32.0	80.48
8.29	29.5	102.92

*Relative position along the neck

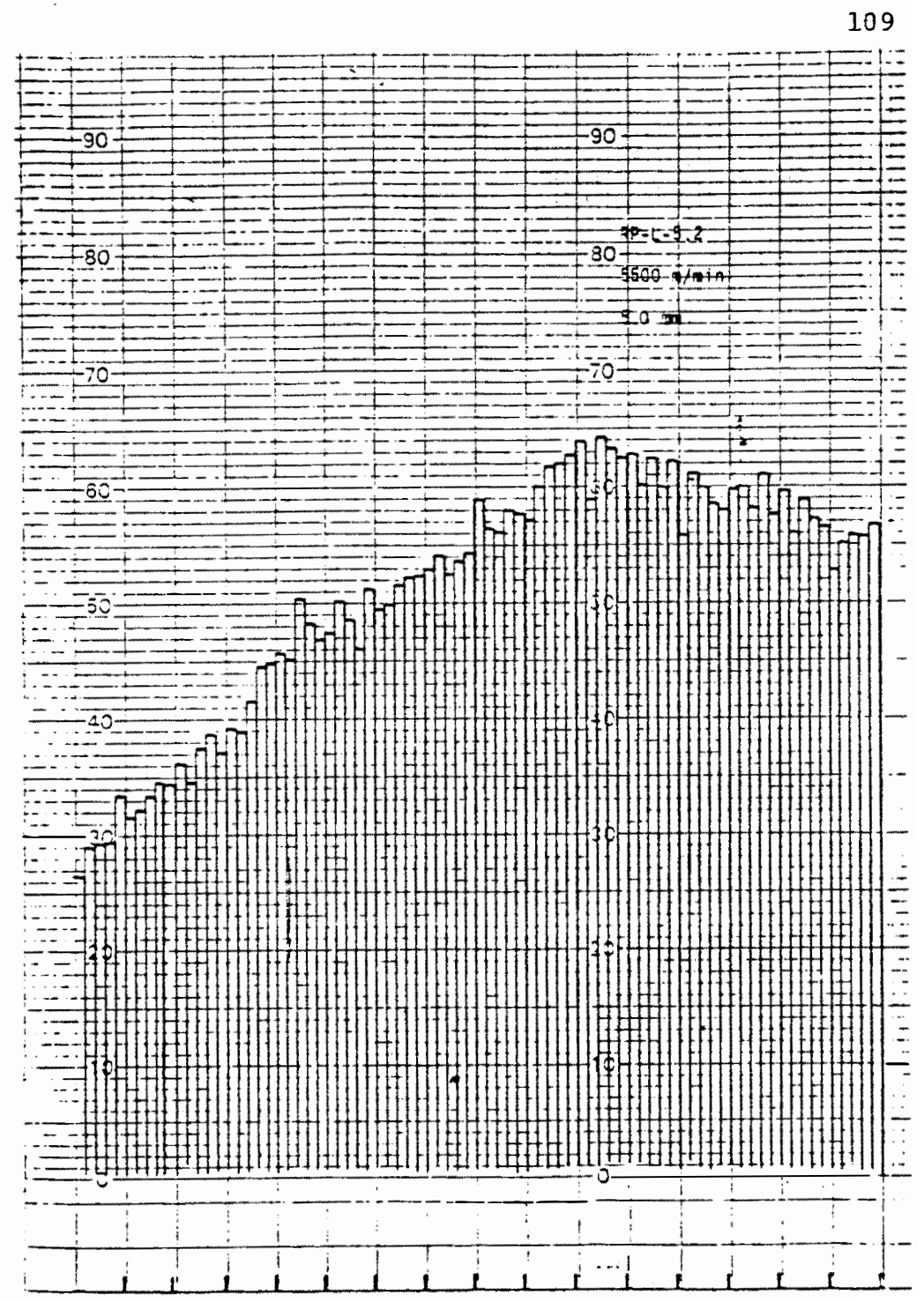

Figure 4.36. Wide angle x-ray diffraction of a neck bundle at relative position of 5.0 mm.

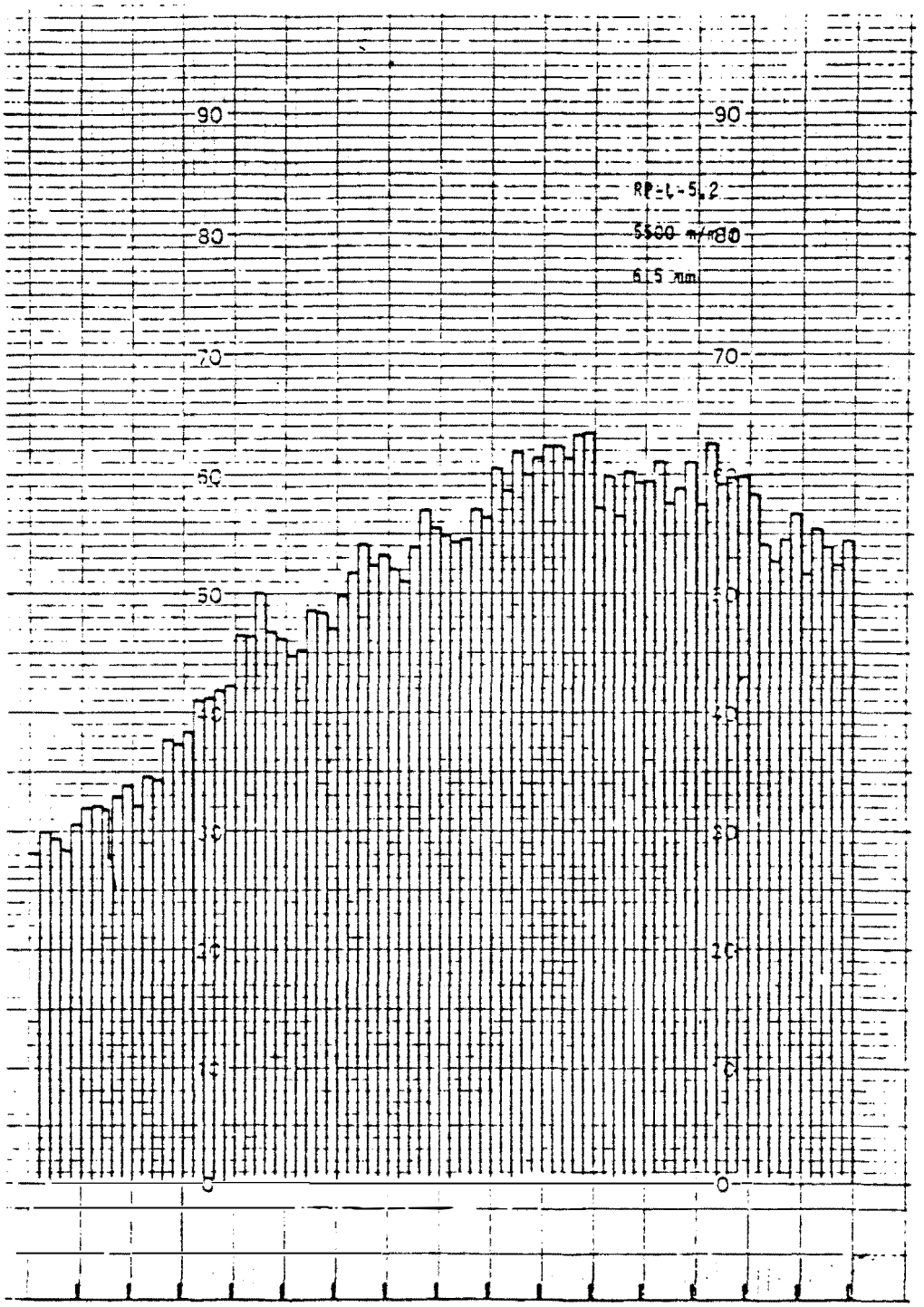

Figure 4.37. Wide angle x-ray diffraction of a neck bundle at relative position of 6.5 mm.

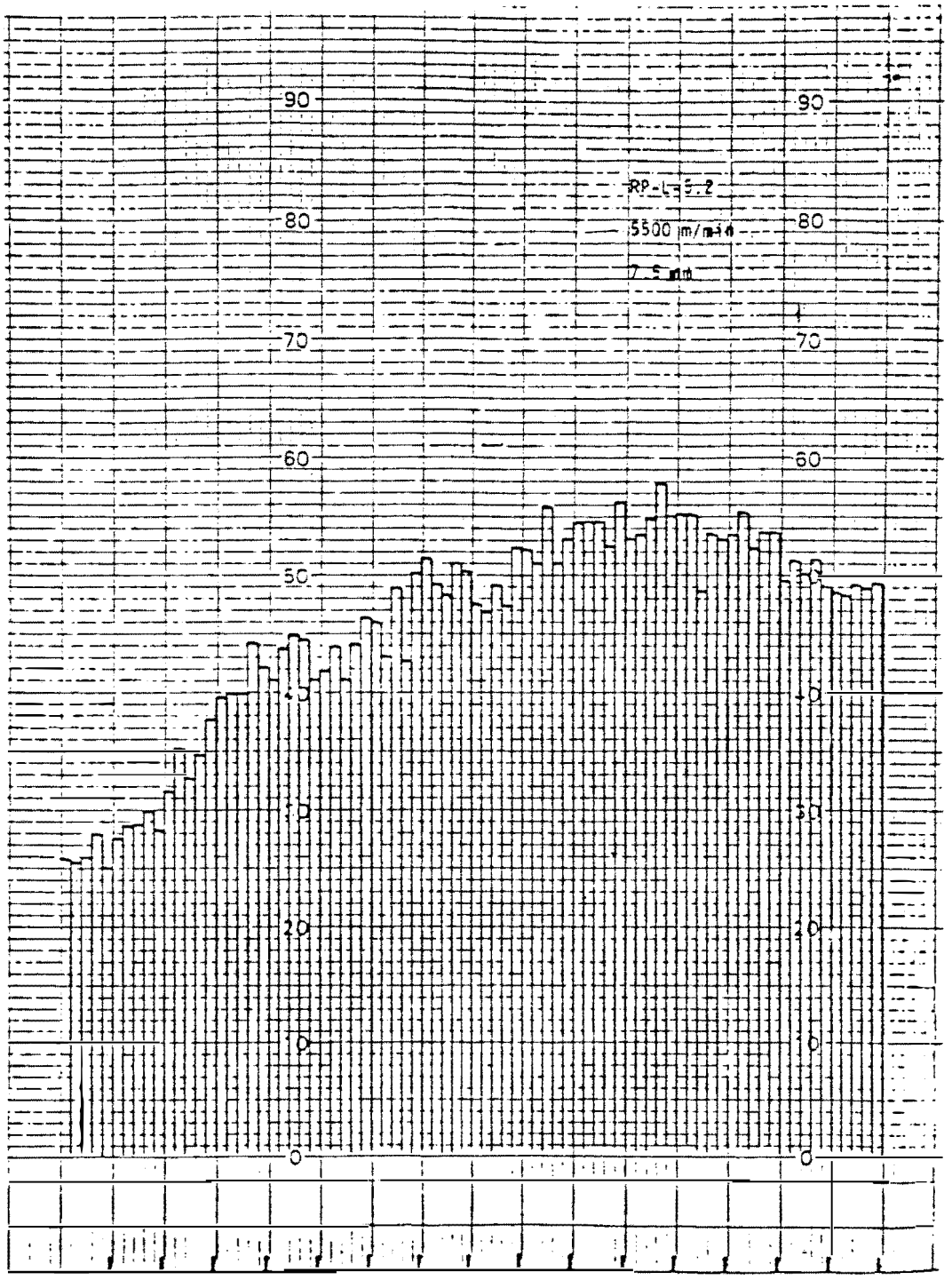

Figure 4.38. Wide angle x-ray diffraction of a neck bundle at relative position of 7.5 mm.

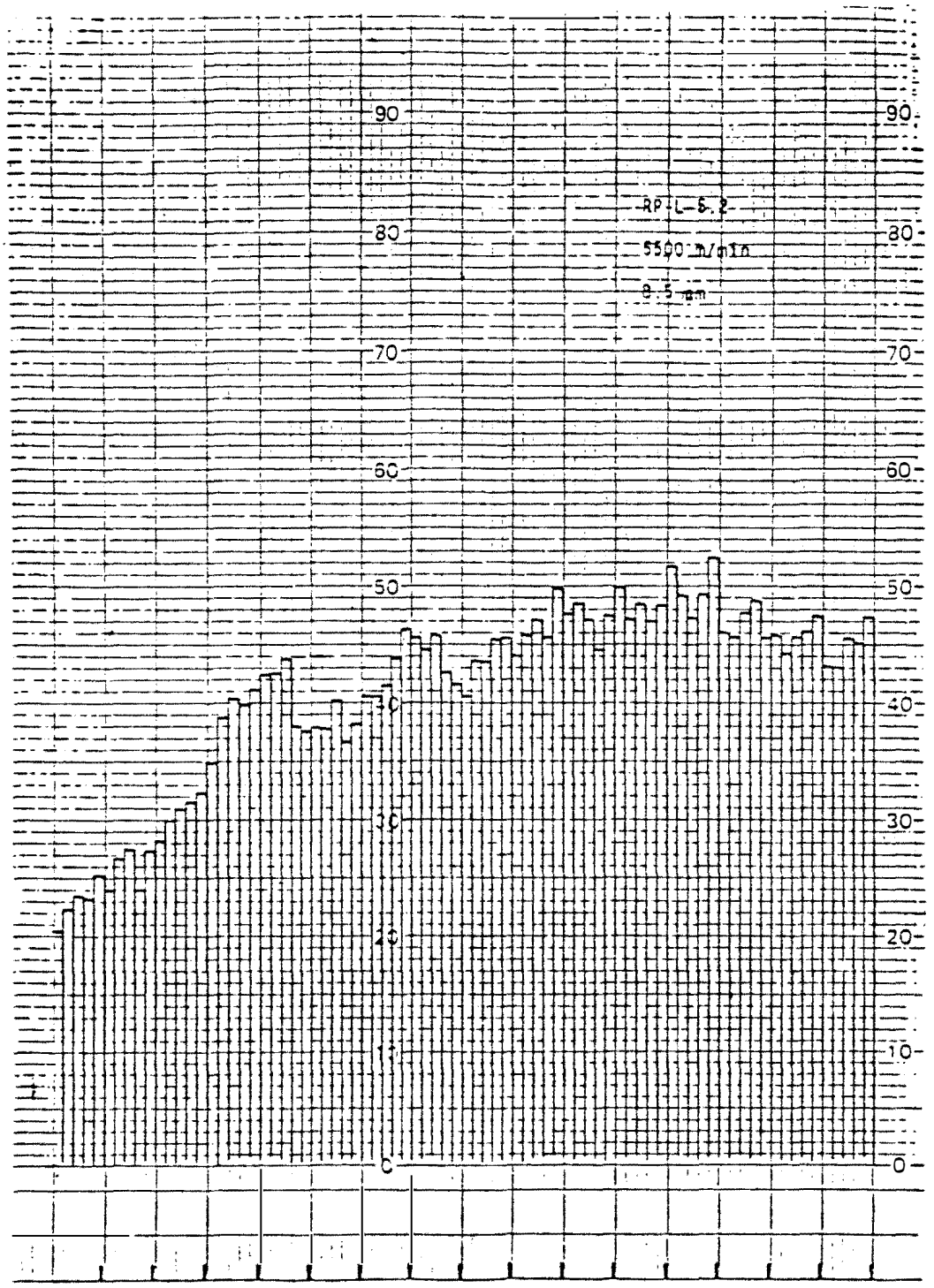

Figure 4.39. Wide angle x-ray diffraction of a neck bundle at relative position of 8.5 mm.

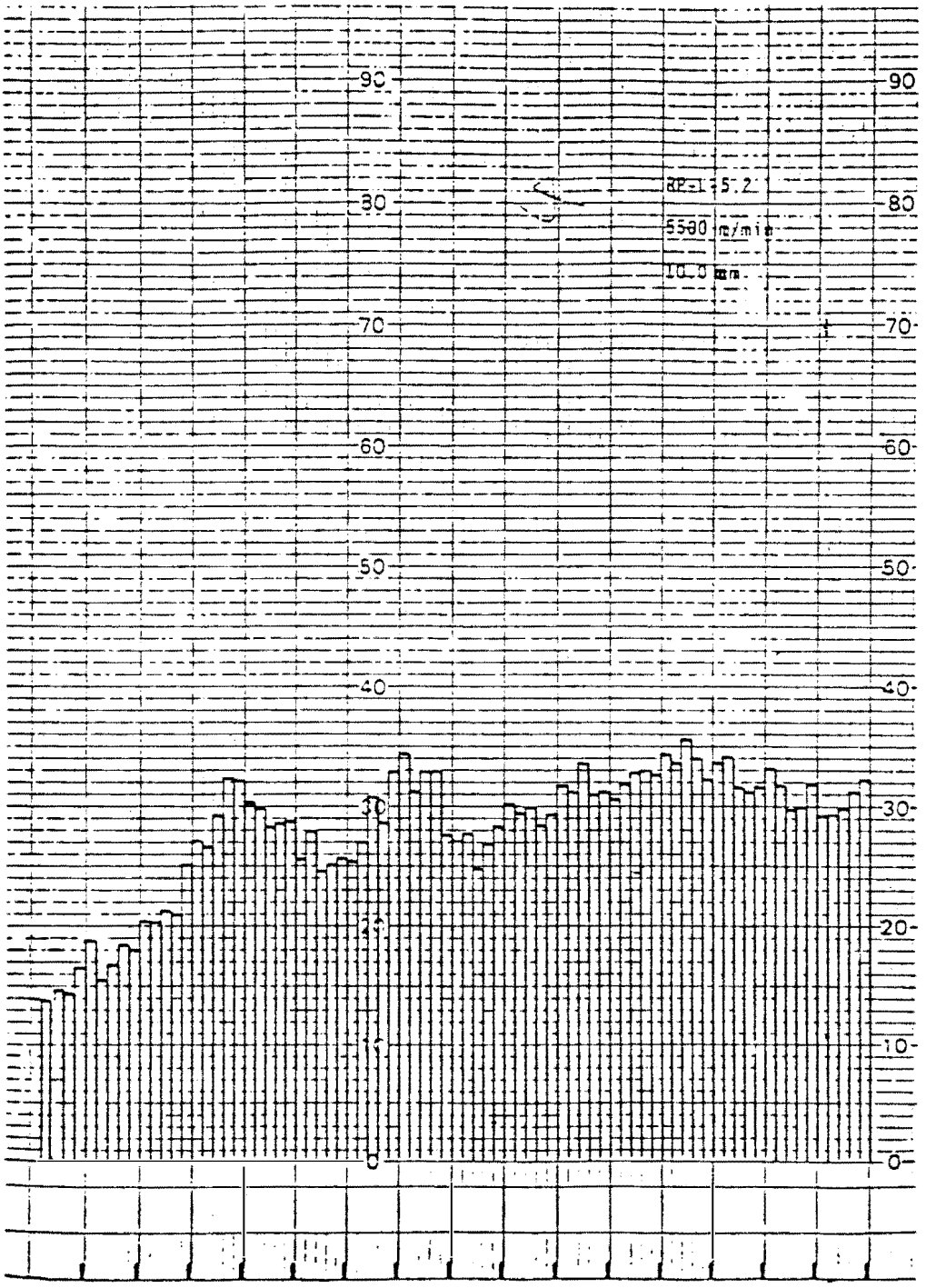

Figure 4.40. Wide angle x-ray diffraction of a neck bundle at relative position of 10.0 mm.

fiber researchers. Several people (25,54,66,73) reported that the spinline temperature profile depended on the polymer type, throughput and take-up velocity. Some of them measured the fiber surface temperature by using a contact thermocouple. Because of low sensitivity, it required a long time to measure the balance temperature of the fiber surface. Friction caused by contacting the fiber moving at high speeds raises some question as to the accuracy of this method. This can be avoided by using an infrared technique since it is a non-contact method.

The principle of this technique is based on measuring the magnitude and spectral distribution emitted by the fiber which indicates the temperature of its surface. The infrared region of the electromagnetic spectrum is generally defined as the wavelength interval between 0.72 and 1000 microns, that is between the visible region and microwave region. Warm objects emit radiation at the longer wavelengths in the infrared region.

Here, the Barnes RM-2B IR microscope system was modified by adding a black surface adjustable heater in front of the IR microscope lens, as a background temperature (see Figure 3.3). The measurement was based on a detectable temperature difference between the

background (heater) and the object (fiber). The IR microscope was moved along the spinline until there was no difference between signal with and without the fiber in the field of view. The fiber temperature at this position was assumed to be the same as the heater temperature.

Figures 4.41 to 4.49 show the temperature profiles of linear, branched, and high molecular weight PET spun at different take-up velocities and mass throughputs. Generally, decreasing the throughput and increasing the take-up velocity produced a more rapid temperature decrease. Within 20 cm of the spinneret the fiber temperature was almost the same for constant throughputs at different take-up velocities. Increasing the spinline length allowed the fiber temperature to decrease further before the filament entered the drawdown device. The temperature profiles exhibited a noticeable slope change at a point which corresponded approximately to the neck region. The temperature profiles indicated that the fiber cooled faster after necking. This rapid cooling may be a result of the increased surface area per unit volume and the increased velocity of the fiber through the ambient air. Since crystallinity increases rapidly at the neck, the latent heat given up would tend to decrease the rate of fiber

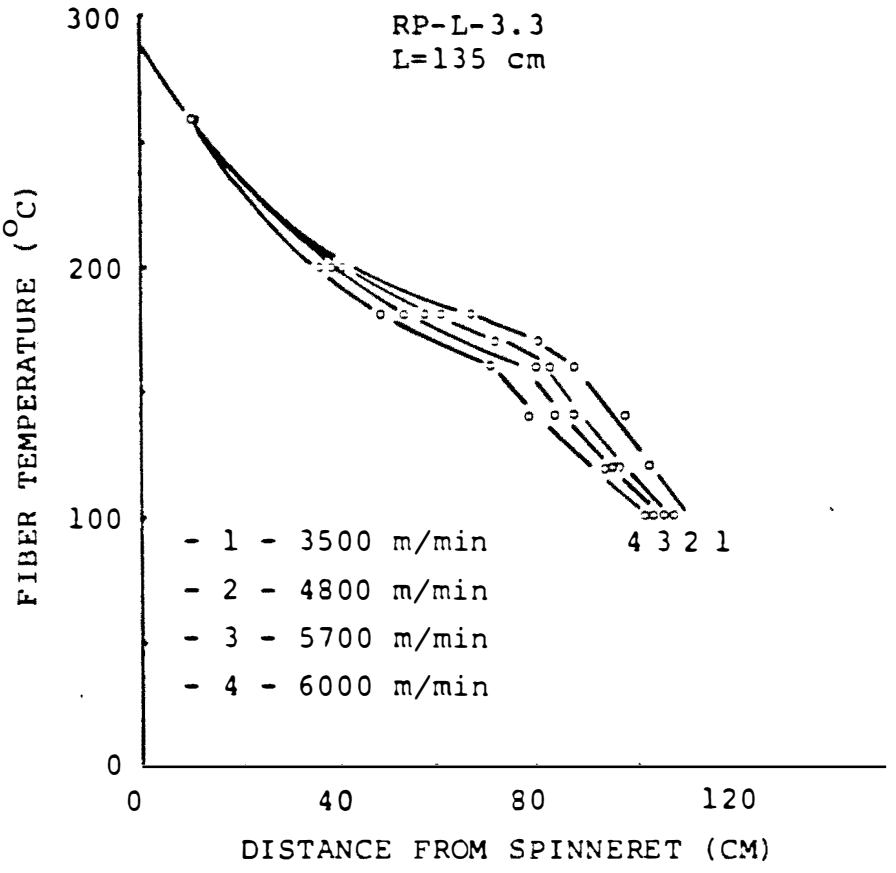

Figure 4.41. Temperature profile of linear PET with a mass throughput of 3.3 g/min and spin-length of 135 cm.

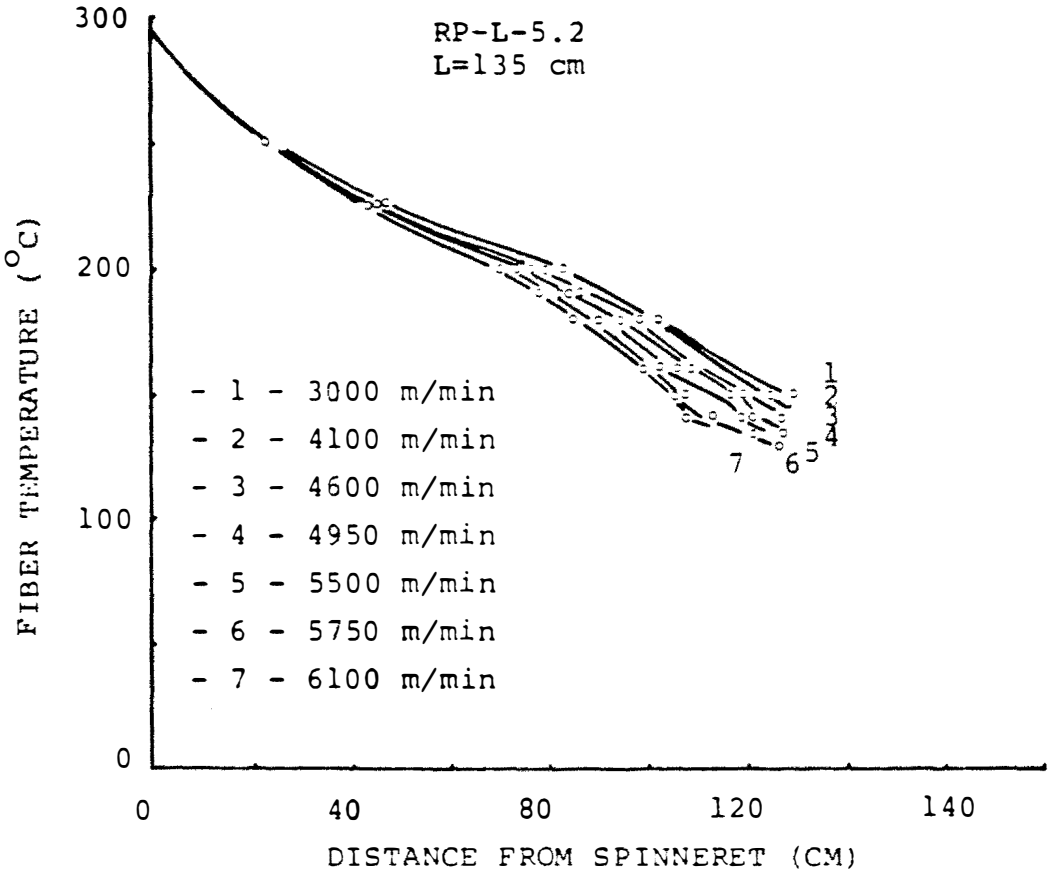

Figure 4.42. Temperature profile of linear PET with a mass throughput of 5.2 g/min and spin-length of 135 cm.

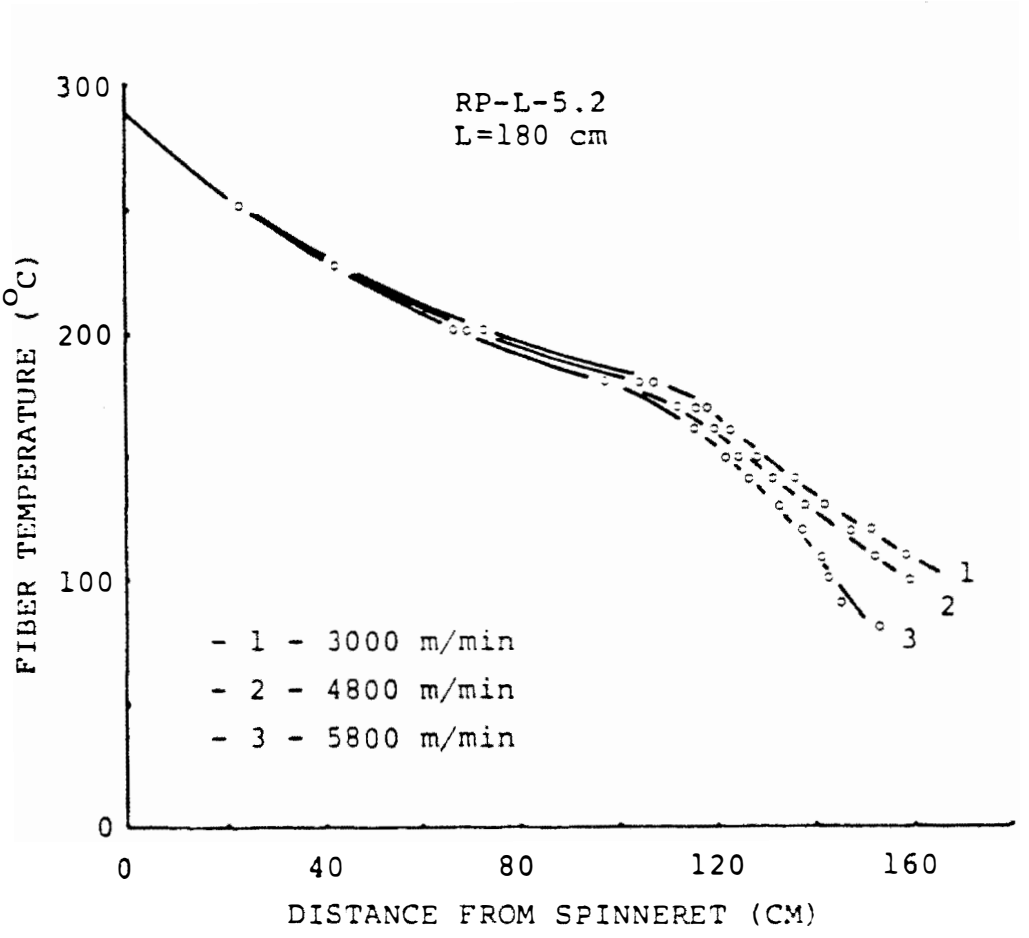

Figure 4.43. Temperature profile of linear PET with a mass throughput of 5.2 g/min and spin-length of 180 cm.

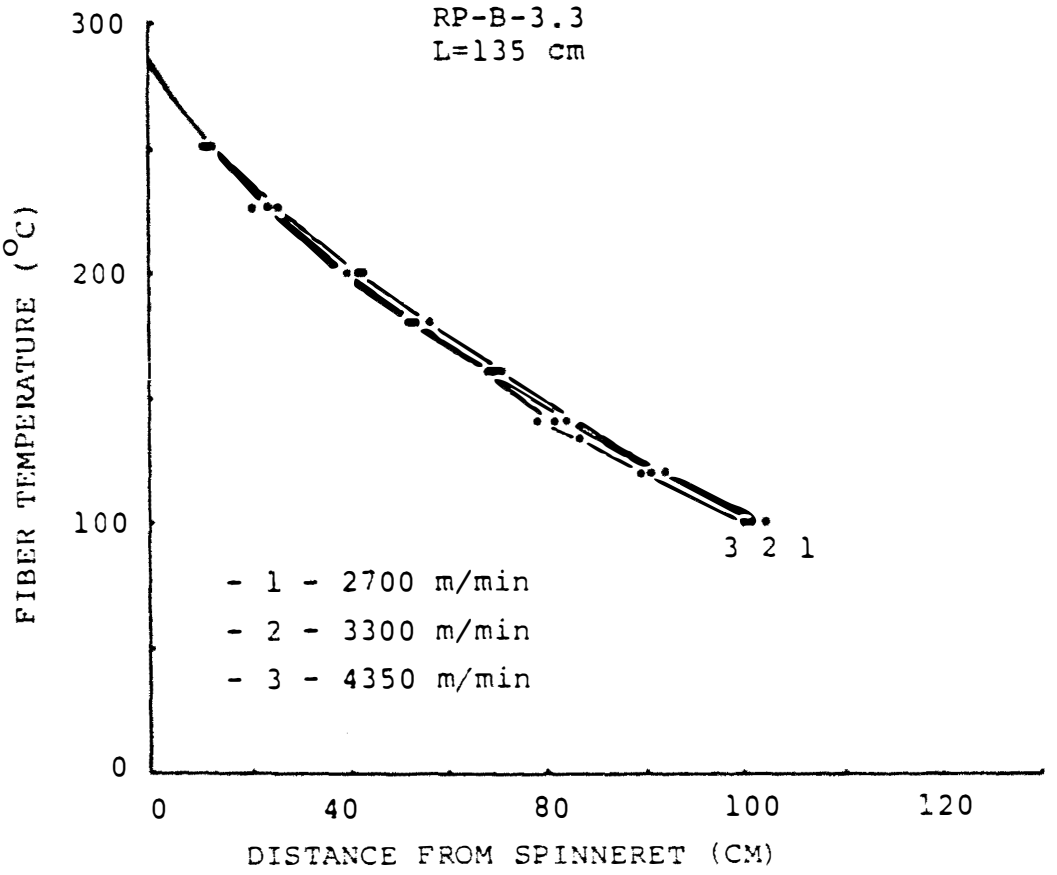

Figure 4.44. Temperature profile of branched PET with a mass throughput of 3.3 g/min and spin-length of 135 cm.

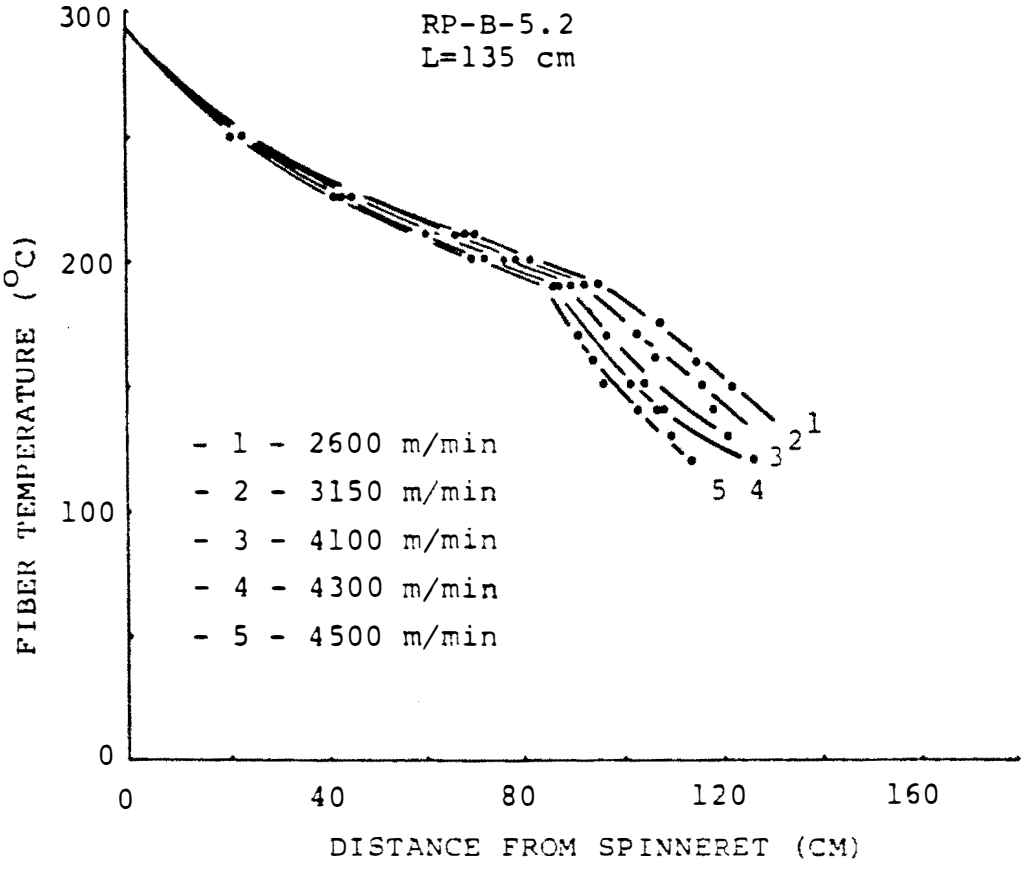

Figure 4.45. Temperature profile of branched PET with a mass throughput of 5.2 g/min and spin-length of 135 cm.

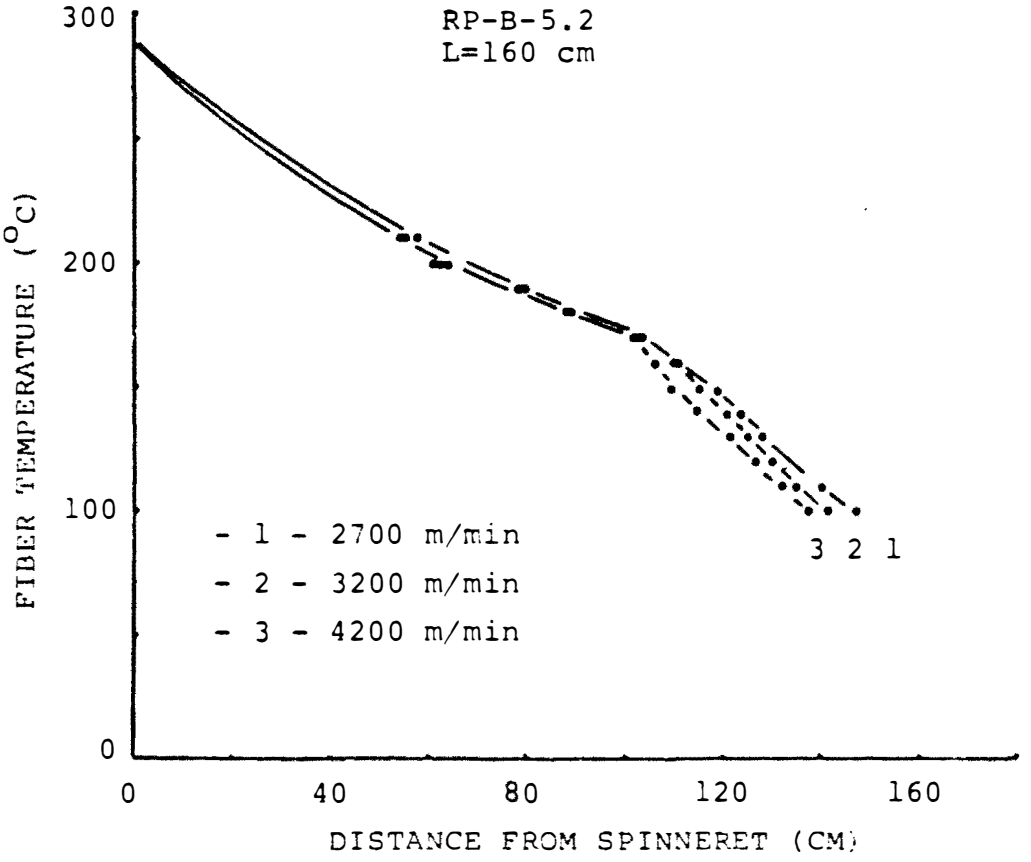

Figure 4.46. Temperature profile of branched PET with a mass throughput of 5.2 g/min and spin-length of 160 cm.

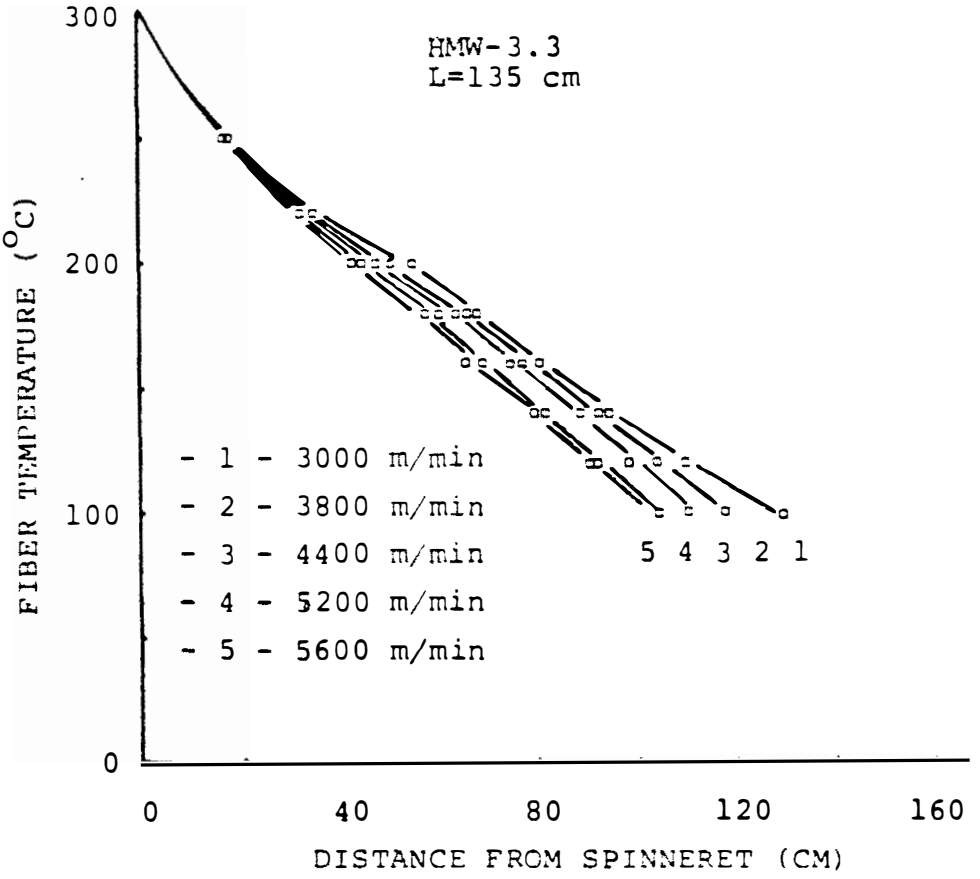

Figure 4.47. Temperature profile of high molecular weight PET with a mass throughput of 3.3 g/min and spin-length of 135 cm.

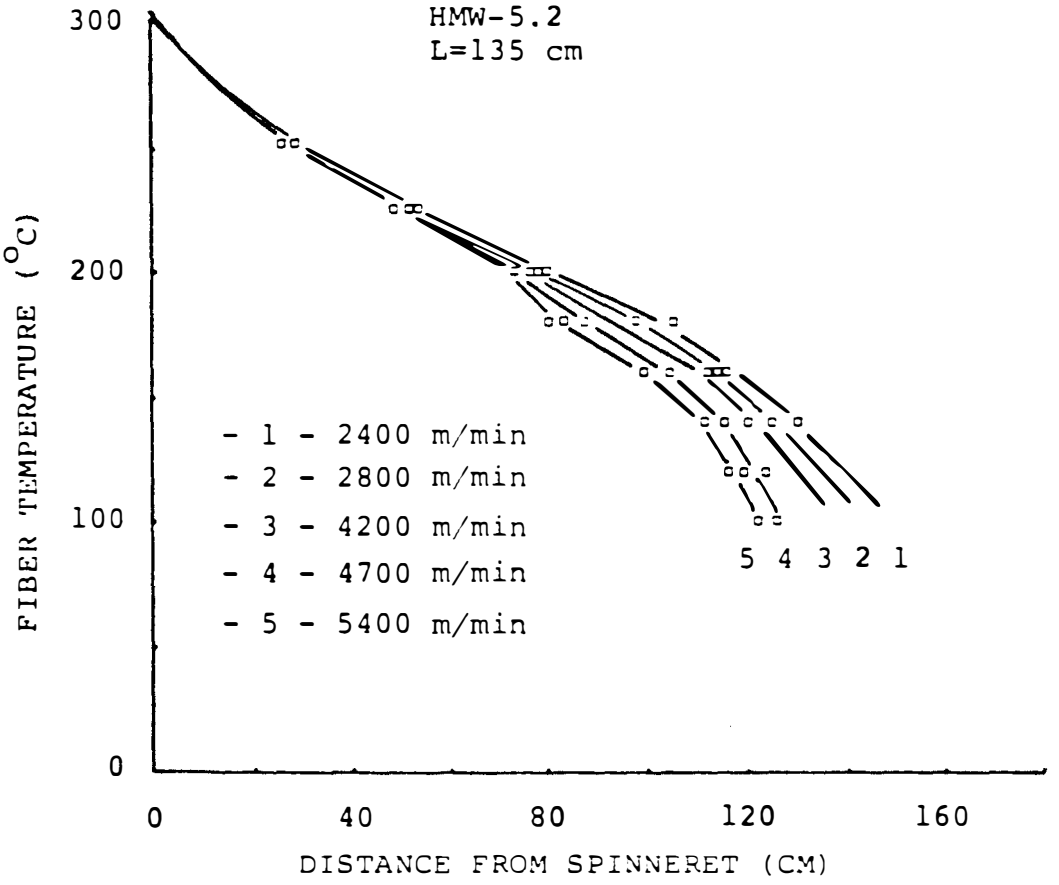

Figure 4.48. Temperature profile of high molecular weight PET with a mass throughput of 5.2 g/min and spin-length of 135 cm.

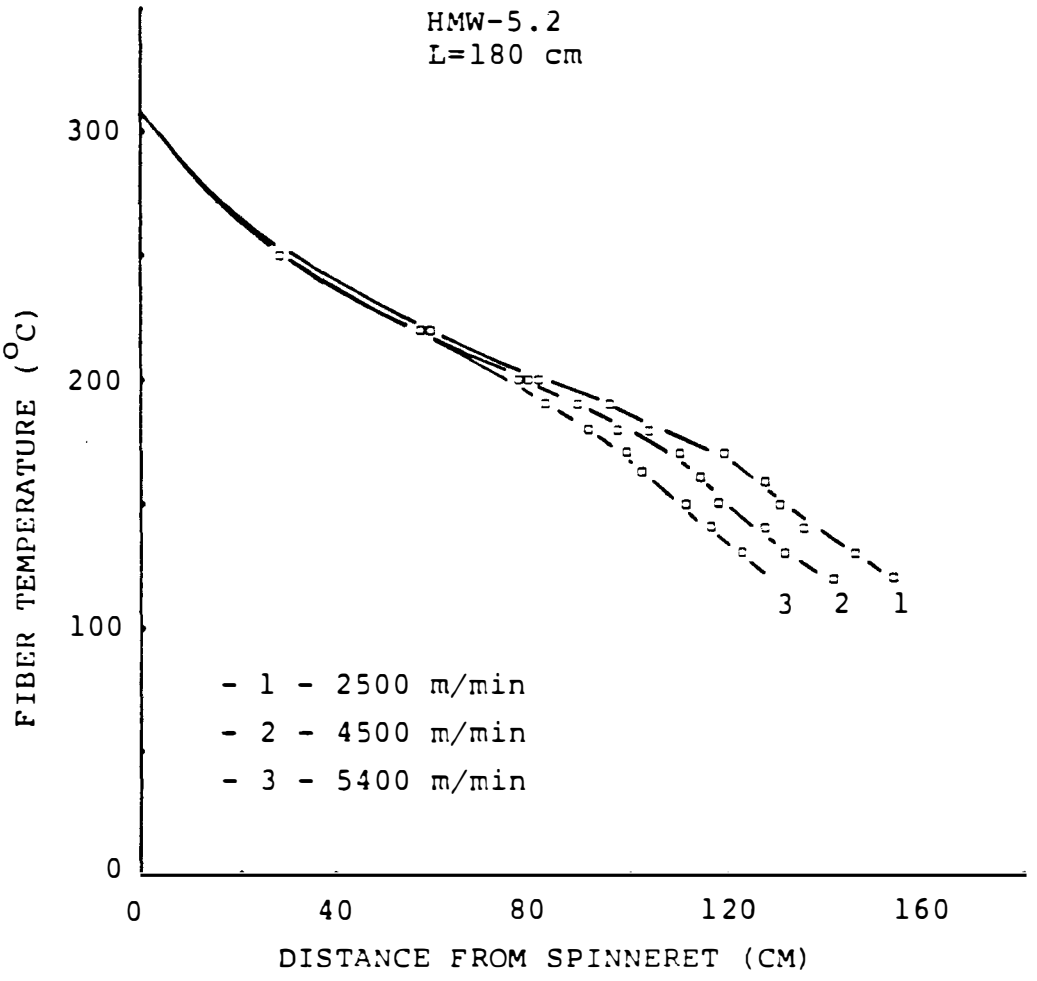

Figure 4.49. Temperature profile of high molecular weight PET with a mass throughput of 5.2 g/min and spin-length of 180 cm.

cooling. This effect opposes that associated with the increased surface area and velocity.

The fiber temperature in the neck region varies with throughput and take up velocity. Measured values range up to 170 ^{o}C for linear PET samples. These values are reasonably consistent with the "freeze point" values reported by George et al. (37).

The temperature in the neck region increased as take-up velocity increased. For high molecular weight PET, as the mass throughput decreased from 5.2 to 3.3 g/min, the "necking temperature" decreased (Figure 4.50). But for linear PET, the "necking temperature" did not change much when mass throughput decreased. When compared with linear PET, the "necking temperature" occurred at higher temperature in high molecular weight PET. This may be because molecular entanglements caused a higher stress build up in the spinline for the high molecular weight PET, and orientation induced crystallization occurred earlier than for linear PET.

4.3.2 Diameter And Birefringence Profile Along The Spinline

The most important aspect of melt spinning is the relationship between the spinning conditions and the structure and properties of the spun fibers.

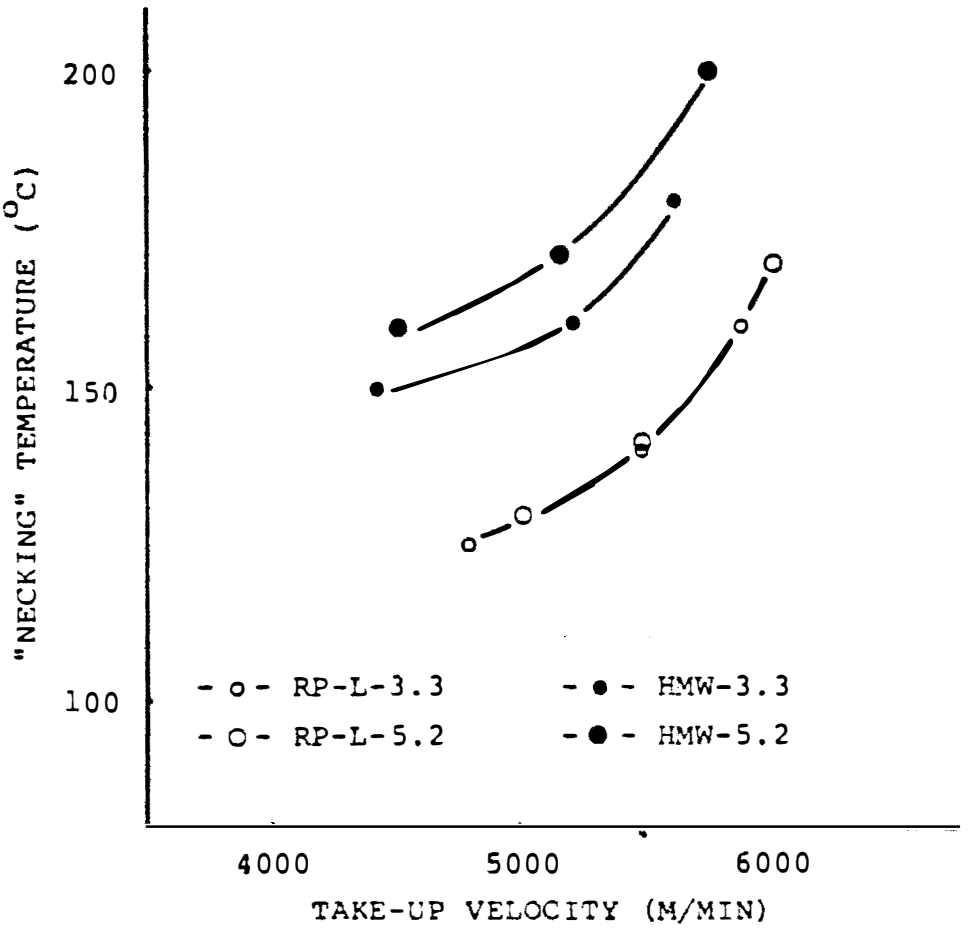

Figure 4.50. Necking temperature vs. Take-up velocities.

Quantitative studies of structure development during melt spinning have been carried out by Kitao et al. (69) and by the researchers at the University of Tennessee (8,9,25,26,79,80,104,107). They quantitatively studied the development of crystallinity and orientation using on-line WAXS and birefringence techniques. They reported the fiber orientation strongly depended upon the spinning conditions. Most of the studies were carried out at low or moderate spinning speeds with large fiber diameters.

In using a pneumatic drawdown device for high speed spinning of PET fibers, the vibration of the spinline increases the difficulty in measuring the fiber diameter and birefringence on the spinline. The effect of vibration was overcome by using a v-groove arc type aluminum guide as shown in Figure 3.7 (p. 53) to guide the filament within the microscope field of view. There was some unavoidable error introduced by the friction between the filament and the guide. A silicon spray was used to prevent sticking between the guide and filament.

Generally, the fiber diameter decreased gradually as the fiber approached the drawdown device at low take-up velocities. At high spinning speeds, necking was observed on the spinline but under microscopic observation there was only a cyclic diameter change

around the necking region. After necking, the filament diameter remained almost constant although it continues to decrease slightly with increasing distance along the spinline (Figures 4.51 to 4.53). The birefringence slightly increased along the spinline at low take-up velocities. At high take-up velocities, it increased slightly before necking and sharply increased after necking for linear PET. Although birefringence was low prior to necking it was still higher for the on-line measurements than for the previously reported samples cut from the threadline. This would appear to result from relaxation after cutting.

Branched PET behaved differently from the linear PET. Branched PET did not exhibit a localized (sudden) increase in birefringence, but a more gradual increase with distance. This appeared to be associated with a more gradual change in diameter than for the linear PET. For branched PET, the on-line birefringence was higher than the values determined from samples cut from the threadline. This would also appear to result from relaxation after cutting.

High molecular weight PET on-line birefringence was lower than linear PET on-line birefringence after necking, but prior to necking, the birefringence of the

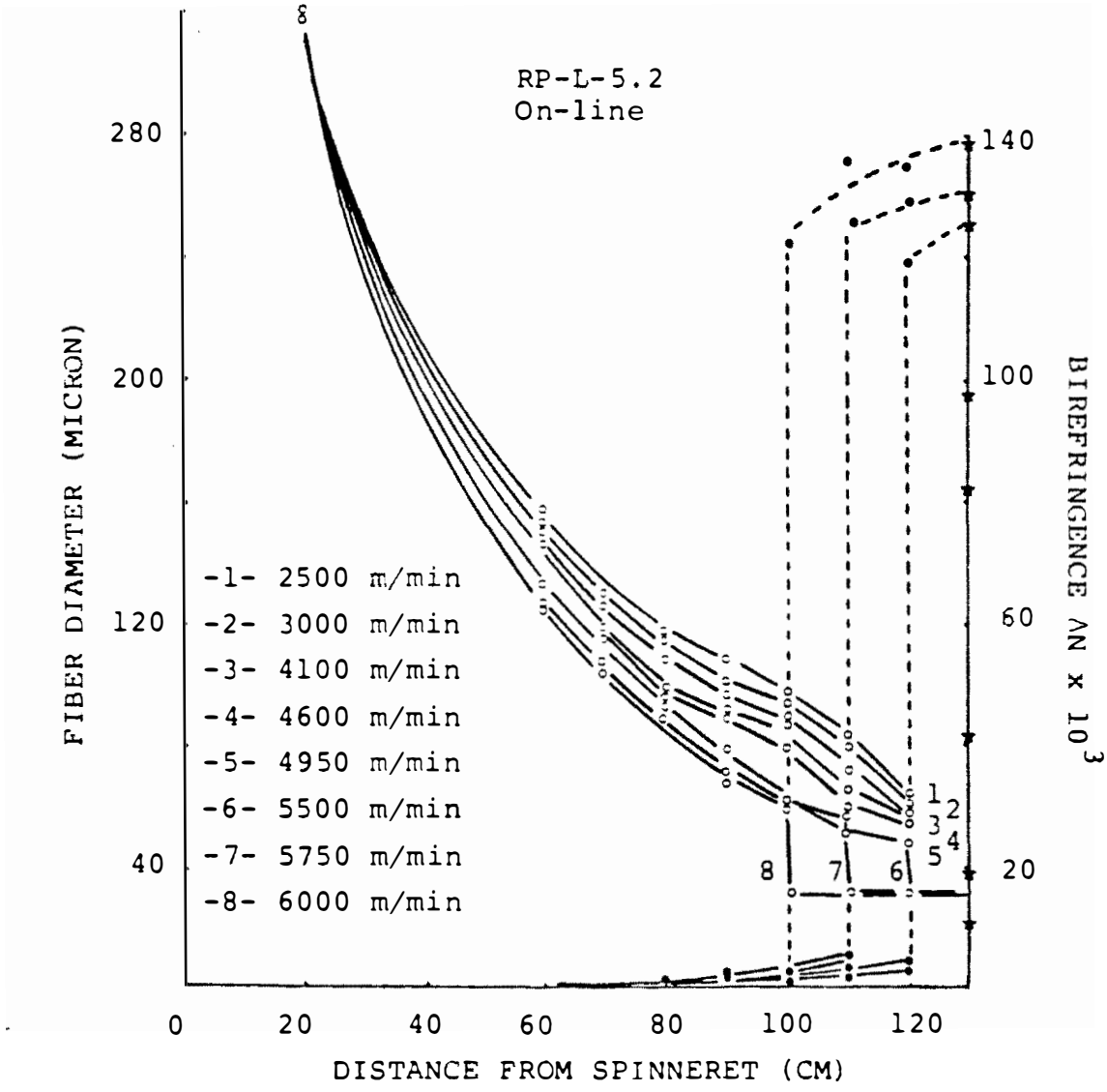

Figure 4.51. On-line diameter and birefringence profile of linear PET with a mass throughput of 5.2 g/min.

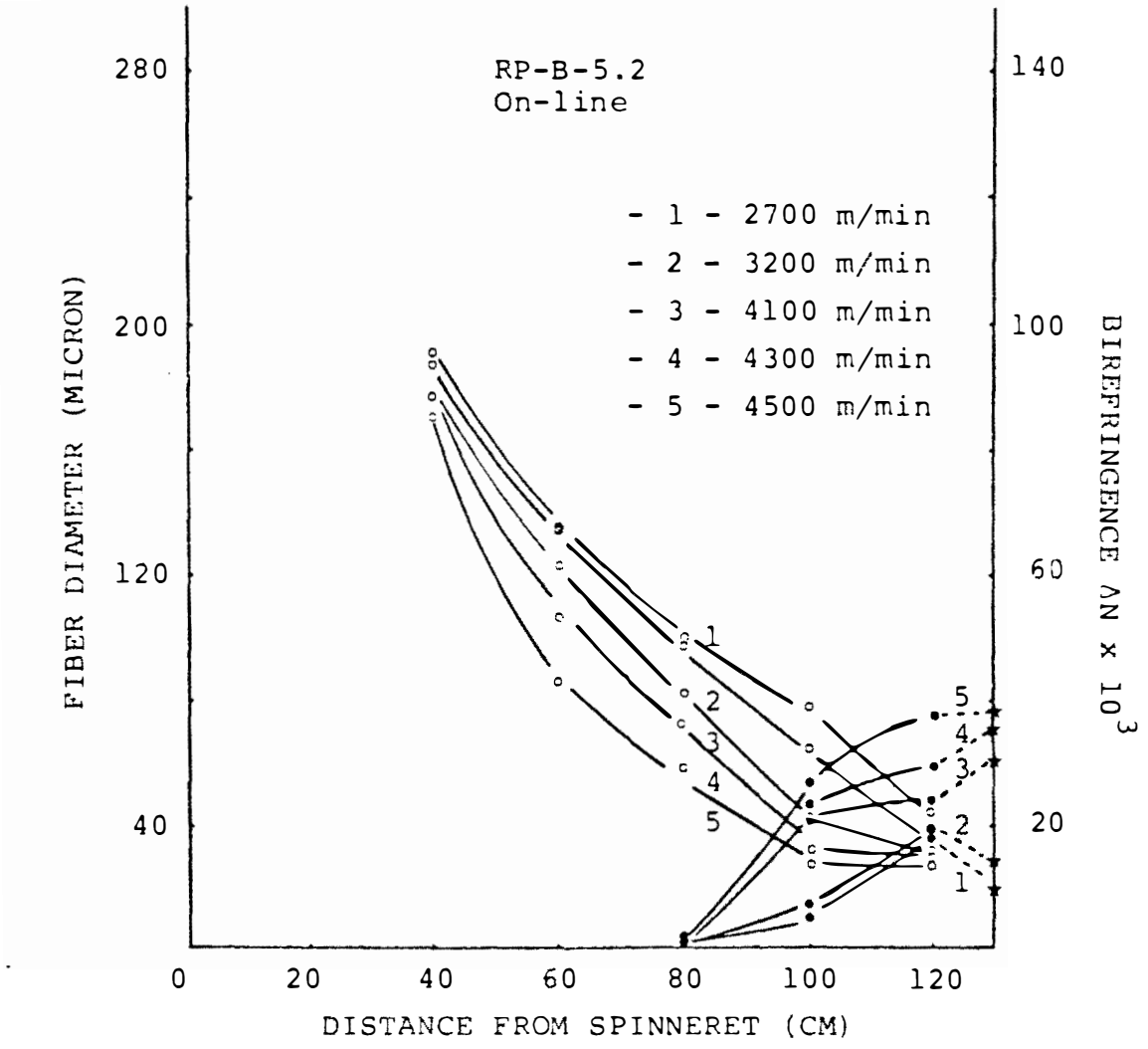

Figure 4.52. On-line diameter and birefringence profile of branched PET with a mass throughput of 5.2 g/min.

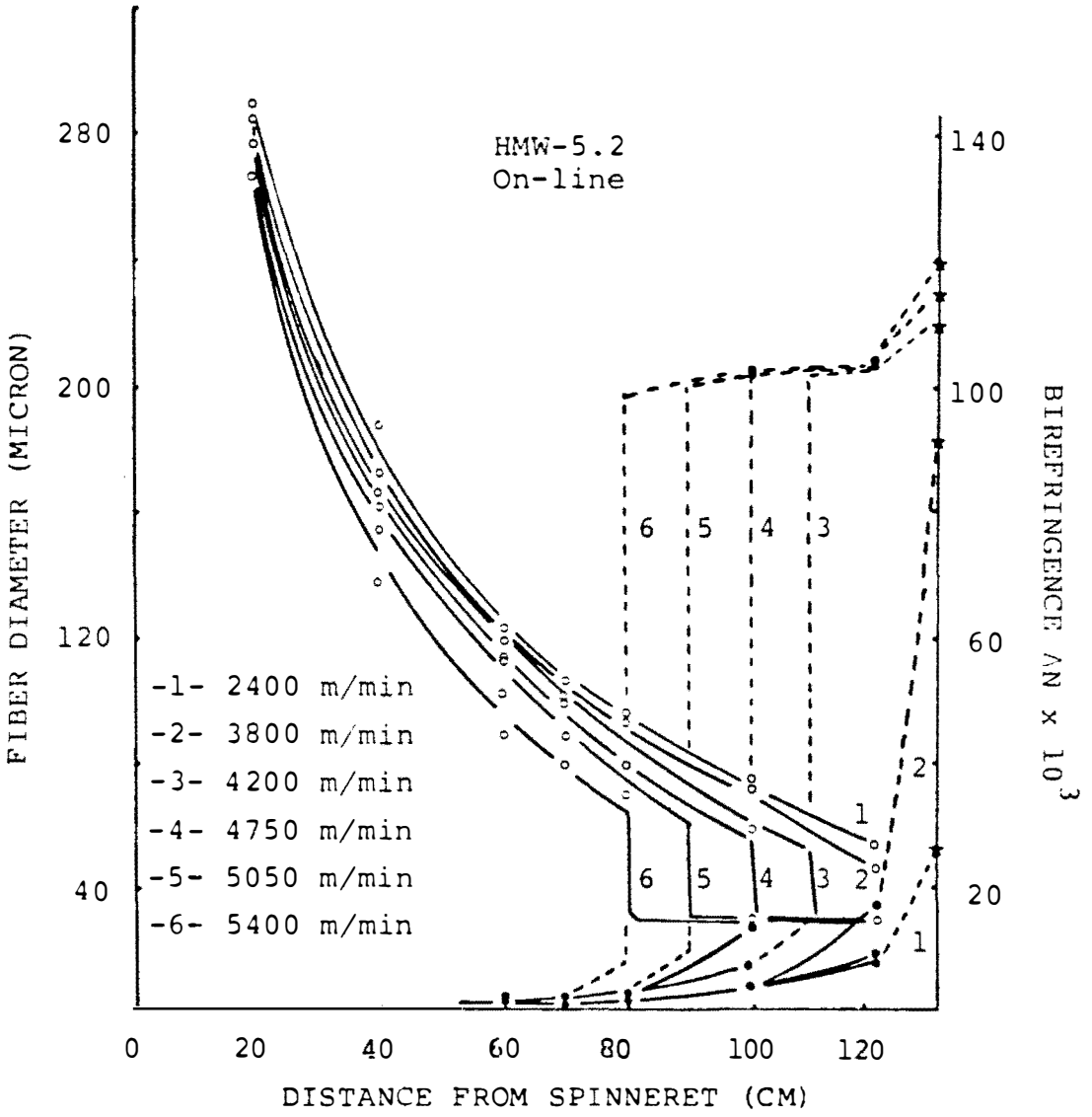

Figure 4.53. On-line diameter and birefringence profile of high molecular weight PET with a mass throughput of 5.2 g/min.

high molecular weight sample was higher than for linear PET.

4.4 Computer Simulation of Fiber Formation and Structure Development on the Spinline

The necking phenomena observed on the spinline, the suddenly increasing birefringence in the necking region, the local change in cooling rate caused by necking and the related release of heat of crystallization, and the strain hardening effect causing filament diameter to remain constant after necking are complex and challenging problems for interpretation of PET high speed spinning. Conventional mass, force, and energy balances alone can not solve these complicated problems of high speed spinning. Kikutani (66) combined birefringence, strain hardening, and crystallization kinetics with the mass, force, and energy balances and successfully predicted the unique behavior of PET high speed spinning along the spinline. His analysis has been used in this dissertation in an effort to try to understand the complex behavior observed experimentally.

The following differential equations were solved simultaneously by a continuous system modeling program (CSMP) method of IBM (97).

Force balance equation

$$\frac{dF}{dx} = W \left(\frac{dV}{dx} - \frac{g}{V} \right) + \pi D \tau_f$$

Rheological equation

$$\frac{dV}{dx} = \frac{F \rho V}{\eta W}$$

Stress hardening equation

$$\eta = 1.3 \exp\left(\frac{4400}{T + 273} \right) \exp\left(2^{18} \chi_c^{16} \right)$$

Energy balance equation

$$\frac{d\chi_c}{dx} = \frac{Cp}{\Delta H} \frac{dT}{dx} + \frac{4h}{\Delta H D \rho V} (T - T_s)$$

Crystallization Kinetics

$$\frac{\chi c}{\chi_\infty} = 1 - \exp \left(-\left(\int_0^\tau K \left(T(\tau) \Delta N \right) d\tau \right)^n \right)$$

Birefringence equation

$$\frac{d\Delta N}{dx} = \frac{Cop}{V} \frac{dV}{dx} - \frac{\Delta N}{V \tau_f}$$

The notations are listed in the Appendix A. The strain-optical coefficient (Cop = 0.53) is from the experimental results of birefringence measurement of PET filament under low take-up spinning carried out by Kikutani (66). The heat of fusion (ΔH = 29.0 cal/g) is from Shimizu's data in reference 96. The tensile viscosity (η = 1.3 exp(4400/T + 273)) (when filament temperature is above Tg) is from Kikutani's experimental results. He compared his simulation results of diameter

profile with his experimental data under 3000 m/min and found reasonable agreement (66).

In this simulation, the constants are the same as Kikutani's. But the initial conditions, for example, the initial fiber temperature, the initial fiber diameter, the mass throughput, etc., are based on the spinning conditions in this research.

In this simulation, only the initial force (Fo) is an unknown parameter. By changing the initial force, the spinline dynamics and fiber structure can be simulated from fully amouphous to semi-crystalline structure in the spinline.

Figure 4.54 shows simulation results for 5.2 g/min mass throughput and 43.35 dynes initial force. For these conditions there was no necking occurring on the spinline, and very low birefringence and crystallinity were computed on the spinline. The results were similar to the experimental data measured at 3000 m/min take-up speed (Figure 4.55).

At an initial force of 46.4 dynes and mass throughput of 5.2 g/min, there was a "neck like" diameter thinning phenomena on the spinline at 120 cm below the spinneret (Figure 4.56). But the simulated diameter thinning phenomena was not as sharp as that of the experimental data (Figure 4.57) at a take-up speed

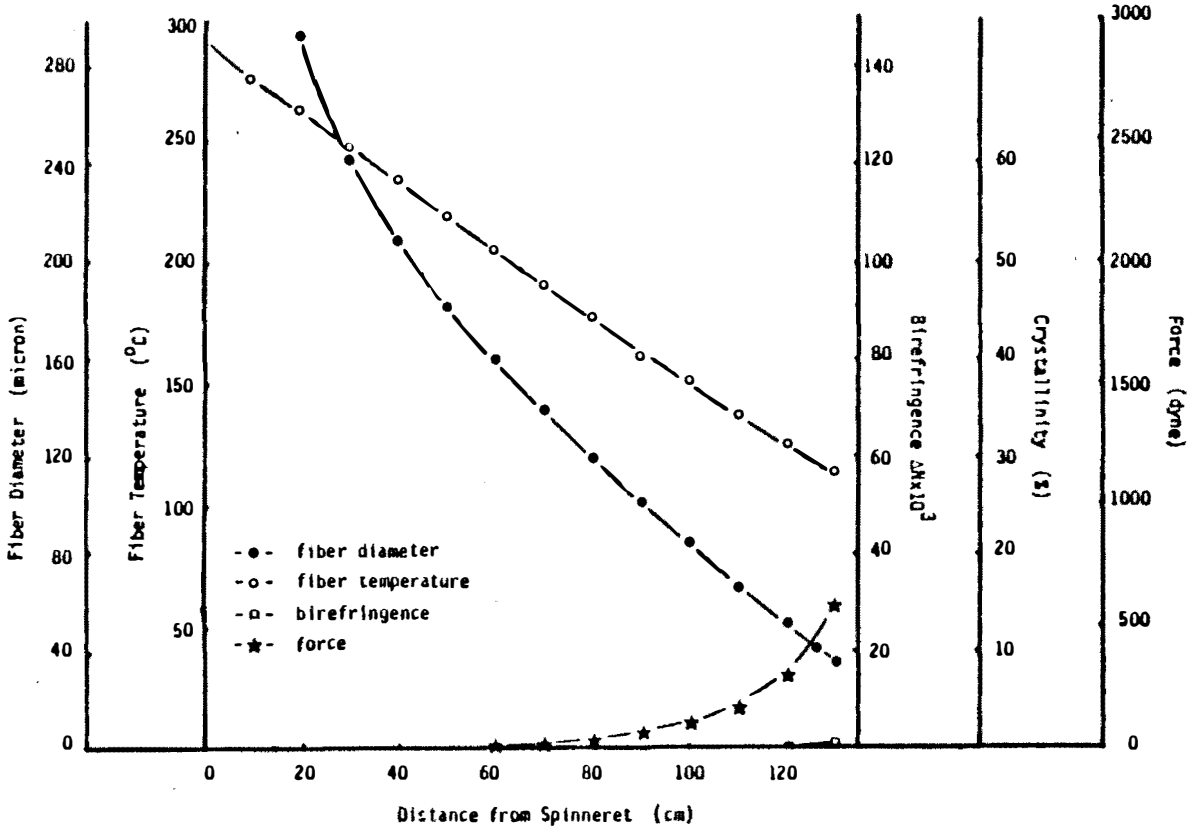

Figure 4.54. Simulation result (F = 46.35 dynes, W= 5.2 g/min).

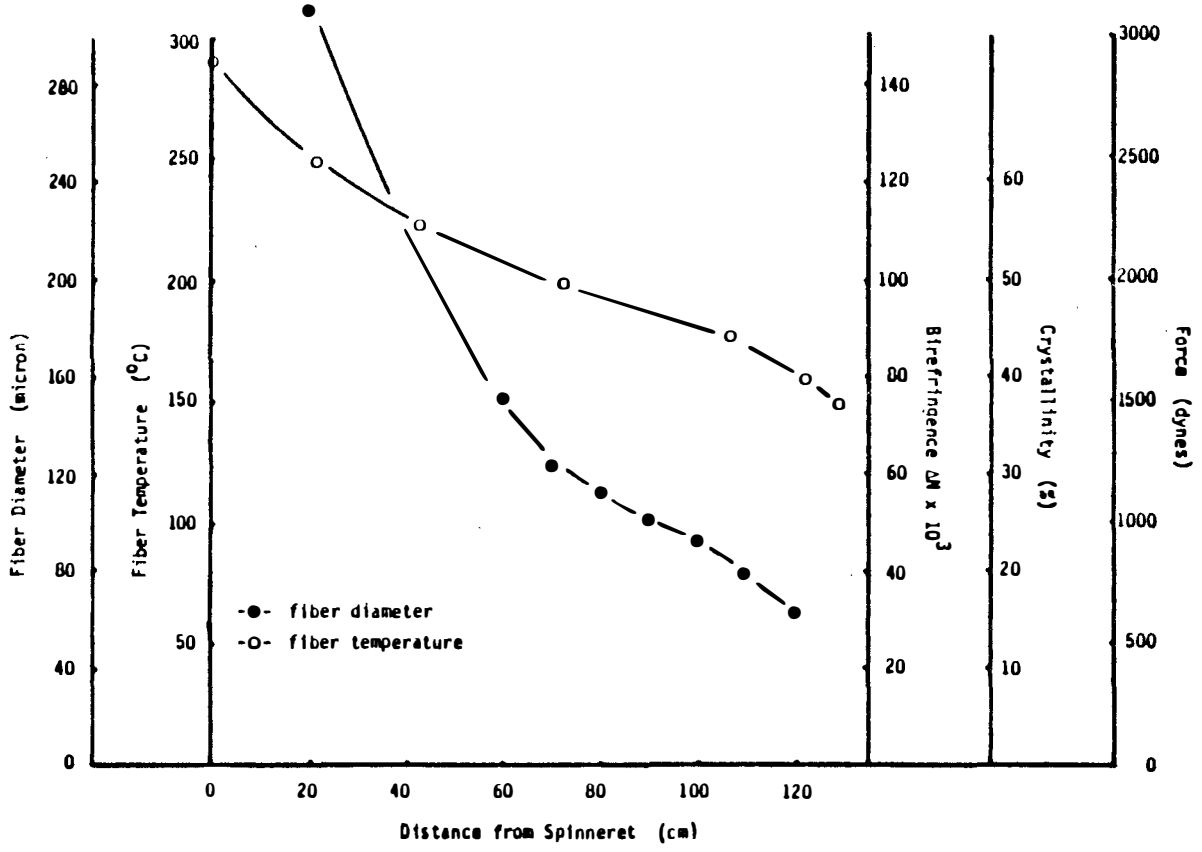

Figure 4.55. Experimental result (velocity= 3000 m/min, mass throughput= 5.2 g/min).

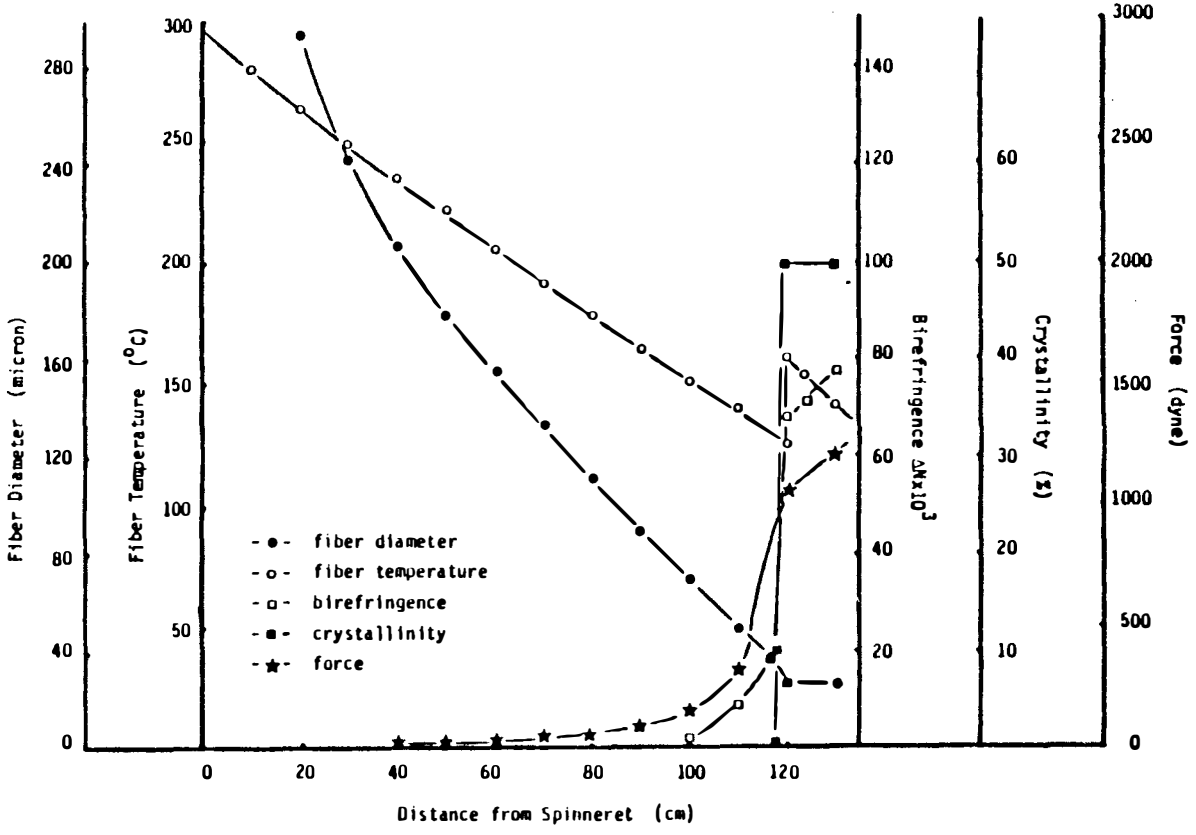

Figure 4.56. Simulation result (F = 46.40 dynes, W= 5.2 g/min).

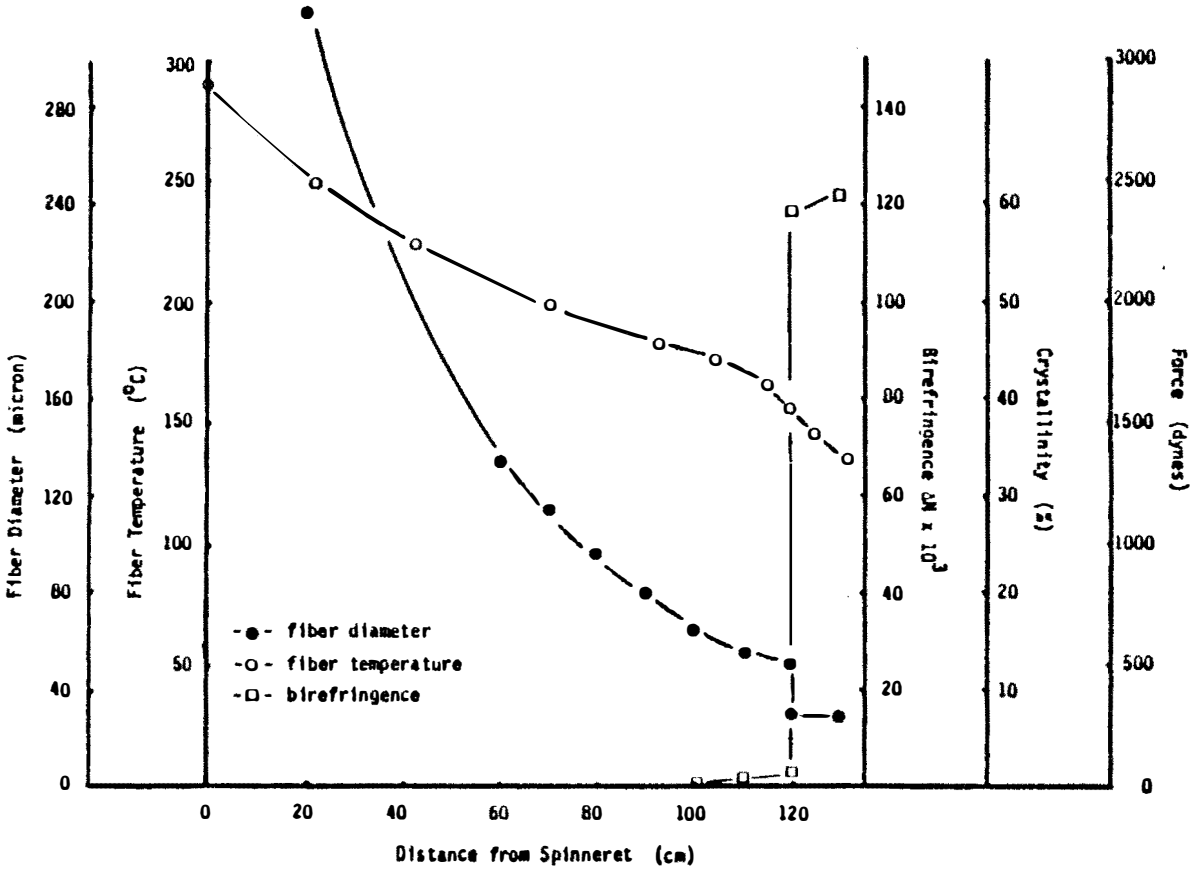

Figure 4.57. Experimental result (velocity=5500 m/min, mass throughput= 5.2 g/min).

of 5500 m/min. After necking, the fiber diameter decreased very slowly, the crystallinity reached its final value, and the birefringence suddenly increased and continued increasing with distance along the spinline. At the same point where crystallization occurred on the spinline, the fiber temperature sharply increased. The amount of heat released depended on the crystallinity of the fiber. As the initial force increased to 46.48 dynes, the necking position moved to 100 cm below the spinneret (Figure 4.58). At the same necking position, the experimental data showed the take-up speed up to be 6000 m/min (Figure 4.59).

These simulation results are qualitatively similar to the experimental results. The simulation revealed that when fiber birefringence (which is the result of molecular orientation) increased to a certain value, stress-induced crystallization initiated in the spinline. When the polymer crystallized on the spinline, the latent heat generated in this region was released and fiber temperature increased locally. This local increase in temperature caused the polymer melt viscosity to suddenly decrease and produced the necessary strain softening effect. Under a constant take-up force, the filament began to undergo a rapid diameter decrease. But when the degree of crystallinity

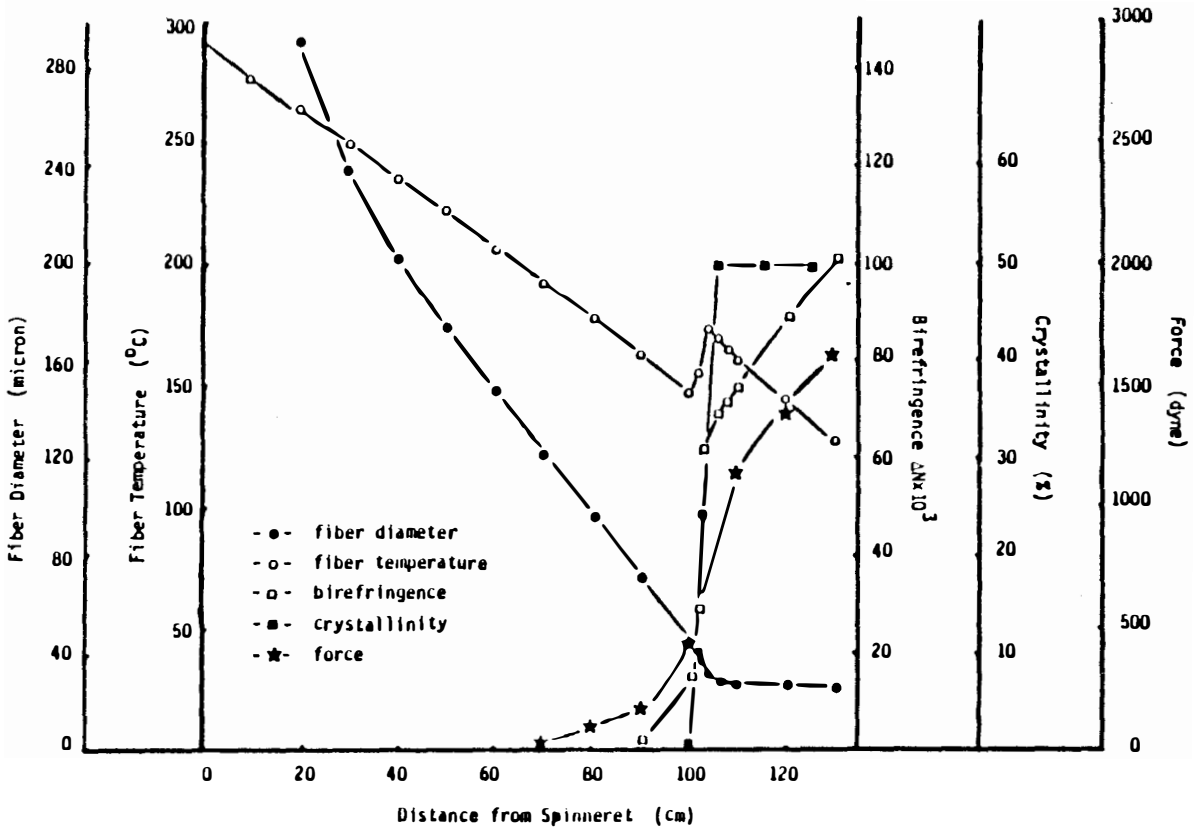

Figure 4.58. Simulation result (F =46.48 dynes, W= 5.2 g/min).

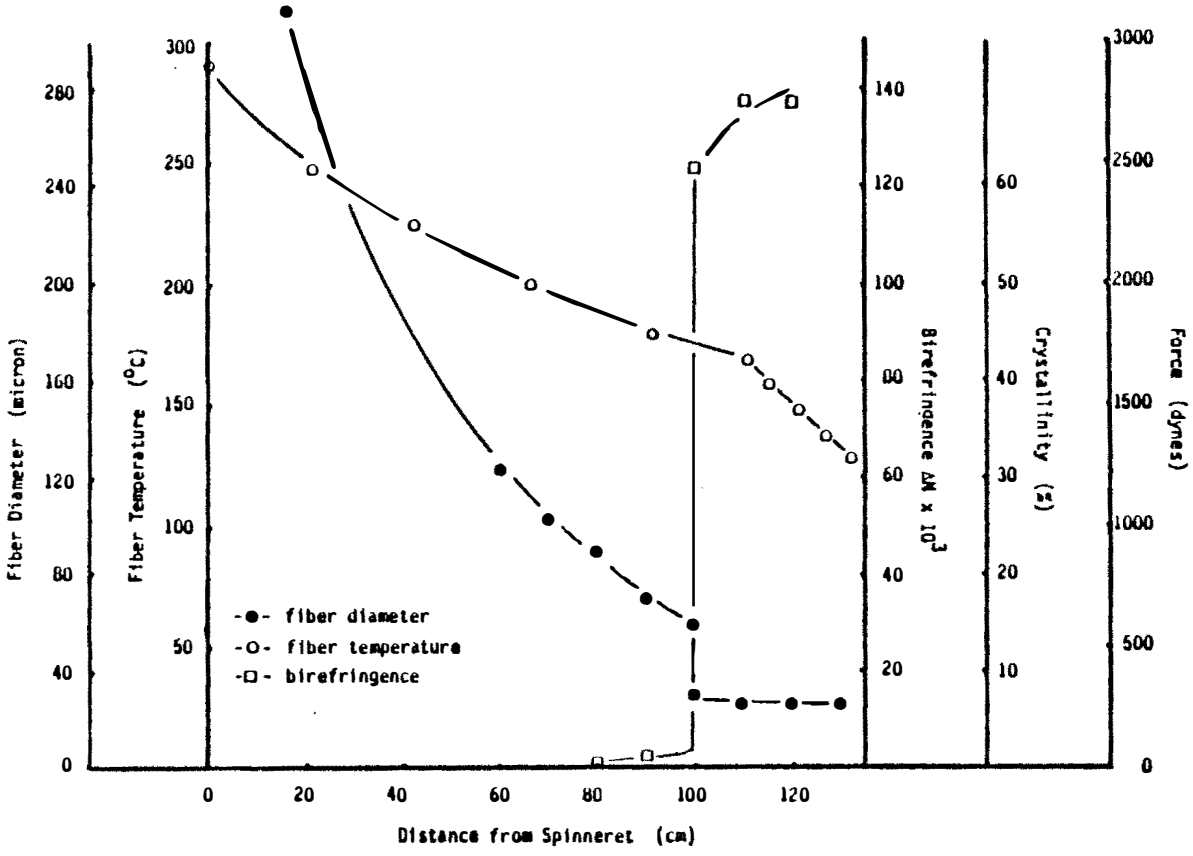

Figure 4.59. Experimental result (velocity= 6000 m/min, mass throughput= 5.2 g/min).

reached a certain level, polymer melt viscosity sharply increased (based on the strain hardening equation). Because of high viscosities, the velocity gradient became small and the diameter of the fiber decreased very slowly and a "neck" was observed on the spinline.

The temperature profile in the necking region did not show a sudden increase in the experimental data. This was probably due to the fact that the necking was not stable at one position. This tended to introduce error in the experimental results.

Figures 4.60 and 4.61 shows the simulation results for a mass throughput of 3.3 g/min. Again, the fiber structure could be simulated from fully amorphous to semi-crystalline on the spinline.

In general, by changing the initial conditions in the simulation, for example, mass throughput, initial fiber diameter, initial fiber temperature, initial forces, etc., the structure development of PET fibers could be simulated from a fully amorphous structure, which exhibited low birefringence and crystallinity, to a semi-crystalline structure, which exhibited high birefringence and crystallinity on the spinline.

But a complete quantitative comparision of the theoretical and experimental results is difficult because of the many parameters which influence the fiber

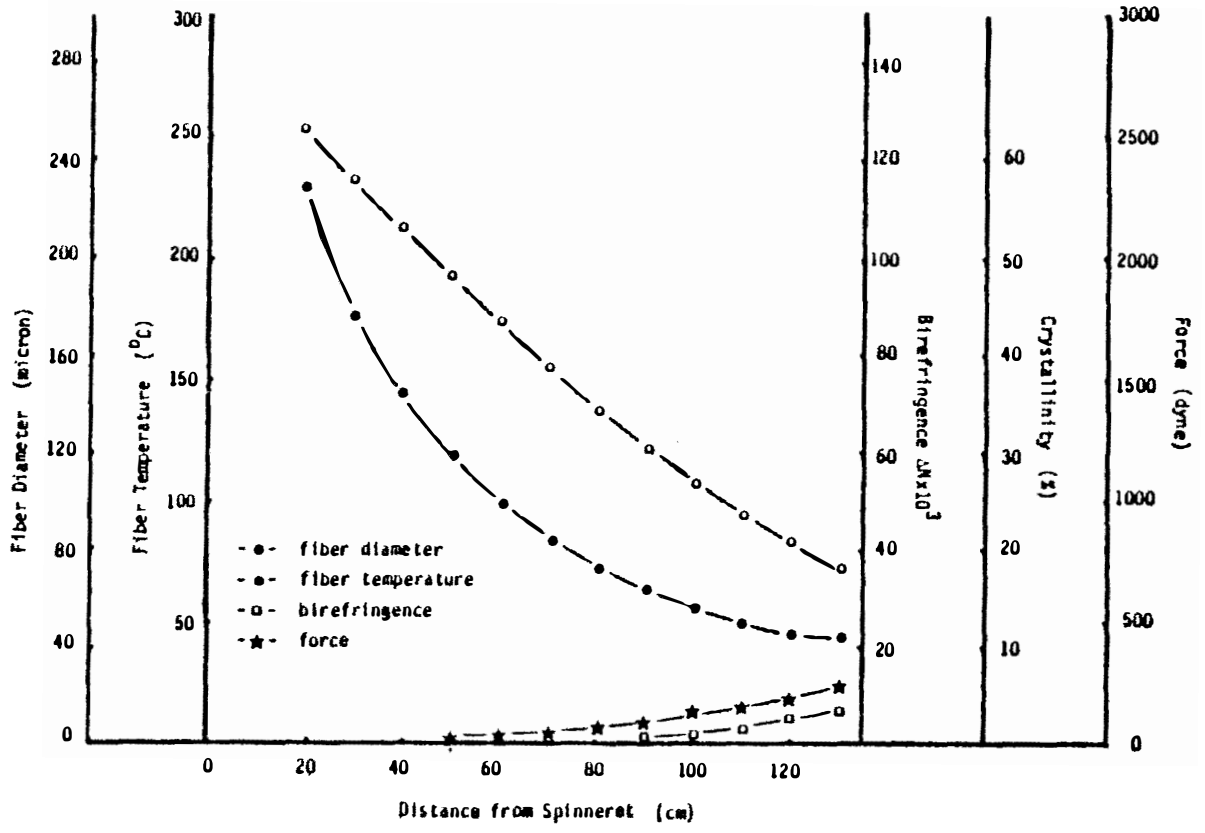

Figure 4.60. Simulation result (F = 39.65 dynes, W= 3.3 g/min).

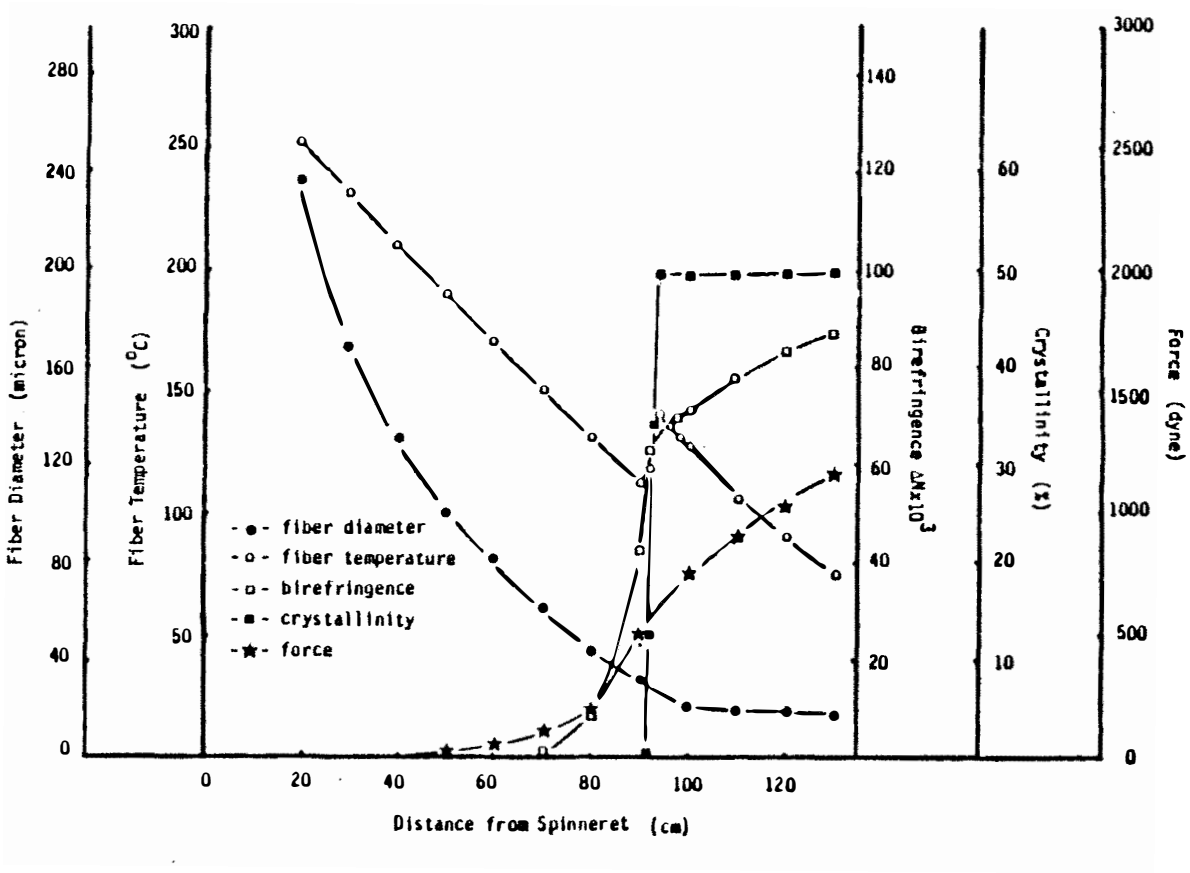

Figure 4.61. Simulation result (F = 40.0 dynes, W= 3.3 g/min).

orientation in the high speed spinning. A complete CSMP program is listed in Appendix B.

4.5 Proposed Neck Formation Mechanism

When molten polymer is extruded from the spinneret, the orientation, which is created by shear flow within the spinneret channel is relaxed by die swell. The extruded polymer is then deformed by the take-up force. Fiber molecules are stretched from a random conformation to an oriented conformation. The molecular orientation actually is a balance between the orientation induced by deformation of the melt stream and relaxation due to thermal motion of the molecules before the glass transition point is reached. Spruiell and White (103) reported that the spinning stress and accompanying molecular orientation decreases the free energy of formation of crystal nuclei and increases the crystallization rate.

The crystallization rate of PET is very low (127). At take-up velocities of 3000 to 3500 m/min, only an oriented amorphous structure was observed (2). At higher take-up velocities, these oriented amorphous molecules serve as a source for nuclei embryo and a rapid crystallization occurs in the spinline (14,76).

In the consideration of possible neck formation

mechanisms it should be realized that the formation of a neck appears to require a sudden strain softening (viscosity decrease) followed by a rapid strain hardening (viscosity increase). This statement is based on the fact that mathematical models that exhibit only a rapid strain hardening at a locallized position do not predict neck formation, but show a smooth drawdown to the final diameter. The final diameter is, of course, reached at approximately the point where the viscosity rises abruptly. In order to explain neck formation then, we must suggest mechanisms that involve a sudden strain softening followed by strain hardening. Based on the present modeling a possible mechanism is as follows: Increased stress and molecular orientation eventually lead to the initiation of stress-induced crystallization. When stress-induced crystallization takes place, the latent heat generated in this region is released and the fiber temperature increases locally. Because the polymer melt is supercooled substantially below the melting temperature of the crystals, there is no remelting but the local increase in temperature causes the polymer melt viscosity to suddenly decrease. This produces the necessary strain softening effect and, under a constant take-up force, the filament begins to undergo a rapid diameter decrease. The deformation

presumably causes considerable molecular orientation and further enhances the crystallization rate. But when the degree of crystallinity reaches a certain level, strain hardening occurs and the highly oriented and crystallized molecules resist further deformation. The fiber diameter becomes constant and a "neck" is observed.

It is speculated that on another possible necking formation mechanism as follows: Prior to necking PET molecules have been oriented. If sufficient orientation is achieved the structure may become a meso-phase (thermotropic liquid crystal) prior to actual crystallization. The viscosity of this meso-phase may be reduced compared to the unordered amorphous phase at the same temperature. This effect would be similar to that observed in the behavior of the viscosity of lyotropic liquid crystalline system on the formation of the meso-phase (22). A mechanism similar to this seems to have been suggested recently by Shimizu et al. (97).

At the present time, we really do not know whether the necking formation mechanism is due to formation of a meso-phase which results in a visocity decrease (strain softing) or the viscosity decrease results from an increase in temperature of the threadline resulting from the liberation of the heat of crystallization.

Although some investigators had argued that the temperature rise may not be sufficient to cause strain softening on the threadline, Warner (112) reported that during deformation of PET fibers in the drawing process, the temperature rise in the necking region was estimated to be about $60^{O}K$ and heat released is sufficient to raise the fiber temperature about $55^{O}K$ under adiabatic conditions. Our calculations indicate that the temperature increase at the neck varies with spinning conditions, but may be locally as high as 20-25 degrees when a sharp neck is observed. A simple adiabatic assumption also indicates that this may not be an unreasonable temperature rise.

In the experimental work, a sharp temperature rise was not observed on the spinline. This probably is because the neck is not stable at one position was not observed on the spinline. The motion of the neck would make measurement of the local temperature rise very difficult, as it would likely smear out the signal being observed by the infrared microscope. Also, after necking the fiber diameter is greatly reduced and fiber velocity sharply increases. This results in faster cooling of the fiber after necking. This would make the experimental observation of a sharp temperature increase in the neck region more difficult.

In summary, then, these simulation results suggest that the neck formation mechanism involves the liberation of crystallization heat which results in a locallized strain softening. Under constant take-up force this results in a high local deformation (necking). At the same time, the crystallization process, which results in strain hardening effect, prevents further deformation of the neck.

4.6 Discussion of the Effect of Polymer Variations on the Spinning Behavior

The molecular orientation is a balance between the orientation induced by deformation of polymer and the relaxation due to thermal motion of the molecules before the glass transition point is reached. Increasing the take-up velocity was found to increase the molecular orientation.

Material properties depend upon the molecular orientation. The fiber molecular orientation depends upon the rheological properties of the polymers and the take-up speeds. The melt viscosity of linear low molecular weight, branched and linear high molecular weight PET behave differently in the spinning process. From the experimental results, a rapid strain-induced crystallization occurred in the spinline for the linear

low molecular weight PET samples at high speed spinning. For the linear high molecular weight samples, the polymer melt viscosity is higher than the linear low molecular weight samples. Because of higher stress build up in the threadline, the neck position is closer to the spinneret. This effect could be predicted by the simulation model. For branched samples, the molecular branching resists polymer crystallization in the spinline. From the experimental results, we did not observe highly crystallized branched PET samples below 5000 m/min. Also we did not easily find necking on the spinline for branched samples. If the branched polymer crystallizes slowly, the strain softening, which is the result of releasing heat of crystallization, would occur over an extended distance in the spinline. This would reduce the sharpness of the necking effect.

CHAPTER 5

SUMMARY AND CONCLUSIONS

High speed spinning of linear, branched, and high molecular weight poly(ethylene terephthalate) (PET) polymers using a pneumatic drawdown device has been carried out. The structure characterization of these as spun fibers and the structure development along the spinline under different mass thrughput and take-up velocities were studied. A computer simulation was also carried out in this research.

From the results of characterization of three different kinds of PET polymers, it was found that the structure and physical properties are greatly affected by take-up velocity. Generally, at low take-up velocities (below 3500 m/min), the as spun fibers exhibited low birefringence, crystallinity, density, and tenacity values, and high elongation and shrinkage properties--typical of an amorphous structure. At high take-up velocities (above 5000 m/min) the (as-spun) fibers exhibited high birefringence, crystallinity, density and tenacity values and correspondingly low elongation and shrinkage values which are indications of a semi-crystalline structure. Differential scanning calorimetry analysis revealed that, below 5000 m/min,

the fiber partially crystallized while heating the sample. Above 6000 m/min, crystallization during heating was no longer observed. The glass transition could not be distinguished at take-up speeds above 5000 m/min. The melting temperature increased as the take-up velocity increased. Both density and DSC results show that PET begins to crystallize on the spinline at speeds in the range of 4000 to 4500 m/min. From density versus birefringence plots, it was found that orientation induced crystallization occurred at fiber birefringences above 45×10^{-3}.

From the analysis of samples cut from the spinline, the fiber diameters were observed to decrease in a very unusual manner. At low take-up velocities, no sharp diameter thinning phenomena (necking) was observed either on the spinline or in the cut specimens, and the birefringence values were low. Necking was observed on the spinline and on the cut samples when the take-up velocity exceeded 4500 m/min for linear PET. The birefringence values reached the final fiber birefringence within a few millimeters in the necking region. The diameter of the filament remained nearly constant after necking. Increasing the take-up velocity moved the position of the neck toward the spinneret. For branched PET, the birefringence increased with

take-up velocity, but the increase was slower than for the linear PET. Necking was not observed for cut branched samples. High molecular weight PET also exhibited necking on the spinline at high take-up speeds. The position of necking was closer to the spinneret compared with linear PET at the same take-up velocity.

Wide angle x-ray diffraction results from a bundle of fibers containing necking regions found amorphous diffraction patterns before necking. Clear crystalline diffraction peaks were detected after necking.

From on-line temperature measurements, it was determined that decreasing throughput and increasing take-up velocity produced a more rapid temperature decrease. The temperature profile indicated that the fiber cooled faster after necking. This increased cooling rate may be a result of the increased surface area per unit volume and increased velocity of the filament through the ambient air. The temperatures in the necking region were different with different PET materials and increased as take-up velocity increased. There was some slight indication that the fiber cooling rate slowed down in the neighborhood of the neck just prior to the increase of cooling rate occurring subsequent to the neck. This effect could have resulted

from the liberation of the heat of crystallization. There was, however, no indication of an actual temperature increase.

The on-line diameter and birefringence profiles showed that a low birefringence was observed before necking and suddenly increased after necking for linear and high molecular weight samples. A more gradual increase in birefringence was observed for branched PET. Prior to necking, the birefringence of the high molecular weight sample was higher than for linear PET.

It was found possible to achieve reasonable qualitative agreement with the experimental data using a computer simulation method first developed by Kikutani (66). This method assumes that when birefringence increases to a certain value, stress-induced crystallization is initiated. When stress-induced crystallization takes place, the latent heat generated in this region is released and the fiber temperature increases locally. This causes the polymer melt viscosity to suddenly decrease and produces a strain softening effect. Under a constant take-up force, the filament begins to undergo a rapid diameter decrease. But when the degree of crystallinity reaches a certain level, polymer melt viscosity increases and this strain hardening effect resists further filament deformation in

the spinline. The filament diameter becomes constant and a "neck" is observed. By changing the initial conditions in the simulation, for example, mass throughput, initial fiber diameter, initial fiber temperature, initial forces, etc., the structure development of PET fibers could be simulated from a fully amorphous structure to a semi-crystalline structure on the spinline.

Based on the experimental data summarized above, the following conclusions were made:

Take-up speed (spinline stress) is a dominate factor for fiber structure development of PET filament in the spinline. At high take-up speeds, the spinline stress is high enough to cause stress-induced crystallization in the spinline. Under certain conditions this also leads to a necking effect on the spinline. The fiber structure changed from amorphous to semi-crystalline structure after the neck.

From DSC analysis it was observed that melting temperature and crystallinity increased as take-up speeds increased. This indicated that the crystalline perfection and crystallinity increased at higher speeds. These data are consistent with online temperature measurements that show that necking occurred closer to the spinneret and necking temperature (crystallization

temperature) was higher at higher take-up speeds. The crystallization rate also increased at high temperature and higher molecular orientation. This produced higher crystallinity and increased the perfection of the crystals.

The difference of rheological properties and crystallization rates of the three different polymers results in different fiber structure and properties. The branched polymer had slower crystallization kinetics and developed lower crystallinity. These differences evidently reduced the propensity for formation of a sharp neck on the spinline. The higher viscosity of high molecular weight polymer results in higher stress build up in the spinline and fibers exhibit higher density and crystallinity at take-up speeds below 4000 m/min. The higher molecular entanglement also restricted further crystallization on the spinline for high molecular weight samples and the crystallization levelled off at higher take-up speeds.

From the present study, it was concluded that the necking formation mechanism is as follows: The formation of a neck appears to require a sudden strain softening (viscosity decrease) followed by a rapid strain hardening (viscosity increase). When sufficient stress-induced crystallization takes place in a

locallized region of the spinline, the heat of crystallization is released in this region and the fiber temperature increases locally. This produces the necessary strain softening effect. Under a constant take-up force, the filament undergoes a rapid diameter decrease. But when the degree of crystallinity reaches a certain level the high viscosity and orientation of filament resists further deformation on the spinline (strain hardening). The fiber diameter becomes constant and a "neck" is observed. Computer simulation results suggest that this is a possible and reasonable mechanism.

Another possible necking formation mechanism is as follows: Prior to necking, PET molecules have been oriented. If sufficient orientation is achieved the structure may become a meso-phase (thermotropic liquid crystal) prior to actual crystallization. The viscosity of this meso-phase may be reduced (viscosity decrease). At a constant take-up force the filament undergoes a rapid diameter decrease. The deformation increases the orientation of the filament and stress-induced crystallization takes place. When the filament is oriented and crystallized on the spinline the molecules resist further deformation of the filament (strain hardening).

While the former mechanism is favored, it is not possible to rule out the latter mechanism on the basis of the present experimental data.

LIST OF REFERENCES

LIST OF REFERENCES

1. Abbot, L. E. and J. L. White, Appl. Polym. Symp., 20, 247 (1973).

2. Abhiinaman, A. S., J. Polym. Sci., 21, 583 (1983).

3. Alexander, L. E., "X-ray Diffraction Method," Polymer Sci., J. Wiley Interscience, New York, (1969).

4. Allison, S. W. and I. M. Ward, Brit. H. Appl. Phys., 18, 1511 (1967).

5. Antwerpen, F. V. and D. W. Van Krevelen, J. Polym. Sci., Polym. Phys. Ed., 10, 2423 (1972).

6. Astbury, W. T., and C. H. Brown, Nature, 158, 871 (1946).

7. ASTM D-2101, 33, 486 (1982).

8. Banker, V., J. E. Spruiell, and J. L. White, J. Appl. Polym. Sci., 21, 2135 (1977).

9. Banker, V., J. E. Spruiell, and J. L. White, J. Appl. Polym. Sci., 21, 2341 (1977).

10. Barnes Infrared Radiometric Microscope Instruction Manual.

11. Bassett, D.C., "Principles of Polymer Morphology," Cambridge University Press, London (1981).

12. Bauer, K., ITB 2, 215 (1978).

13. Benaim, E., M.S. Thesis, The University of Tennessee, Knoxville (1978).

14. Binsbergen, J. L., Ph.D. Dissertation Holland, (1969).

15. Bragato, G. and G. Gianotti, Eng. Polym. J. 19 801 (1983).

16. Brandrup, J. and E. M. Immergut, "Polymer Handbook," J. Wiley Interscience, New York, (1975).

17. Brennan, W. P. "Thermal Analysis Application Study," Perkin-Elmer Corp., 6, (1973).

18. Brennan, W. P. "Thermal Analysis Application Study," Perkin-Elmer Corp., 7, (1973).

19. Bromley, J. E., U. S. Patent 4,128,,989 (1978).

20. Carothers, W. H. and J. W. Hill, J. Amer. Chem. Soc., 54, 1579 (1932).

21. Cakmak, M., Ph.D. Dissertation, The University of Tennessee, Knoxville, (1982).

22. Ciferri, A., W. R. Krigbaum, and R. B. Meyer, "Polymer Liquid Crystals," Academic Press, New york, (1982).

23. Cobbs, W. H., and R. L. Burton., J. Polym. Soc., 10, 275 (1953).

24. Daubeny, R. P., C. W. Bunn, and C. J. Brown, Proc. Roy. Soc., A 226, 531 (1955).

25. Dees, J. R. and J. E. Spruiell, J. Appl. Polym. Sci., 18, 1055 (1974).

26. Dees, J. R., Ph.D. dissertation, The University of Tennessee, Knoxville, (1974).

27. Dumbleton, J. H., J. Polym. Sci. A-2 6, 795 (1968).

28. Dumbleton, J. H., Textile Res. J. 40, 1035 (1970).

29. Fakirov, S., E. W. Fischer, R. Hoffman, and G. F. Schmidt, Polymer, 18, 1121 (1977).

30. Farrow, G. and D. Preston, Brit. J. of Appl. Phy. 11, 353 (1960).

31. Farrow, G. and J. Bagley, Textile res. J., 32, 587 (1962).

32. Fellous, J., U. S. Patent 3,576,284 (1971).

33. Fiber Producer Editors, Fiber Producer, 12, 19 (1976).

34. Frankfort, H. R. and B. H. Knox, U. S. Patent 4, 134,882 (1978).

35. Garg, S. K., J. Appl. Polym. Eng. Sci., 29, 2111 (1984).

36. George, H. H., Polym. eng. Sci., 22, 292 (1982).

37. George, H. H., A. Holt and A. Buckley, Polym. Eng. Sci., 23, 95 (1983).

38. George, V., European Patent 0,089,819 (1983).

39. Goswami, B. C., J. G. Martindale, and F. L. Scardino, "Textile Yarns-Technology, Structure and Application," John Wiley and Sons, New York, (1977).

40. Gupta, V. B. and S. Kumar, J. Polym. Si., Polym. Phys. Ed., 17, 1307 (1979).

41. Gupta, V. B. and S. Kumar, J. Appl. Polym. Sci., 26, 1865 (1981).

42. Gupta, V. B. and S. Kumar, J. Appl. Polym. Sci., 26, 1877 (1981).

43. Gupta, V. B. and S. Kumar, J. Appl. Polym. Sci., 26, 1885 (1981).

44. Gupta, V. B. and S. Kumar, J. Appl. Polym. Sci., 26, 1897 (1981).

45. Hamidi, A., A. S. Abhiraman and P. Asher, J. Appl. Polym. Sci., 28, 567 (1983).

46. Han, C. D., and R. R. Lamonte, J. Appl. Polym. Sci., 16, 3307 (1972).

47. Hearle, J. W. S. and R. H. Peters, "Fiber Structure," Manchester, (1968).

48. Heberler, H. H., U. S. Patent 2,604,667 (1968).

49. Henson, H. M. and J. E. Spruiell, Paper Presented at The Div. of Cellulose, Paper and Tex. Chem., Philadelphia (1975).

50. Hermans, P. H., J. H. Hermans, D. Vermoas and A. Weidinger, J. Polym. Sci., 3, 1 (1947).

51. Heuvel, H. M. and R. Huisman, J. Appl. Polym. Sci., 22, 2229 (1978).

52. Heuvel, H. M. and R. Huisman, J. Appl. Polym. Sci., 26, 713 (1981).

53. Heuvel, H. M. and R. Huisman, J. Appl. Polym. Sci., Polym. Phys. Ed., 19, 121 (1981).

54. Hill, J. W. and J. A. Cuculo, J. appl. Polym. Sci., 18, 2569 (1974).

55. Hoffmeister, R. and Landenberger, P., Fiber Producer, 12, 5 (1979).

56. INDA, "Guide To Nonwoven Fabrics," INDA Public Co., 1978.

57. Ishibashi, T. and T. Ishii, J. Appl. Polym. Sci., 20, 335 (1976).

58. Ishizuka, O. and K. Koyama, Sen-I Gakkaishi, 35, T-453 (1979).

59. Ishizuka, O. and K. Koyama, Polym., 12, 735 (1980).

60. Joseph, M. L. "Introductory Textile Science" CBS College Publishing New York (1981).

61. Kase, S., and T. Matsuo, J. Polym. Sci., A-3, 2541 (1965).

62. Kase, S., and T. Matsuo, J. Appl. Polym. Sci., 11, 251 (1967).

63. Kase, S., and T. Matsuo, J. Appl. Polym. Sci., 18, 3267 (1974).

64. Kase, S., and T. Matsuo, J. Appl. Polym. Sci., 18, 3279 (1974).

65. Kase, S., and T. Matsuo, J. Appl. Polym. Sci., 19, 557 (1975).

66. Kikutani, T., Ph.D. Dissertation, Tokyo Institute of Technology, Tokyo, Japan (1984).

67. Killian, H. G., H. Halboth, and E. Jenkel, Kolloid Z, Z. Polym., 172, 166 (1960).

68. Kinney, G. A. U.S. Patent 3,338,992 (1965).

69. Kitao, T., S. Ohya, J. Furukaw, and S. Yamashita, J. Polym. Sci., Poly. Phys., 11, 1091 (1973).

70. Kubo, S., Sen-I Gakkaishi, 38. P-429 (1982).

71. Lecluse, C., "High Speed Spinning of Polyamide 66," Rhone Poulenc Fibers, (1984) Unpublished.

72. Lemanska, G. and A. Nerbska, J. Polym. Sci., Polym. Phys. Ed., 18, 917 (1980).

73. Lin, L. C. and J. Hauenstein, J. Appl. Polym. Sci., 18, 3509 (1974).

74. Ludewig, H., "Polyester Fibers-Chemistry and Technology," J. Wiley Interscience, New York (1971).

75. Mark, H. F. and N. G. Gaylord, "Encyclopedia of Polym. Sci. and Techn.," Interscience Publishers, New York, 11, 1 (1969).

76. Matsui, M., Sen-I Gakkaishi, 38, T-508 (1982).

77. Miller, R. W., J. H. Southern and R. L. Ballman, Textile Res. J., 53, 670 (1983).

78. Misra, A. and R. S. Stein, J. Polym. Sci., Polym. Phys. Ed, 17, 235 (1979).

79. Nadella, H., J. E. Spruiell and J. L. White, J. Appl. Polym. Sci., 21 3003 (1977).

80. Nadella, H., H. M. Henson, J. E. Spruiell and J. L. White, J. Appl. Polym. Sci., 22, 2131 (1978).

81. Nakamura, K., T. Watanabe, K. Katayama and T. Amano, J. Appl. Polym. Sci., 22, 2131 (1978).

82. Perez, G. and C. Lecluse, 18th"International Man-Made Fiber Conference" at Dorbirn, June (1979).

83. Perez, G., "Some Effect of the Rheological Properties of PET on Spinning Line Profile and Structure Development in High Speed Spinning," Rhone Poulenc Fibers, France (1982).

84. Perkin-Elmer DSC-2 Operation Manual.

85. Pizza, S., U.S. Patent 3,772,872 (1973).

86. Samuels, R. J., "Structureed Polym. Properties," John Wiley, New York (1974).

87. Shimizu, J., A. Watanabe and K. Toriumi, Sen-I Gakkaishi, 30, T-53 (1974).

88. Shimizu, J., Ka Sen Kes Po, 27, 42 (1977).

89. Shimizu, J., K. Toriumi and K. Tamai, Sen-I Gakkaishi, 33, T-208 (1977).

90. Shimizu, J., K. Toriumi and Y. Imai, Sen-I Gakkaishi, 33, T-255 (1977).

91. Shimizu, J., N. Okui, t. Kikutani and K. Toriumi, Sen-I Gakkashi, 34, T-93 (1978).

92. Shimizu, J., N. Okui, A. Kaneko and K. Toriumi, Sen-I Gakkaishi, 34, T-64 (1978).

93. Shimizu, J., N. Okui and Y. Imai., Sen-I Gakkaishi, 35, T-405 (1979).

94. Shimizu, J., N. Okui and Y. Imai, Sen-I Gakkaishi, 36, T-166 (1980).

95. Shimizu, J., N. Okui and T. Kikutani, Sen-I Gakkaishi, 37 T-135 (1981).

96. Shimizu, J., N. Okui, T. Kikutani, A. Ono and A. Takaku, Sen-I Gakkaishi, 37, T-143 (1981).

97. Shimizu, J., Sen-I Gakkaishi, 38, T-499 (1982).

98. Shimizu, J., N. Okui, and K, Tamai, Sen-I Gakkashi, 39, T-398 (1983).

99. Shimizu, J. and N. Okui, Sen-I Gakkaishi, 39, T-445 (1983).

100. Shimizu, J., N. Okui, Y. Imai, S. Nishide and A. Takaku, J. Polym. Sci., 21, 275 (1983).

101. Shimizu, J., T. Kikutani and A. Takaku, Sen-I Gakkaishi 40, T-63 (1984).

102. Speckhart, F. H., and W. L. Green, "A Guide to Using CSMP-The Continuous System Modeling Program" Prentic-Hall Inc., Englewood Cliffs, N.J. (1976).

103. Spruiell, J. E. and J. L. White, in "Fiber and Yarn Processing," J. L. White, Ed., Appl. Polym. Symp., 27, 121 (1975).

104. Spruiell, J. E. and J. L. White, Polym. Eng. Sci. 15, 660 (1975).

105. Stein, R. S., J. Polym. sci., 24, 383 (1957).

106. Stein, R. S., S. Onogi and D. A. Keedy, J. Polym. Sci., 57, 801 (1962).

107. Suryadevara, J., M.S. Thesis, The University of Tennessee, Knoxville (1984).

108. Tompson, A. B., J. Polym. Sci., 34, 741 (1959).

109. Tsou, J. D., Ph.D. Dissertation, The University of Tennessee, Knoxville, (1984).

110. Vincent, P. I., Polymer, 1, 7 (1960).

111. Ward, I. M., "Mechanical Properties of Solid Polymers," John Wiley and Son, New York (1974).

112. Warner, S. B., J. Appl. Polym. Sci., 29, 219 (1984).

113. White J. L., K. C. Dharod, and E. S. Clark, J. appl. Polym. Sci., 18, 2539 (1974).

114. White, J. L., Polym. Eng. Review, 1, No.4 (1981).

115. Wilchinsky, Z. W., J. Appl. Phys., 30, 792 (1959).

116. Wilchinsky, Z. W., J. Appl. PhYs., 31, 1969 (1960).

117. Yasuda, H. and Sugiyama, J., Sen-I Gakkaishi, 37, T-497 (1981).

118. Yasuda, H., Sen-I Gakkaishi, 38, P-514 (1982).

119. Yeh, G. S. Y. and P. H. geil, J. Macromol. Sci., Phys., B1, 251 (1967).

120. Zachmann, H. G., Polym. Eng. Sci., 19, 966 (1979).

121. Zahn, H. and R. Krzikalla, Makromol. Chem., 23, 31 (1957).

122. Ziabicki, A. and K. Kedzierska, J. Appl. Polym. Sci., 11, 14 (1959).

123. Ziabicki, A. and K. Kedzierska, Kolloid Z. A. Polym., 171, 51 (1960).

124. Ziabicki, A. and K. Kedzierska, Kolloid Z. A. Polym., 171, 111 (1960).

125. Ziabicki, A. and Kolloid Z. A. Polym., 175, 14 (1960)

126. Ziabicki, A. and K. Kedzierska, J. Appl. Polym. Sci., 6, 111 (1962).

127. Ziabicki, A., "Fundamentals of Fiber Formation," John Wiley and Sons New York (1976).

128. Ziabicki, A., Sen-I Gakkaishi, 38, T-417 (1982).

129. Ziabicki, A. and H. Kawai, "High Speed Melt Spinning--Science and Engineering" will be publish (1985).

APPENDIXES

APPENDIX A

Notations

NOTATIONS

A	(cm^2)	cross-section area of filament	
Cop	(---)	strain-optical coefficient	
Cf	(---)	coefficient of air friction	$Cf = 0.5Re^{-0.61}$
Cp	(cal/g^oC)	heat capacity of polymer	$Cp = 0.3 + 6.0 \times 10^{-4}T$
D	(cm)	diameter of filament	
F	(dyne)	tension of spinning filament	
g	(cm/sec^2)	gravity	$g = 980$
G	($dyne/cm^2$)	modulua	$G = 1 \times 10^9$
h	($cal/cm^2 sec^oC$)	heat transfer coefficient	$h = (ks/D)\ Nu$
k	($cal/cm\ sec^oC$)	heat conductivity of polymer	$k = 5.2 \times 10^{-4}$
ks	($cal/cm\ sec^oC$)	heat conductivity of air	$ks = 0.66 \times 10^{-4}$
n	(---)	Avrami number	
Nu	(---)	Nusselt number	$Nu = 0.42(1 + (8Vy/V)^2)^{0.167}Re^{0.334}$
Re	(---)	Reynolds number	$Re = DV/\nu_s$
t	(sec)	time	
$t_{1/2}$	(sec)	crystallization half-time	
$t_{1/2}^*$	(sec)	minimum crystallization halt-time	
T	(^oC)	temperature of filament	
Ts	(^oC)	temperature of surrounding air	
T*	(^oC)	maximum crystallization rate temperature	

V	(cm/sec)	velocity of spinning filament	
Vy	(cm/sec)	velocity of quenching air	
W	(g/sec)	extrusion rate	
x	(cm)	distance from spinneret	
χ_c	(---)	crystallinity	
β	(deg)	half-width of temperature vs. crystallization curve	
ΔH	(cal/g)	heat of fusion	
ΔN	(---)	birefringence	
ε	(---)	strain	
η	(poise)	tensile viscosity of polymer	$\eta = 1.3 \exp(4400/(T + 273))$ $(T>70^{o}C)$ $\eta = \infty$ $(T<70^{o}C)$
ν_s	(st)	kinetic viscosity of air	$\nu_s = 0.16$
ρ	(g/cm^3)	density of polymer	$\rho = 1.356 - 5.0 \times 10^{-4} T$
ρ_s	(g/cm^3)	density of air	$\rho_s = 1.2 \times 10^{-3}$
σ	($dyne/cm^3$)	spinning stress	
τ_f	($dyne/cm^3$)	stress of air friction	$\tau_f = (1/2)\rho_s V^2 Cf$
t_m	(sec)	relaxation time	$t_m = \eta/G$

SUBSCRIPTS

0	value at the spinneret
L	value at x = L

APPENDIX B

Continuous System Modeling Program

Continues System Modeling Program (CSMP) is an applicationoriented program specially written for scientist, engineers, and analysts who are involved in work that requires the solution of ordinary differential equations or in simulating a system that has been modeled as a block diagram.

The program structure of CSMP is composed of three segments: Initial, Dynamic, and Terminal. Generally, data statements will appear in the Initial segment. In addition, calculations that are required to be performed only one time during a simulation can conveniently placed in this segment. The Dynamic segment is usually vomposed of structure statements that describe the dynamics of the system or explicity describe a set of differential equations. The Terminal segment is the last segment in the program and is usually made up of control statements.

The utility and ease of using stems mainly from:

(1) simplified program statements

(2) flexibility of program structure

(3) a basic set of preprogrammed function blocks.

The CSMP program for high speed spinning of PET is listed below.

CSMP Program

```
$$$CONTINUOUS SYSTEM MODELING PROGRAM  III   V1M3   TRANSLATOR OUTPUT$$$

CONSTANT TS=25.
CONSTANT COP=.53,DELH=29.
CONSTANT TC=290.
CONSTANT AKS=.016
CONSTANT AKSO=.66E-4
CONSTANT PI=3.14159,G=980.
CONSTANT ALCS=0.0012,AMUS=0.16
CONSTANT DO=0.076
*CONSTANT FO=46.288
PARAMETER FO=(46.33,46.34,46.35)
INITIAL
W=5.2/60.
ALCO=1.356-5.E-4*TC
VO=W**4./ALCO/PI/DO/DO
XCO=.44
DELNO=COP*FO*ALCO*VO/10.**9/W
DYNAMIC
LABEL W=5.2,VY=0.
ANU=.42*RE**.334
H=AKSO/D*ANU
CP=.3+0.E-4*T
DF=W*(DV-G/V)+PI*D*TAUF
ALC=1.356-5.E-4*T
F=INTGRL(FO,DF)
D=SQRT(W**4./V/PI/ALC)
TAUF=0.5*ALCS*V*V*CF
CF=0.5*RE**(-0.61)
RE=D*V/AMUS
DV=F*ALC*V/W/ATA
*ATA=0.73*EXP(5300./(T+273.))*EXP(2.**2*(2.*XC)**16)
ATA=1.3*EXP(4400./(T+273.))*EXP(4.*(2.*XC)**16)
*ATA=0.0282*EXP(4375./(T+273.))*EXP(4.*(2.*XC)**16)
V=INTGRL(VO,DV)
VPL=V*60./100.
DT=-PI*D*H*(T-TS)/W/CP+DXC*DELH/CP
T=INTGRL(TO,DT)
DDELN=COP*DV/V-DELN/V/TAUM
DELN=INTGRL(DELNO,DDELN)
TAUM=ATA/10.**9
XC=INTGRL(0.,DXC)
DXC=DY*(XOO-XC)/V
DY=AKS*EXP(-Y1)*EXP(4000.*DELN*DELN)
Y1=4.*ALOG(2.)*(T-TSTAR)**2/B/B
TSTAR=190.+75.*DELN/.22
 PROCEDURE B=REDY(T,TSTAR)
       IF (T.GT.TSTAR) GO TO 10
       B=(TSTAR-70.)/1.2
       GO TO 20
 10    B=(265.-TSTAR)/1.2
 20    CONTINUE
 ENDPROCEDURE
DD=ALOG(DUM)
DUM=D*10000.
XCP=XC*100.
METHOD STIFF
PRTPLT DUM,T,VPL,DY,XCP
PAGE HEIGHT=50,WIDTH=50
PRTPLT F,DELN,XCP,T,ALC
```

```
PAGE HEIGHT=50,WIDTH=5C
RELERR DELN=0.00005,T=C.0001
ABSERR DELN=0.0C0001,T=C.0001
NOSORT
CALL DEBUG(1,0.)
TERMINAL
TIMER FINTIM=135.,PRDEL=8.,DELMIN=1.E-12
END
STOP
```

VITA

Chi-Chung Bai (白志中) was born in Hsinchu, Taiwan, R.O.C. on Nov. 10, 1950 as the third son of Mr. & Mrs. Hsi Chih Bai (白曦之). He graduate from Hsinchu High School and joined Feng Chia University at Taichung, Taiwan in 1969. After four years he received his Bachelor's degree in Textile Engineering. In 1975, he received his Master's degree in Textile Engineering at the same university. Upon completion of two years of millitary service, he had worked for Union Chem. Res. Lab. of Industrial Techn. Res. Inst. in Taiwan, Rep. of China.

He married Hsin-Shen Chin (秦新生) in Dec. 3, 1977 and they have two sons, Jong-Woen Bai (白仲文) and Young-Weon Bai (白仰文).

In Jan. 1981, he received a fellowship from National Sci. Council of Rep. of China and attended the University of Tennessee, Knoxville. He received his Ph.D. degree in June 1985. He will rejoined the Union Chem. Res. Lab.

He is a member of Text. Eng. Soc. and Material Sci. Soc. of R.O.C., Soc. of Plas. Eng. and Amer. Asso. of Text. Chem. and colorist of U.S.A., the Text. Inst. of U.K. and the Soc. of Fiber Sci. of Japan.

He receive Jeme Tein-yau (詹天佑) Gold Medal from Chinese Institute of Chinese Engineers in 1978.